2021

A Proteomic Approach to Elucidating the Function of Picornavirus 2A Protease

Artem Serganov

A Proteomic Approach to Elucidating the Function of Picornavirus 2A Protease

A Thesis Presented to the Faculty of
The Rockefeller University
in Partial Fulfillment of the Requirements for
the degree of Doctor of Philosophy

by
Artem Serganov
June 2021

A Proteomic Approach to Elucidating the Function of Picornavirus 2A Protease

Artem Serganov, Ph.D.
The Rockefeller University 2021

Human-infecting viruses have evolved diverse strategies to enter cells and hijack the host machinery to promote their self-replication. Viruses deploy their proteins to subvert a number of host functions, such as the cell cycle, cellular metabolism, protein synthesis, nuclear and RNA transport across the nuclear pore complex, apoptosis, and innate immune responses. Picornaviruses are the most dominant human disease-causing viruses and present an excellent clinical target for research studies into their molecular mechanisms. Picornaviruses have an RNA genome that is translated as a single polyprotein, which is processed into individual components by two proteases, termed 2A and 3C. In addition to polyprotein processing, these proteases also subvert host cell function through cleavage of specific protein targets. The 2A protease is especially critical during the initial stages of picornaviral infections.

We developed protein expression platforms to further characterize the 2A protease's function, interacting partners, and targeting mechanisms, showing that it makes surgical strikes against eIF4G and Nup98, key players in host protein synthesis and nucleocytoplasmic trafficking of proteins and RNA, respectively. We subsequently utilized those protease expression platforms in combination with transport reporter assays to interrogate nuclear import and export through the NPC. By studying the interactome of 2A protease, we discovered that it seems to employ two different cleavage mechanisms for its primary targets, Nup98 and eIF4G. It directly binds and degrades Nup98, and may alternatively bind eIF3L and utilize the eIF3 complex as a targeting platform to cleave eIF4G. Cellular fractionation revealed Nup98 cleavage by 2A protease results in observable dissociation of Rae1 from the NPC as well as cytoplasmic accumulation of proteins normally transported by Karyopherins that interact with Nup98 FG motifs. We developed fluorescent transport reporters with various nuclear import and export signals to elucidate their transport mechanism and dependence on Nup98. Nuclear localization signals promiscuously recognized by a variety of Importins were marginally, if at all, affected by Nup98 depletion, while export and import signals depending on Crm1 or Rae1 mediated RNA export were severely affected by the absence of full-length Nup98. We propose a novel cleavage mechanism for the 2A protease, as well as report on our development of a suite of molecular tools to further characterize 2A protease function and nucleocytoplasmic transport mediated by Nup98. These tools can be

adapted to include a diverse variety of viral proteins to further characterize host subversion mechanisms as well as other aspects of nuclear pore complex function.

ACKNOWLEDGMENTS

Throughout my 7-year journey as a Ph.D. student, I was fortunate to work with a number of incredible and supportive people.

First and foremost, I would like to thank my supervisor Prof. Mike Rout for giving me the opportunity to work in his laboratory and for years of guidance and mentorship. I would like to thank past and current members of the Rout laboratory that helped me with my research project, fielding questions and always happy to offer help and advice. Thank you Yael Udi, Samson Obado, Peter Fridy, Dan Simon, Jill Trivedi, John LaCava, and Javier Martinez Fernandez. I would also like to thank Erica Jacobs of the Chait laboratory for her generous help with my project, from experiments and data analysis, to big-picture guidance on the direction of my thesis work.

I would like to thank my thesis committee members Profs. Charles Rice and Brian Chait. Both have been instrumental to my success, from the beginning of my project to its conclusion. You helped shape my thesis work, helped provide the tools for me to solve problems, and helped me prioritize the most valuable questions to pursue. I would also like to thank Prof. John Aitchison for agreeing to be a part of my thesis defense as an external committee member.

I would like to my Fiancée Bailey Carroll for her continued patience and endless support throughout my endeavor. From weekends and late nights to holidays and odd-hours, you always had my back and were ready to help however you could. I could not have done this with you.

Finally, I would like to thank my incredible and loving parents Prof. Alexander Serganov and Dr. Inna Serganova. Thank you for fostering my interest in science when I was a teenager and for helping me get started in a research laboratory when I was in high school. Thank you for a lifetime of support and for making me into the man I am today.

TABLE OF CONTENTS

LIST OF FIGURES

LIST OF TABLES

LIST OF ABBREVIATIONS

2AC110A	2A protease with Cysteine 110 mutated to Alanine
$2A^{pro}$	Catalytically active, wild type 2A protease
$3C^{pro}$	Catalytically active, wild type 3C protease
AdV	Adenovirus
APD	Autoproteolytic Domain
BSA	Bovine Serum Albumin
Cryo-EM	Cryogenic electron microscopy
CVB3	Coxsackievirus B3
Da	Dalton
DMSO	Dimethyl Sulfoxide
DNA	Deoxyribonucleic acid
Dox	Doxycycline
DSS	Disuccinimidyl suberate
DTT	Dithiothreitol
EDTA	Ethylenediaminetetraacetic acid
EGFP	Enhanced green fluorescent protein
eIF	Eukaryotic initiation factor
$eIF4G^{cp}$	eIF4G cleavage product
EMCV	Encephalomyocarditis Virus
ER	Endoplasmic Reticulum
FG Nup	Nup rich in FG repeats
FG Repeat	Phenylalanine-Glycine Repeat
FISH	Fluorescent in situ hybridization
fmk	Fluoromethyl ketone
GFP	Green fluorescent protein
GFP_2	Two GFP molecules fused together
GTP	Guanosine triphosphate
H.p.i.	Hours post-infection
HCV	Hepatitis C Virus
HIV-1	Human Immunodeficiency Virus 1
HPV	Human papillomavirus
HTLV-1	Human T-cell leukemia virus type 1
IRES	Internal Ribosome Entry Site
ITAF	IRES trans-acting factor
ITR	Inverted Terminal Repeats
Kaps	Karyopherins
Kb	kilobases
MeOH	Methanol
mRNA	Messenger Ribonucleic acid
mRNP	Messenger Ribonucleoprotein
MX2	Human myxovirus resistance 2
NaCl	Sodium Chloride
NES	Nuclear export signal
NFDM	Non-fat dry milk
NHS	N-hydroxysuccinimide

NLS	Nuclear localization signal
NPC	Nuclear Pore Complex
Nup	Nucleoporin
O.N.	Overnight
PABP	Poly-A Binding Protein
PBS	Phosphate buffer saline
PCBP2	Poly(rC)-binding protein 2
PCR	Polymerase Chain Reaction
PIC	Preinitiation complex
PMSF	Phenylmethylsulfonyl fluoride
PSM	Peptide spectral mass
PTBP1	Polypyrimidine Tract-Binding Protein 1
PV	Poliovirus
PVP	Polyvinylpyrrolidone
PY	Proline-Tyrosine
RanGEF	Guanine nucleotide exchange factor
RBD	RNA binding domain
RNA	Ribonucleic acid
Rpm	Rotations per minute
RRE	Rev-responsive element
RRM	RNA recognition motif
RV	Rhinovirus
RxRE	Rex-responsive element
SRSF3/SRp20	Serine/Arginine-Rich Splicing Factor 3
TBST	Tris-buffered saline with Tween-20
Tm	Melting temperature
VP1-4	Viral coat proteins 1-4
VSV	Vesicular stomatitis virus

CHAPTER 1. Introduction

1.1 Viral hijacking and control of host functions during replication life cycles

Viruses are obligate intracellular parasites with relatively small genomes that depend on their infected hosts for perpetuation of their life cycle. Viruses constantly evolve new strategies to evade detection and subvert their host's cellular functions[1]. These targeted functions include regulation of the cell-cycle[1], cellular metabolism[2], host protein synthesis[3], intracellular protein and nucleic acid transport[4], apoptosis[5], autophagy[6], cytokine-mediated signaling[7], and immune responses[8]. During infection of cells, viruses normally provide some of their own enzymes, such as DNA/RNA polymerases, helicases, and proteases, to promote their self-replication[9]. Viruses also quickly interfere with host cell regulation as soon as a cell is invaded to attenuate host response of infected cells and drive viral replication. In the initial stages of infection, a variety of host machinery is subverted by viruses for promotion of self-replication. Two specific examples relevant to this thesis include translation components such ribosomes and related factors as well as nuclear pore complex (NPC) components that regulate trafficking of proteins and nucleic acids. Both sets of machinery are often targeted by viruses to co-opt translation machinery and nuclear-localized RNA-binding proteins that contribute to formation of Internal Ribosome Entry Sites (IRESes) to facilitate cap-independent translation of viral proteins. Among many viruses that target both translation and transport machinery are picornaviruses.

Picornaviruses are small, non-enveloped RNA viruses with a positive-sense RNA genome of approximately 8 kilobases (kb) in length. There are over 63 genera of picornaviruses, with 147 species and over 500 strains identified, distributed ubiquitously all over the world, and capable of infecting vertebrates of all classes[10]. The genus *Enterovirus* includes most of the human disease-causing picornaviruses. Symptoms of picornaviral infections vary widely and can present as disease of the central nervous system leading to paralysis (poliovirus - PV), of the respiratory system (rhinovirus - RV), and heart (Coxsackievirus B3 – CVB3), among many others (cdc.gov). Clinically, picornaviruses pose one of the biggest threats to human health. Infection rates in the human population are impossible to calculate precisely due to the varied prevalence of viruses, their infectivity, and rate of severe clinical symptoms, but are predicted to be 10-15 million cases annually in the USA alone (cdc.gov). Overall, picornaviruses present diverse and impactful clinical presentation of symptoms and widespread infectivity. Elucidating mechanisms of picornaviral replication, specifically how they subvert infected host cells and what host proteins they manipulate, would prove invaluable towards development of treatment strategies for picornaviral infections. Furthermore, we can develop picornaviral proteases as novel tools to interrogate the various host pathways that they subvert.

1.2 Picornaviral replication cycle

Picornaviral virions bind specific receptors on cell membrane surfaces, triggering entry of the virion and subsequent release of the RNA genome. Different picornaviruses bind different cell surface receptors. For example, rhinoviruses bind ICAM-1[11], polioviruses bind PVR[12], and coxsackieviruses and adenoviruses bind CAR[13]. The replication cycle of picornaviruses starts and stays in the cytosol of the infected cells (Fig. 1.1) and involves host machinery for replication, such as ribosomes and other proteins. The picornaviral genome is a positive-sense strand mRNA that is translated by host ribosomes into a polyprotein comprising of capsid and nonstructural replication proteins. The polyprotein is co-translationally processed into individual components by two proteases, 2A ($2A^{pro}$) and 3C ($3C^{pro}$). $2A^{pro}$ makes the initial cleavage during translation to

separate all of the viral coat proteins (VP1-4)[10], while $3C^{pro}$ makes all subsequent polyprotein cleavages (Fig. 1.1).

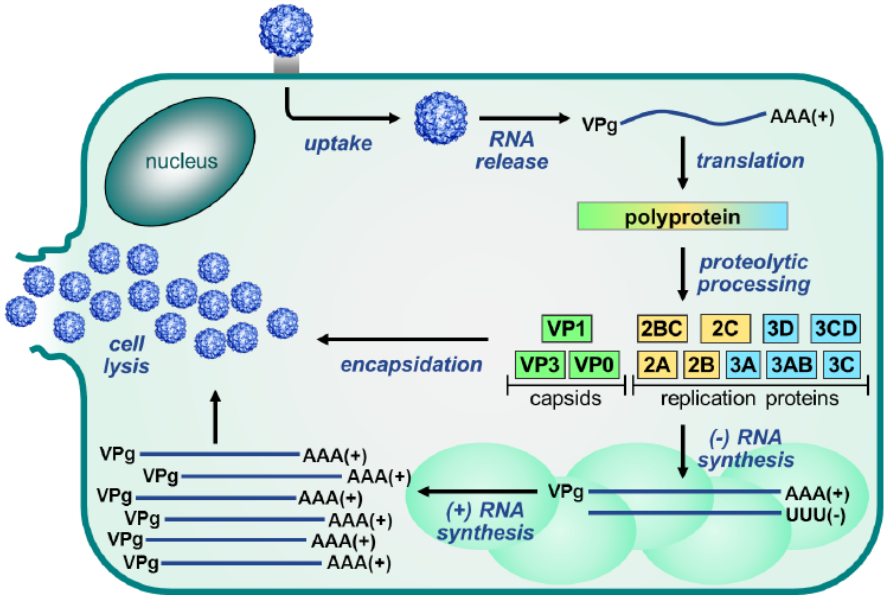

Figure 1.1. Viral replication cycle and polyprotein processing.[14]
Picornaviral virions attach to the membrane surface of cells, release the RNA genome, which is subsequently translated as a polyprotein by host machinery. The polyprotein is processed into individual components by two proteases: 2A and 3C. Viral proteins contribute to the replication of new viral coat proteins and transcription of the RNA genome, which combine to form novel virions. Adapted from Linden et al[14].

Among the two proteases, other nonstructural proteins include a viral RNA polymerase (3D) that catalyzes genome replication[15], a protein (3A) that inhibits endoplasmic reticulum (ER)–to–Golgi transport[16], an NTPase (2C) that rearranges the cytoplasm to form vesicle "webs" for viral replication[17], and a transmembrane protein (2B) that localizes to the ER where it forms pores to reduce Ca^{2+} levels and inhibit intracellular protein trafficking[18]. These proteins clearly serve a diverse set of roles, from directly contributing to viral replication (3D), to preparing a cellular environment that promotes replication (2C), to stopping core host cell functions such as protein trafficking (3A and 2B). Many of these proteins still have poorly defined or characterized roles, and may contribute to viral replication in undetermined, secondary ways. An example of secondary function is the two picornaviral proteases 2A and 3C, for which researchers have identified roles beyond polyprotein processing. Indeed, both proteases cleave dozens of different host proteins, ranging from translation factors, RNA binding proteins, NPC components involved in protein and nucleic acid trafficking, innate immune proteins, and many others. The cleavage of these proteins is critical for promoting picornaviral replication and preventing a host response.

1.3 Viral subversion of eukaryotic translation

Eukaryotic translation involves approximately 50 different proteins and is a highly regulated process in gene expression[19, 20]. Translation can be subdivided into four major steps: initiation, elongation, termination, and ribosome recycling. Translation initiation involves over 30 proteins (the majority of translation-related proteins) and is the most regulated step of translation,

and effectively constituting a rate-limiting step of protein synthesis[20]. Cap-dependent translation initiation begins with the formation of the 43S preinitiation complex (PIC), which includes the 40S small ribosomal subunit, a GTP-bound eIF2, eIF3, and eIF5. In parallel, eIF4G, eIF4A, and eIF4E form the eIF4F complex, which engages the 5' cap and PABP, which coats the poly-A tail of mRNA (Fig. 1.2)[21]. The PIC attaches to the eIF4F complex engaged with the mRNA and forms the 48S pre-initiation complex, which will subsequently scan the mRNA for an appropriate start codon to begin translation.

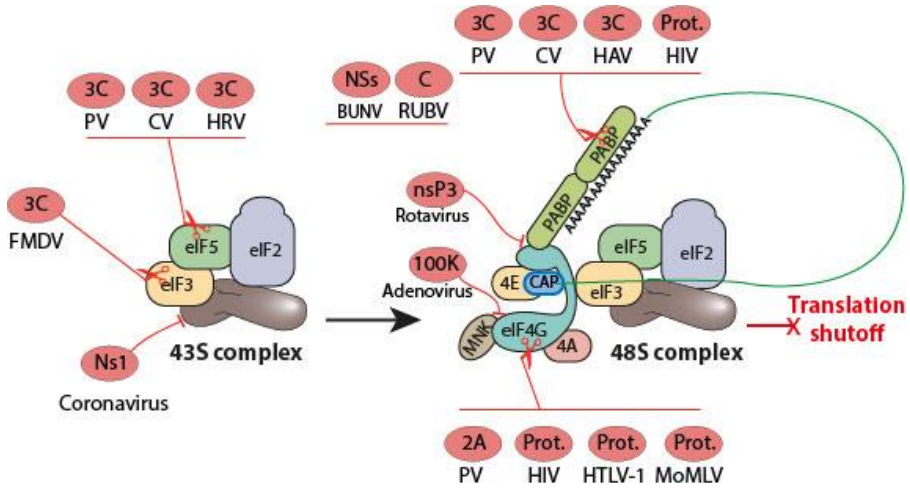

Figure 1.2. Viral subversion of eukaryotic translation initiation.
The first step in eukaryotic translation is the formation of the 43S PIC by combining the 40S ribosomal subunit, eIF2, eIF3, and eIF5. The PIC engages the eIF4F complex (eIF4G and eIF4E) which is bound to the capped and poly-adenylated mRNA. The resulting 48S complex would normally initiate start-codon scanning and eventually translate peptides. Almost all factors involved in translation initiation are targeted by viruses during infection. Some viral proteins affect the phosphorylation state of various proteins, other viral proteins directly compete with normal translation factor binding partners, and finally some viruses (retroviruses and picrornaviruses) express proteases that cleave translation machinery. Figure legend: $3C^{pro}$ (3C), $2A^{pro}$ (2A), Non-structural Protein 1 (Ns1), Non-structural Protein 3 (nsP3), Nonessential protein (NSs), Capsid protein (C), L4-100K Assembly Protein (100K), Poliovirus (PV), Coxsackievirus (CV), Human Rhinovirus (HRV), Foot-and-Mouth Disease Virus (FMDV), Bunyamwera orthobunyavirus (BUNV), Rubella Virus (RUBV), Hepatitis A Virus (HAV), Human Immunodeficiency Virus (HIV), Human T- cell leukemia virus type 1 (HTLV-1), Moloney Murine Leukemia Virus (MoMLV). Adapted from ViralZone at ExPASy.org.

Given the number of factors involved in translation initiation, it is unsurprising that many viruses target them during infection to subvert host protein synthesis (Fig. 1.2). For instance, adenoviruses inhibit phosphorylation and subsequent activation of eIF4E through its viral protein 100K. Similarly, influenza virus dephosphorylates eIF4E through an unknown mechanism. Rotaviruses express the NSP3 protein that evicts and re-localizes PABP by competitively binding eIF4G. Coronaviruses, such as SARS-CoV, express Nsp1, which binds to host 40S ribosomal subunits and prevents PIC assembly. Retroviruses like HIV-1 express a protease that cleaves eIF4G and PABP, shutting off translation. Finally, in a similar vein, picornaviral proteases 2A and 3C have been reported to cleave eIF4G, PABP, and numerous other translation factors, shutting off host translation. These examples of translation machinery subjugation by viruses are only a

sampling. Indeed, there are dozens of types of viruses that impair host translation by directly targeting translation factors, as well as upstream signaling pathways that activate the translation machinery[3].

1.4 IRES-driven viral translation and co-opting of host proteins

Despite the diversity of functions that viruses encode for their propagation, they remain dependent on the translational machinery of cells they infect and, therefore, have evolved elaborate mechanisms to ensure that cellular ribosomes are recruited to viral mRNAs. Furthermore, while traditional mRNA translation in eukaryotic cells depends on dozens of translation factors described in the previous section and Figure 1.2, viruses evolved different streamlined mechanisms to recruit ribosomes for viral mRNA translation. Internal ribosome entry sites (IRESes) are distinct regions normally present in the 5' UTR of viral mRNAs that recruit ribosomes for cap-independent translation initiation. IRESes were first discovered in poliovirus (PV) and encephalomyocarditis virus (EMCV) in 1988 and were eventually found in dozens of viral families, including lentiviruses (such as HIV-1) and picornaviruses[3]. IRESes fold into specific spatial structures to confer ribosome binding and translation initiation, incorporate host factors that promote IRES-driven translation efficiency, and are categorized accordingly into four different types (Fig. 1.3)[22].

Viral species employing different IRES types widely vary in their need for canonical initiation factors (Fig. 1.3). For example, picornaviruses such as PV and CVB3 utilize the Type I IRES, which uses eIF2, eIF3, eIF5, and the C-terminal fragment of eIF4G during translation initiation[22]. *Flaviviruses* such as EMCV and FMDV utilize the Type II IRES, which associates with the same factors as Type I IRESes but has a divergent sequence and structure. *Pestiviruses* (*Flavivirus* family) utilize a minimized Type III IRES that does not require eIF4G or eIF4A. Finally, the *Dicistroviridae* family (within the order Picornavirales) of insect-infecting viruses such as the cricket paralysis virus, evolved an absolutely minimal IRES (Type IV) that only requires the 40S ribosomal subunit for translation and no other initiation factors[23]. It is unclear how important every factor is for translation initiation, and if it is possible that the various types of IRESes merely operate at peak efficiency in the presence of each required factor, and at decreased efficiency when lacking some of the factors. For instance, previously published literature suggests that Type I IRES translation can be promoted during picornavirus-mediated cleavage of eIF4G[24]. Other work suggested a species-dependent translation activity, specifically with CVB3 activity promoting enterovirus IRES-driven translation, whereas PV showed no species depdendancy[25].

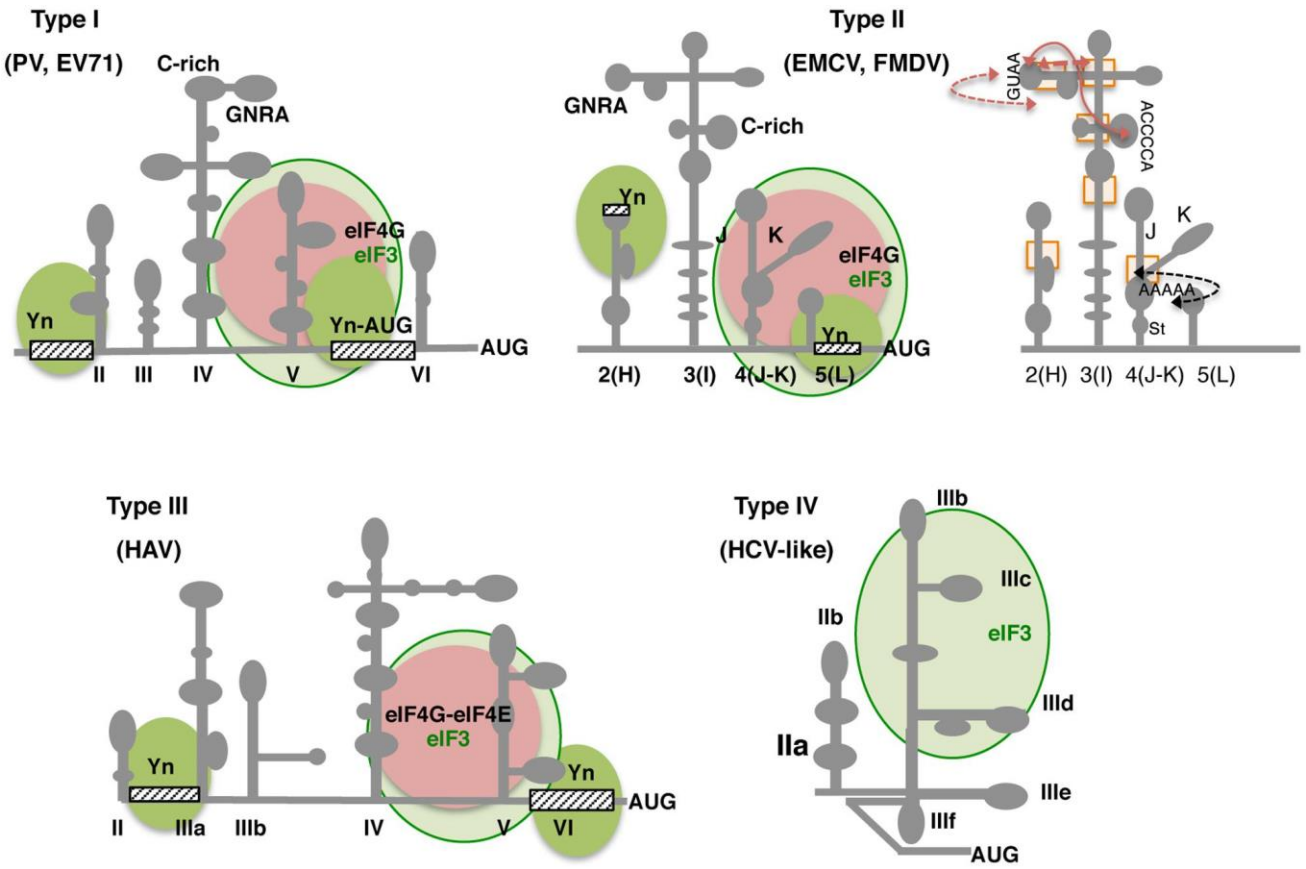

Figure 1.3. IRES types (I-IV), their secondary structures, and required components for function.

Gray lines depict IRES domains. Conserved motifs are indicated in dark green ovals (GNRA, C-rich, Yn, A-rich). Approximate binding sites of eIF3 in all IRES types are indicated by light green circles. eIF4G binding sites are indicated with pink ovals. Beyond secondary structure, the various types of IRESes require a variety of additional proteins for formation, some of which are indicated. Figure legend: Poliovirus (PV), Enterovirus 71 (EV71), Encephalomyocarditis Virus (EMCV), Foot-and-Mouth Disease virus (FMDV), Hepatitis A Virus (HAV), Hepatitis C Virus (HCV). Adapted from Martinez-Salas et al, 2018[22].

In addition to incorporating varying components of the host translation machinery, picornaviral IRESes promote translation efficiency by co-opting other proteins, termed IRES trans-acting factors (ITAFs), of which many are compartmentalized in the host nucleus or shuttle between it and the cytosol. During the course of picornaviral infection, nuclear localized ITAFs can often be found in increased concentrations in the cytosol, relative to a non-infected steady-state, suggesting that picornaviruses employ mechanisms to actively or passively drive mislocalization of these nuclear proteins. Most of these ITAFs have RNA-binding capabilities and control many features of RNA biology and gene expression, such as splicing, mRNA transport, and mRNA stability[26, 27]. Some notable examples include (i) Polypyrimidine Tract-Binding Protein 1 (PTBP1) that was found to be associated with Type I, II and III IRESes, in literature dating as far back as 1990[27], (ii) Lupus La protein has also been implicated in translation of Type I and II IRESes by binding the picornaviral mRNA[27], (iii) Serine/Arginine-Rich Splicing Factor 3 (SRSF3/SRp20) is a splicing factor with many functions related to mRNA processing and

promotes cap-independent translation of Type I IRESes[27-30]. SRSF3 co-localizes with PCBP2 during PV infection to promote IRES-mediated translation. Researchers found expressing a mutated SRSF3 that lacks its RNA recognition motif (RRM) decreased IRES translation by up 100-fold, reinforcing the paradigm of ITAFs being crucial in cap-independent viral translation[30]. A number of other proteins, their reported affected IRES types, and effects on translation can be found in Table 1.1. One especially challenging aspect of studying ITAFs and understanding their roles in IRES-driven translation is species variability. For instance, PTBP1 has been reported to promote Type I IRES translation in FMDV and TMEV but is unnecessary for translation of EMCV RNA[27].

Table 1.1. IRES types (I-IV) and their structures and required components for function.

Nuclear-resident protein	Picornavirus IRES type	Effect
Polypyrimidine tract-binding protein 1 (PTBP1)	I, II, III	Promotes translation through stabilization of IRES structure
Lupus La protein (La)	I, II, III	Stimulates translation from Type I and Type II IRESs; suppresses translation from Type III IRES structures
Poly(rC)-binding protein 2 (PCBP2)	I, III	Stimulates translation from Type I and Type III IRESs but does not bind Type III IRES element
Serine/arginine-rich splicing factor 3 (SRSF3/SRp20)	I	Acts synergistically with PCBP2 to increase efficiency of poliovirus translation
Proliferation-associated protein 2G4 (PA2G4/EBP1)	II	Necessary for FMDV translation but not required for TMEV or EMCV translation
Nucleolin	I	Stimulates translation
Heterogeneous nuclear ribonucleoprotein A1 (hnRNP A1)	I	Interacts with EV71 IRES, depletion results in reduced reporter gene translation
Far upstream element-binding protein 1 (FBP1)	I	Interacts with EV71 IRES
KH domain-containing, RNA-binding, signal transduction-associated protein 1 (Sam68)	II	Promotes FMDV translation
Double-stranded RNA binding protein 76 (DRBP76)	I	Heterodimerizes with nuclear factor of activated T-cells, 45 KDa (NF45) and inhibits HRV 2 translation
Far-upstream element-binding protein 2 (FBP2)	I	Inhibits EV71 IRES-driven translation
AU-rich binding factor 1 (AUF1/hnRNP D0)	I	Binds IRES element and inhibits translation
Gem-associated protein 5 (Gemin5)	II	Likely inhibits FMDV translation through competitive inhibition of PTBP1 binding

Picornaviruses have at least four different types of IRESes, each consisting of various proteins that facilitate IRES formation, and increase picornaviral translation. This table lists nuclear-localized proteins that promote IRES formation. These proteins are relocalized to the cytosol during picornaviral infection. Most are RNA binding proteins and components of mRNPs. Adapted from Flather et al, 2015[27].

1.5 The nuclear pore complex and mechanisms of nuclear-cytoplasmic trafficking

The nuclear pore complex (NPC) acts as a gateway regulating the flow of genetic information between the nucleus and cytosol of eukaryotic cells. Signaling cascades often begin in the cytosol in reaction to a variety of stimuli and continue in the nucleus, where transcription factors upregulate genetic responses. These factors promote transcription of mRNAs, which are shuttled back to the cytoplasm for translation of specific proteins in response to the original stimuli.

The entire gene expression paradigm is complex and is tightly regulated not only by myriad of signaling molecules and various macromolecules, such as transcription factors, chromatin associating factors, and ncRNAs, among others, but also by the NPC itself. Transport across the nuclear envelope is mediated by the NPC, usually with the assistance of karyopherins that shuttle proteins and nucleic acids through the NPC. In this section, I will discuss the structure and function of the NPC and disease implications resulting from alterations to NPC

1.5.1 Nuclear pore complex structure

The NPC is an approximately 50-100-megadalton protein complex (its size varies between organisms) consisting of multiple copies of approximately 30 different proteins called nucleoporins (Nups) (Fig. 1.4)[31-34]. The NPC's primary and critical role is to regulate the exchange of macromolecules like RNAs and proteins between the nucleus and the cytoplasm[35-39]. Each NPC is organized around a central channel, which is surrounded by eight symmetrical spokes joined together by rings. The Nups that form the various architectural features of the NPC are diverse in size and structure[40]. Nups contain a variety of secondary structure elements, recurrent motifs, and domains. Structural features include α-helices, β-propellers, Phe-Gly (FG) repeats, WD and transmembrane domains[41]. Nups rich in FG repeats are typically found along the central axis of the NPC, where they both set up the barrier to passive diffusion of macromolecules and mediate active trafficking. However, the disordered nature of the FG Nups makes it challenging to discern their mechanism of action[36, 39, 42, 43].

Peripheral filaments formed by Nups protrude from the core of the NPC into both the nucleoplasm and cytosol. Cytoplasmic filaments on the NPC are structurally disorganized. They mediate traffic through the NPC, couple mRNA export and translation, and connect the NPC to the cytoskeleton[33]. NPC nuclear filaments are more structured and form a basket-like assembly, which plays a role in regulation of mRNP assembly and export[34]. Furthermore, the nuclear basket connects RNA export and regulation of transcription[44], organizes RNP complexes in the vicinity of the NPC to control DNA damage repair[44], engages in chromatin silencing[45], and mediates transcriptional activation of genes[46].

The exact mechanics of how the NPC functions is being elucidated with 3-D structures from X-ray crystallography and cryogenic electron microscopy (Cryo-EM)[47]. Such integrated 3-D structures are reported for yeast NPCs, but still not available for entire human NPCs, which are twice as large. However, given the NPC is an evolutionarily conserved protein assembly, insights derived from the yeast structure can be adapted to its human counterpart. For example, the overall architecture in the yeast NPC suggests a framework of sturdy diagonal "columns" and "connector cables" that provide the NPC both strength and flexibility and associate the "core" of NPC with peripheral NPC elements, such as membrane-interacting regions, outer rings, and RNA-processing platforms[47]. FG Nups are evenly distributed across the length of the central transport channel and anchored inwards with FG regions thus forming a highly concentrated milieu within the NPC[47].

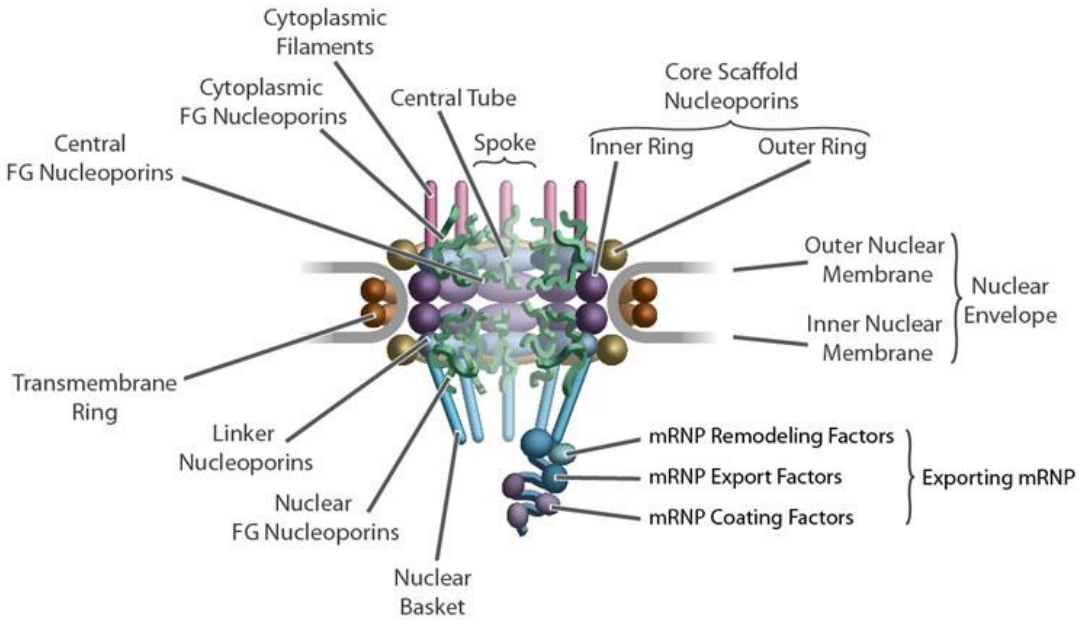

Figure 1.4. Structure of the NPC.
The NPC is made up of an 8-fold symmetrical framework which surrounds a central channel utilized for transport. Nucleoporins surround the central core, form rings at both sides of the nuclear envelope, and protrude filaments into both the cytosol and nucleus. The cytosolic filaments play a role in mediating traffic through the NPC and couple mRNA export and translation. The nuclear filaments form a basket which is involved in regulation of mRNP assembly, among other roles. Adapted from Simon, DN and Rout, MP 2014[48].

1.5.2 Nuclear-cytoplasmic trafficking of macromolecules

As previously mentioned, FG Nups line the central channel of the NPC and engage traffic through it. Most cargoes are carried by members of a large family of trafficking proteins known as Karyopherins (Kaps), which interact with these FG Nups to cross the NPC[39, 49-51]. Each Kap identifies its cognate cargoes by binding specific signals in the cargoes, termed Nuclear Localization Signals (NLSs) and Nuclear Export Signals (NESs), and utilizes a RanGTP gradient for the energy required during transport (Fig 1.5)[39]. An exception is the RNA exporter Mex67, which does not require GTP hydrolysis to power active transport, and instead terminates its export cycle through RNA remodeling by ATP-driven helicases on the cytoplasmic face of the NPC[52].

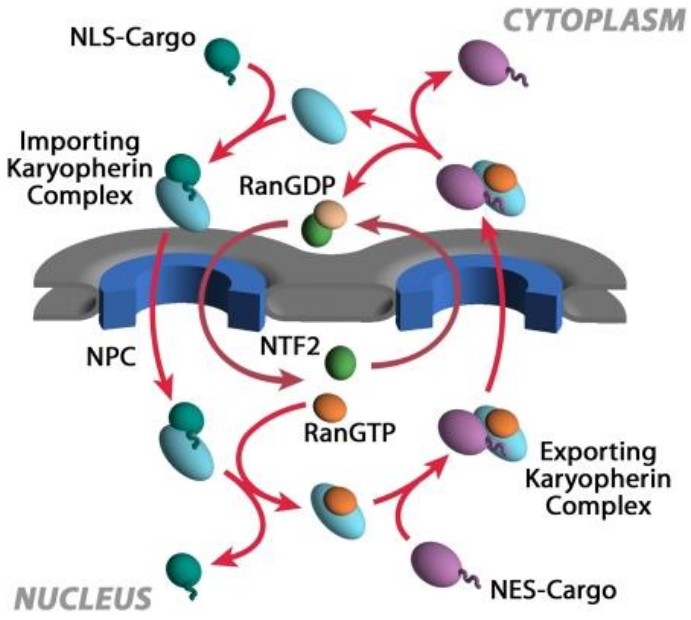

Figure 1.5. Karyopherin mediated transport across the NPC. Nuclear-cytoplasmic transport of proteins depends on Karyopherins that detect specific NLS and NES sequences on their cargo. Importins bind NLS-cargo and transport it to the nucleus, where RanGTP catalyzes the disassociation of the cargo by binding importin. The Importin-RanGTP complex returns to the cytoplasm where GTP is hydrolysed to GDP, and Ran dissociates from Importin. NTF2 recycles RanGDP back to the nucleus with GTP by RCC1, a guanine nucleotide exchange factor (RanGEF). Export pathways function in a reverse manner, whereby Exportin has to bind RanGTP prior to export of NES-cargo into the cytoplasm. Adapted from Aitchison et al[39].

There are at least 26 different Kaps in humans (19 Kap-βs and 7 Kap-αs), each interacting with a subset of proteins and RNA and mediating distinct nuclear import, export, or bi-directional transport pathways[53, 54] (Table 1.2). Similarly, various transport proteins recognize a variety of NLS and NES signals, including both human and viral sequences. Nup98 is a mobile FG Nup that interacts with import proteins such Importin-α1/β1, as well as export proteins such as Crm1 (Table 1.2). Many transport proteins that engage FG Nups also have promiscuous binding capacities, for example Importin-β1 can interact with FxFG domains of Nup62, Nup153, and Nup214[55, 56].

Table 1.2. Nuclear Transport Receptors.

Nuclear Import		**Nuclear Export**
KPNB1/Importin-β1/Kap-β1	*KPNA2/Importin-α1*	*XPO1/Exportin-1/Crm1*
TNPO1/Transportin-1/Kap-β2	KPNA4/Importin-α3	XPO2/Exportin-2/Cas
TNPO2/Importin-β2b	KPNA3/Importin-α4	XPO5/Exportin-5
IPO4/Importin-4	KPNA1/Importin-α5	XPO6/Exportin-6
IPO5/Transportin-5/Kap-β3	KPNA5/Importin-α6	XPO7/Exportin-7
IPO7/Importin-7	KPNA6/Importin-α7	XPOT/Exportin-tRNA
IPO8/Importin-8	KPNA7/Importin-α8	RanBP17
IPO9/Importin-9	**Bi-directional Transporters**	
IPO11/Importin-11	IPO13/Importin-13	
TNPO3/Transportin-3	XPO4/Exportin-4	

Transport proteins with their various gene and protein names are listed under three categories, Nuclear Import, Nuclear Export, and Bi-directional Transport proteins. Import and export proteins implicated with Nup98 interactions are italicized. Adapted from Beck et al[57] and Wu et al[58].

1.5.3 Nuclear pore complex implicated in diseases

Given its role in regulation of transport and gene expression, it is unsurprising that NPC alterations are implicated in a number of diseases, such as neurological syndromes (e.g. Alzheimer's Disease)[59], autoimmune disorders[60], and cardiological diseases (Fig. 1.6)[61]. For example, Nup98 has been shown to directly associate with Tau, which is a major constituent of neurofibrillary tangles in Alzheimer's disease also found affecting NPC structure and function[59]. Furthermore, Nup98 can accumulate in cell bodies of neurons and promote cellular aggregation of Tau[59]. Relatively rare Nup62 and Nup210 autoantibodies serve as biomarkers for an autoimmune disease primary biliary cholangitis (PBC) and associate with more severe symptoms and prognosis[60]. Homozygous genetic mutations in Nup155 were linked to inherited cardiac disease and sudden childhood death[61]. Nups37, 43, and 188 were also suspected to be involved in cardiovascular disease. Interestingly, these Nups and Nup155 are scaffolding proteins, suggesting a shared function for Nups that are associated with cardiovascular diseases[61].

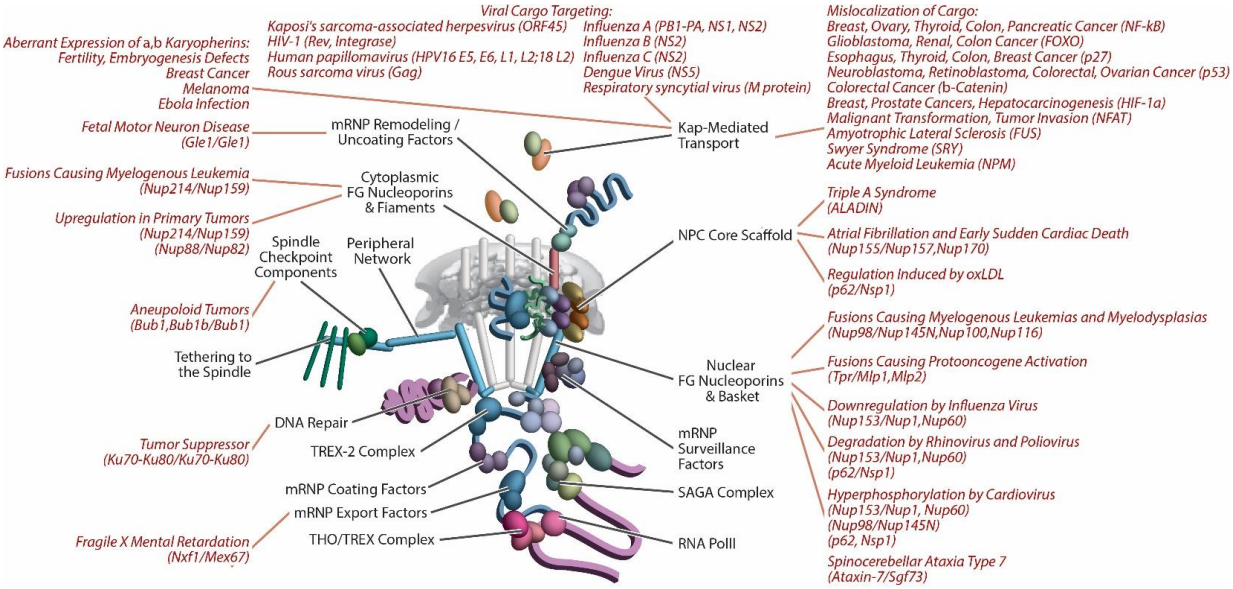

Figure 1.6. Diseases implicated in the NPC.
Major scaffolds of the NPC and engaged platforms are linked to the associated disease states (in red), with specific Nups and transport proteins identified. Every component of the NPC is implicated in a disease state, ranging from neurodegenerative syndromes and cardiovascular diseases to cancers and viral infections. Adapted from Simon, DN and Rout, MP 2014[48].

More frequently, however, various Nups have been linked to different cancers and infections caused by pathogens, such as viruses and parasites[48]. In cancers, Nup alterations do not appear to be 'driver' mutations that are critical for transformation of a cell to a tumorigenic state, but are believed to be complimentary mutations that occur after transformation to promote oncogenesis. Most examples of oncogenic Nups are associated with aberrant chromosomal translocations that result in fusion proteins with novel characteristics. For instance, the coiled-coil region of Tpr, which dimerizes the protein, has been found fused to kinase domains of HGFR, FGFR, and NTrk1, thereby creating constitutively active upregulators of Ras/MAPK, PI3K, FRS,

FGFR, and many others signaling pathways and stimulating unlimited cell division and other pro-tumor phenotypes[48, 62]. Similar paradigms of fusion events also occur with Nup98, 214, and 358. However, some Nups, such as Nups62 and 88, are not components of fusions but are rather found overexpressed in tumors. For instance, Nup88 is overexpressed in ~75% of ovarian cancers[63].

1.6 Viral subversion of protein and nucleic acid trafficking

There is a striking overlap between Nups implicated in cancers and those targeted during pathogenic infection, specifically among the transport factor that docks Nups 62, 88, 98, 153, 214, 358 and Tpr (Fig. 1.6)[48]. For instance, a parasitic trypanosome *Leishmania* produces a virulence factor, GP63, which cleaves Nups62, 98, and 358[64]. Most common, however, are viruses that cleave Nups or manipulate transport of proteins and nucleic acids across the NPC through other means.

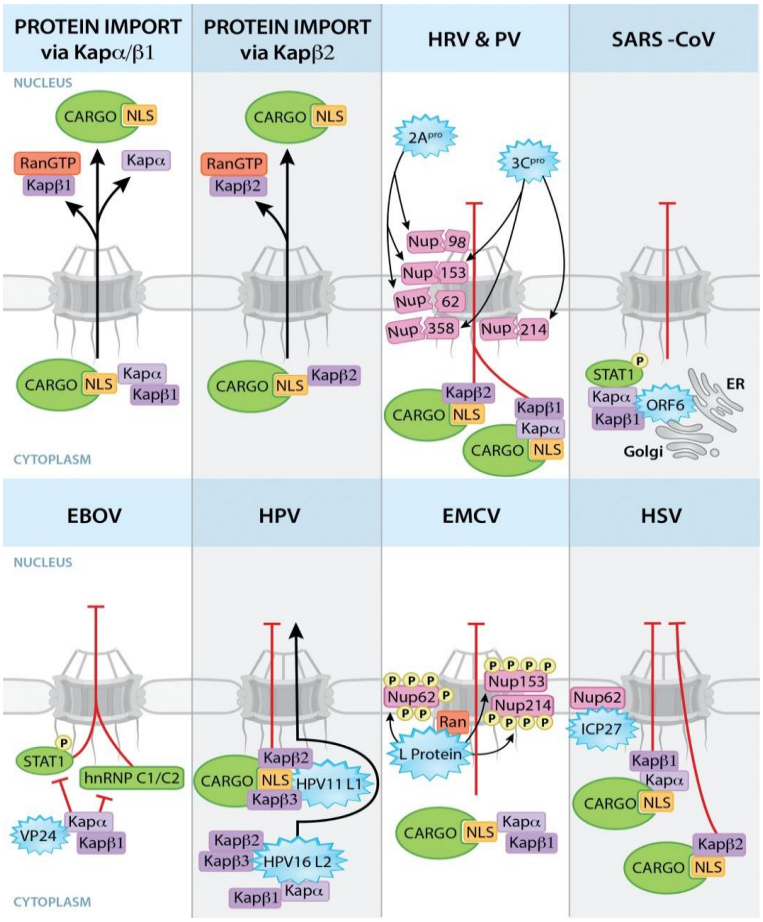

Figure 1.7. Viral subversion of nuclear protein trafficking.
Viral proteins (blue) disrupt trafficking of proteins across the NPC. Picornavirus $2A^{pro}$ and $3C^{pro}$ cleave Nups to block nuclear import of proteins via Kap-α/β1 and Kap-β2 pathways. SARS-CoV ORF6 blocks nuclear import of phosphorylated STAT1 by tethering STAT1 bound by Kap-α/Kap-β to cellular organelles. Ebola virus (EBOV) VP24 binds Kap-α and stops it from transporting STAT1 and hnRNP C1/C2, resulting in their cytoplasmic accumulation. HPV protein L1 binds Kap-β2/β3 and disrupts cargo import. EMCV L protein hyperphosphorylates Nups, causing them to bind Ran and create an import blockade. ICP27 protein of HSV binds Nup62 and blocks import of proteins. Figure adapted from Yarbrough et al[4].

Such capabilities are shared by a number of viral families, including Hepatitis C virus (HCV), Picornaviridae family viruses, coronaviruses, human papillomavirus (HPV), herpes simplex virus (HSV), Vesiculoviruses like vesicular stomatitis virus (VSV), influenza viruses, HIV, and adenoviruses[4]. For instance, HCV expresses the Core protein, which hijacks host Nup98 for use in viral replication[65]. VSV expresses the M protein, which binds at nucleic acid interacting sites of the Nup98-Rae1 export complex[66] (Fig. 1.7). Picornaviruses, specifically proteases 2A and 3C, have been reported to cleave the FG-repeat containing Nups62 and Nup98 during infection and inhibit proper protein and RNA trafficking between the nucleus and cytoplasm (Figs. 1.7 and 1.8)[4]. Similarly, SARS-CoV ORF6 protein binds Nup98-Rae1 and impedes protein import, especially of STAT1.

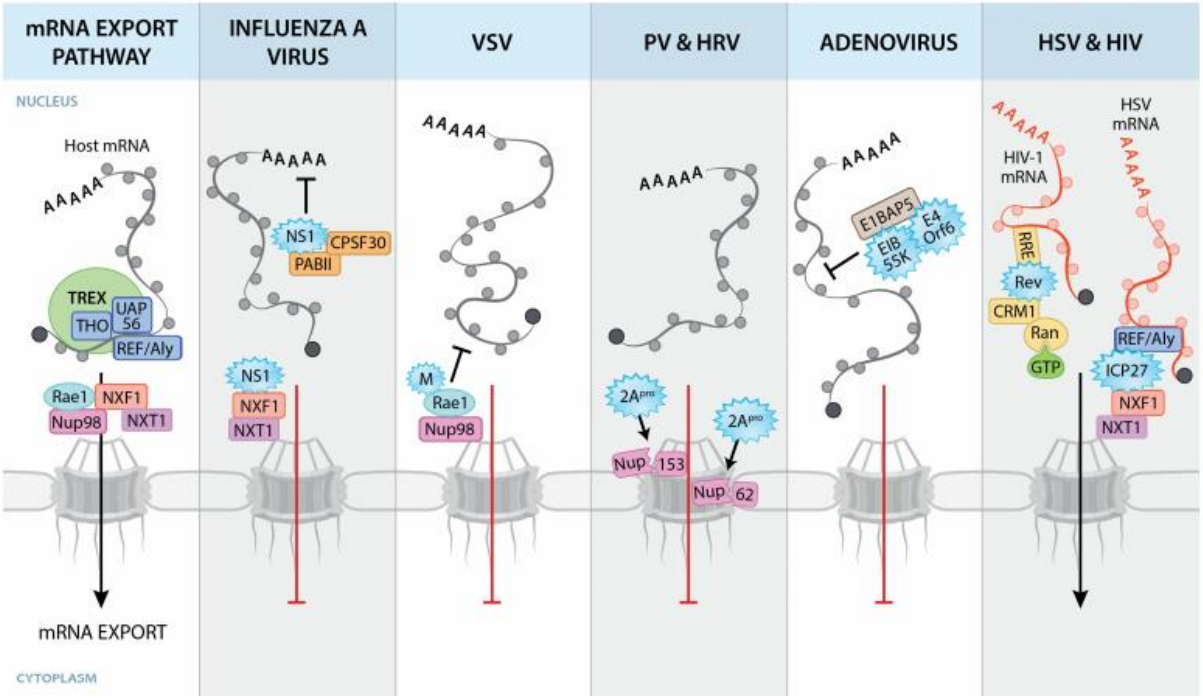

Figure 1.8. Viral disruption and manipulation of host mRNA nuclear export pathways[4]. Viral proteins (blue) disrupt mRNA export from the nucleus by interacting with various host factors. Circles surrounding mRNAs depict RNA-binding proteins. Influenza A (IAV) NS1 protein binds and abrogates factors involved in mRNA processing and export. VSV M protein binds Rae1-Nup98, resulting in mRNA nuclear export block. Picornavirus $2A^{pro}$ cleaves Nups, including Nup98, involved in mRNA export. Adenovirus (AdV) E1B protein binds E1BAP5, disrupting NXF1-mediated mRNA export. Conversely, HSV and HIV hijack host transport pathways to promote viral mRNA export. HSV ICP27 protein enriches viral mRNA export by binding REF/Aly and NXF1. The HIV-1 Rev protein facilitates nuclear export viral mRNAs by directly binding the RNA motif Rev-responsive element (RRE), which triggers export of RNA through CRM1. Figure adapted from Yarbrough et al[4].

1.7 Picornaviral proteases and catalytic activity

As previously mentioned, in addition to their roles during viral replication, picornaviral proteases have many other targets within their host cells. $2A^{pro}$ cleaves eIF4G, an important translation initiation factor, thus inhibiting host translation[67]. $3C^{pro}$ cleaves IRF-7 and -9, both key

transcription factors that regulate the expression of interferons[68]. Both proteases have also been implicated in the cleavage of Nups involved in transport (specifically, Nups62, 98, 153, 214, and 358); the targeted cleavage of these Nups significantly reduces nuclear import and leads to accumulation of nuclear proteins in the cytoplasm[48]. As previously mentioned, it is hypothesized that picornaviruses disrupt nucleocytoplasmic trafficking not only as a method of host gene expression control, but to also relocalize proteins, especially RNA binding proteins, necessary for viral replication[4]. An example is SRp20, a splicing factor that is predominantly found in the nucleus of uninfected cells, but is overwhelmingly localized to the cytoplasm during infection, where it facilitates recruitment of host ribosomes to viral RNA[28-30]. Despite evolutionary conservation of protease sequences, both proteases were reported to have functional differences between viral species[69], and even among strains of the same virus attacking different species[70]. These differences likely account for species-related viral phenotypes and resulting distinct patterns during patient infections. Given that these two proteases play critical roles in picornaviral replication, they were intensively studied by virologists, with hundreds of articles dedicated to understanding their diverse functions and properties, including cleavage mechanisms, cleavage targets, and species-related differences.

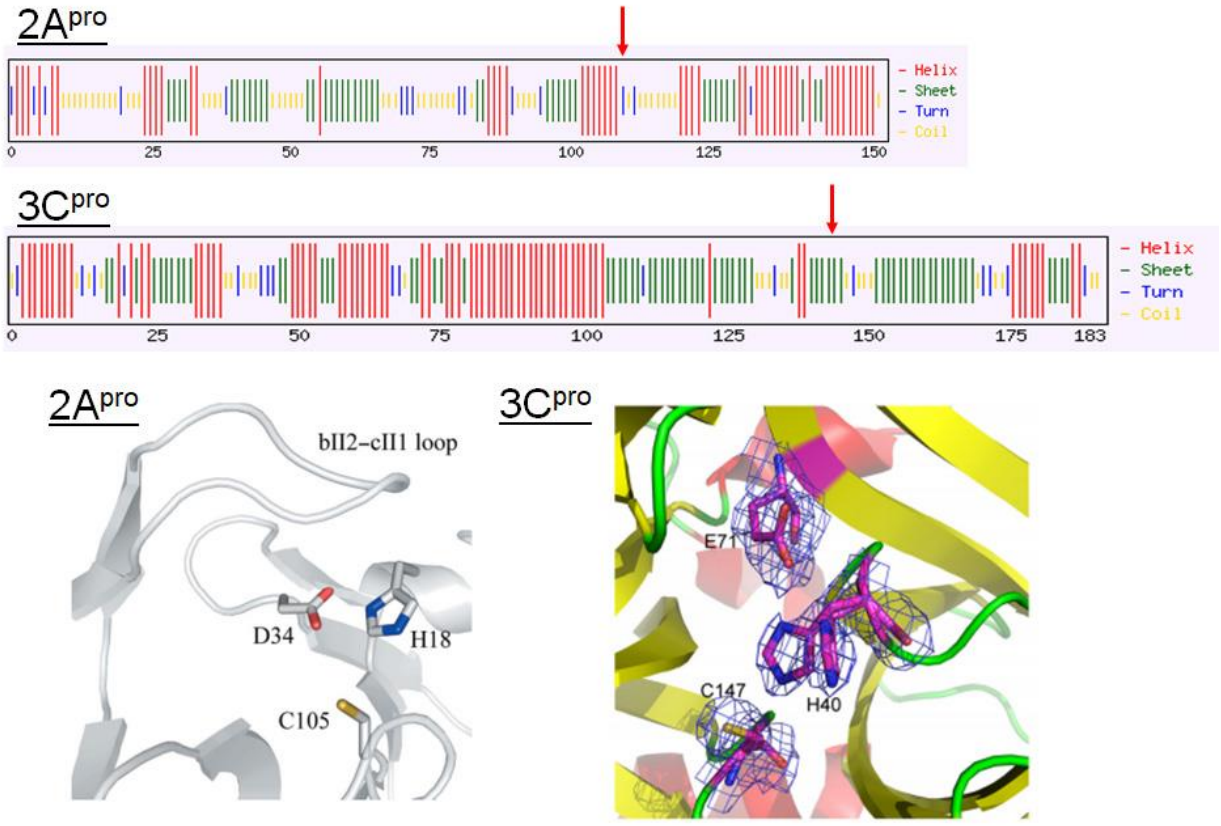

Figure 1.9. Secondary structures of Coxsackie Virus B3 proteases and their proteolytic active sites.

Secondary and 3-D structures of $2A^{pro}$ and $3C^{pro}$. Active site structures for $2A^{pro}$ and $3C^{pro}$ showcase the proteases' catalytic triads of Asp/Glu-His-Cys. Active site Cysteines can be mutated to Alanines to design proteolytically inactive mutants. Adapted from Ling et al[71] and Tan et al[72].

$2A^{pro}$ is approximately 150 amino acids long with a molecular weight of ~16 kDa, while $3C^{pro}$ is approximately 180 amino acids in length, with a larger ~27 kDa mass (Fig. 1.9). The 3-D crystal and solution NMR structures of both proteases have been determined from a number of picornaviruses, and their respective active site and proteolytic mechanisms have been extensively characterized (Fig. 1.9)[71, 73-75]. $2A^{pro}$ is chymotrypsin-like protease, with its active site forming a canonical catalytic triad of Cysteine-Histidine-Aspartate. $3C^{pro}$'s active site adopts a trypsin-like fold, with a catalytic triad of Cysteine-Histidine-Aspartate/Glutamine. Studies on viral proteases have enabled researchers to design catalytically inactive mutants to specifically characterize protease functions directly related to catalytic activity (Fig. 9). This progress is especially important given that genetic manipulation of the picornaviral genome is difficult, and as such, most research is done by validating hypothesized effects of proteases with ectopic protein expression systems.

1.8 Reported picornaviral protease cleavage targets

Picornavirus proteases play an integral role in their replication, not only through polyprotein processing but through cleavage of specific host proteins to further promote viral replication and downregulate the host response. When analyzing the scope of literature specifically related to understanding cleavage targets of $2A^{pro}$ and $3C^{pro}$, researchers investigated both proteases relatively evenly, with 55% of the focus on $3C^{pro}$ and 45% on $2A^{pro}$ (Fig. 1.11). Most studies on picornaviral proteases involved the use of ectopic protease expression systems to validate findings from picornavirus infections (Fig. 1.12). Over 50% of researchers cloned picornaviral proteases into vectors for protein expression in mammalian cell lines and compared effects between wild type and catalytically inactive proteases (Fig. 1.12a). Another avenue for characterizing protease function is to prepare cell extracts and combine them with purified proteases (Fig. 1.12a), with more than half of published literature featuring experiments of this nature. A less common experimental method (~20% of published research) involved direct cleavage assays with purified proteases and their potential cleavage partner (Fig. 1.12a).

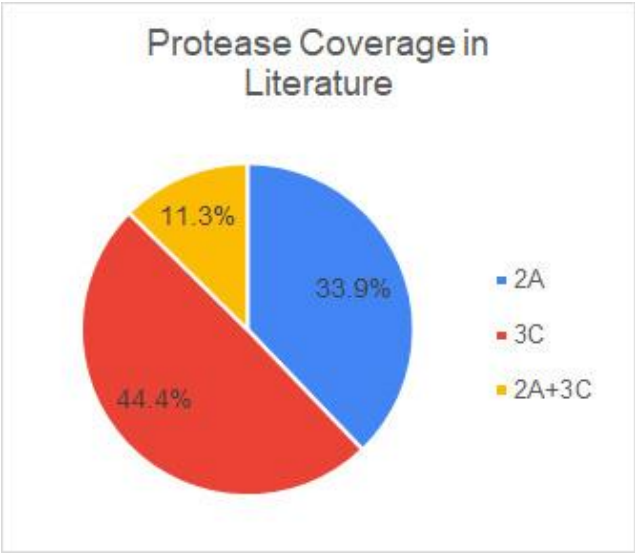

Figure 1.11. Approximate coverage of proteases in published literature. The focus of researchers characterizing picornaviral proteases was relatively even, with 55% of published work focusing on $3C^{pro}$ and 45% on $2A^{pro}$. This includes all methodology for characterizing the proteases.

Over a dozen picornavirus species were studied by scientists according to published literature, with the major focus on the most clinically relevant species, such as Poliovirus, Coxsackie Virus B3, Rhinovirus, and Enterovirus 71 (Fig. 1.12b). Given high clinical relevancy

in the 90s and 2000s, poliovirus was a frequent model system to characterize proteases from, with ~30% of published studies on PV-related proteins. CVB3 has a similar publication rate (~32%), with species such as HRV, EV71, and EMCV making up the rest of the majorly studied picornaviruses (Fig. 1.12b).

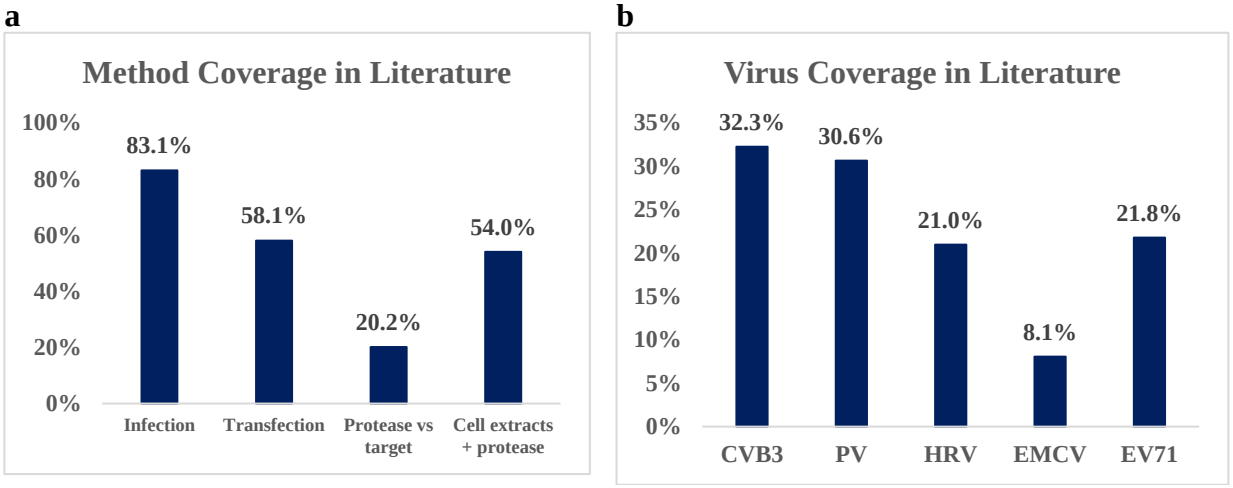

Figure 1.12. Coverage of methods employed by researchers to characterize different picornaviral proteases.
a, analysis of method types in picornavirus protease research efforts. Infection – mammalian cell lines infected with live virus and assayed for cleavage of specific target proteins. Transfection – cell lines transiently or stably transfected to ectopically express proteases of interest. Protease versus target – biochemically purified proteases are incubated with their predicted targets and assayed for target protein degradation. Cell extracts and protease – Mammalian cells are lysed in buffer conditions and clarified, often with a high speed centrifugation step, to leave a cellular extract with soluble proteins and potential cleavage targets that are assayed for degradation by addition of biochemically purified proteases. **b**, most commonly researched picornaviral species. While literature published in ~20 years covers over a dozen various picornaviruses, the majority of scientific research focused on five specific picornaviruses. Published work often included research on multiple picornaviruses.

CVB3 is one of the most well studied Enteroviruses (Fig. 1.12b), with a well characterized life-cycle[76] and many reported cleavage targets for CVB3 $2A^{pro}$. Clinically, CVB3 is one of the most common causes of viral myocarditis, a condition that can end in acute heart failure[76]. This virus also causes hand, foot and mouth disease (HFMD) among children[77]. CVB3 is especially common serotype responsible for epidemics in infants in countries like China[77], as well as the 5th most common Enterovirus in the USA, causing ~40,000 annual infections[78, 79]. Because of the combination of clinical relevance and necessity to improve our understanding of this virus, as well as extensive published research, CVB3 presents a perfect model system for our studies focused on picornaviral proteases and their use as molecular tools. To this end, we prepared a list of CVB3 proteins identified as cleavage targets in published literature. These protease targets were identified by various methodologies (Fig. 1.12a) and were curated into three types either specifically targeted by $2A^{pro}$, $3C^{pro}$, or both proteases (Table 1.3). We anticipated that collection of published cleavage targets would be invaluable during our studies of CVB3 $2A^{pro}$.

Table 1.3. Published cleavage targets of Coxsackie Virus B3.

CVB3 2A targets	CVB3 3C targets	CVB3 2A+3C targets
eIF4G[29, 80-85]	G3BP1[81, 85, 86]	GSDMD
GAB1[87, 88]	RIG-I[89]	MDA5[89]
GAB2[88]	AUF1[90-92]	MAVS[89, 93]
Thrombin[83]	PABP[85, 86, 91, 94, 95]	NFAT5[96]
DAP5[97]	Unc93b[98]	PARP[98]
IPS-1[81]	TDP-43[99]	TRIF[81, 93]
Dystrophin[80, 100]	PCBP2[86, 101]	
SQSTM1[102]	hnRNP[86]	
SRF[103]	eIF5B[104]	
Nup62[29]	IκBα[105]	
Nup98[29, 106]	SNAP29[107]	
Nup153[29]	PLEKHM1[107]	
	PTB[101]	

Cleavage targets for CVB3 are separated into three categories, proteins targeted by $2A^{pro}$, $3C^{pro}$, and both proteases. Each individual protease target has references cited.

1.9 Investigative aims and research hypothesis

Despite our knowledge of multiple potential cleavage targets and mechanisms of host subversion, many properties of picornaviral proteases remain unclear. Therefore, we decided to focus our research efforts on elucidating the exact function and specificity of CVB3 $2A^{pro}$.

Our project goals were to characterize interacting partners, cleavage targets, and $2A^{pro}$ protease specificity by biochemical and proteomics approaches. We were keen on understanding whether $2A^{pro}$ cleaves many targets promiscuously and simultaneously, as suggested by a vast array of putative cleavage targets (Table 1.3), or whether it displays more precise affinity and temporal targeting. We expected these studies to shed light on the target selection mechanisms by $2A^{pro}$ and further our understanding of how host cells are hijacked during picornaviral infection. We were subsequently keen on converting $2A^{pro}$ to a molecular tool for studying biological questions about the function and structure of the NPC as well as characterizing protein and nucleic acid transport across the nuclear envelope. During the course of our study, we established a unified hypothesis of the function of $2A^{pro}$ in mammalian cells, which combines both previously published results and our own data.

Hypothesis: In the earliest stages of infection, the 2A protease performs surgical strikes on a small number of specific host targets, and over the course of infection eventually broadens its target list as more viral protease accumulates through continuous polyprotein translation.

Investigative aims:

Aim 1: Characterize the interacting partners of $2A^{pro}$ to determine targeting mechanisms and novel characteristics

1a. Develop a stable and tunable picornavirus protease expression system in mammalian cell lines.

1b. Characterize the interacting partners, specifically NPC components, of catalytically inactive viral proteases to elucidate novel functional characteristics.

Aim 2: Analyze the effects of viral proteases on the mammalian NPC function

2a. Develop pipeline to investigate effects of picornaviral proteases on mammalian NPC composition and stoichiometry.
2b. Characterize the mechanisms by which picornavirus proteases create an import blockade and otherwise affect nucleocytoplasmic trafficking.

CHAPTER 2. Results

Methodological rationale: Given the clinical relevance of CVB3 across the world[77-79], how extensively CVB3 was utilized as a model system for research[108], and how well its cleavage targets were characterized (Table 1.3), we chose to focus our research efforts on CVB3 $2A^{pro}$. Dr. Mohsan Saeed, our collaborator from the Rice laboratory (The Rockefeller University, currently in Boston University) generously provided us plasmid vectors for exogenous expression of GFP-tagged CVB3 $2A^{pro}$, as well as the catalytically inactive mutant variant, 2AC110A[108]. Mutation of Cys110 to alanine removes a critical component of the $2A^{pro}$ catalytic triad (Fig. 1.9), rendering the protease catalytically inactive[71, 73, 109]. This mutant is especially useful for our proteomics approach focused on identifying interacting partners for $2A^{pro}$. The lack of catalytic activity may permit the protease to bind the would-be cleavage targets, and remain bound throughout affinity capture experiments. The GFP tag on the N-terminus of the protease serves to facilitate detection of the protease in cells with fluorescent microscopy as well as in cell lysates through immunoblotting with GFP-specific antibodies. The GFP tag can also serve as the handle during immunoprecipitation experiments. Expression and affinity capture of GFP-tagged $2A^{pro}$ and 2AC110A would lay the foundation for our efforts on identifying the interacting partners of $2A^{pro}$ and understanding whether and how these partners affect the function of the protease. The expression platforms we establish in the course of our study could subsequently serve as the basis for developing $2A^{pro}$ as a molecular tool to characterize the NPC and nucleocytoplasmic trafficking of RNA and proteins.

2.1 Establishing picornaviral protease expression platforms

It is well established that the $2A^{pro}$ shuts down host translation through eIF4G cleavage during picornaviral infections[24, 84, 110]. This serves to not only reduce the use of host energy and available resources towards housekeeping functions, but to diminish any cellular response to infection[111]. Similarly, any ectopic expression of this protease quickly depletes cellular eIF4G levels and stops host translation[112, 113]. In an *in vitro* setting, this translational arrest creates an unfortunate situation where expression of the wild type $2A^{pro}$ prevents and limits its own detectable accumulation by immunoassays (Fig. 2.1). As such, it became imperative to develop an alternative detection method for the protease.

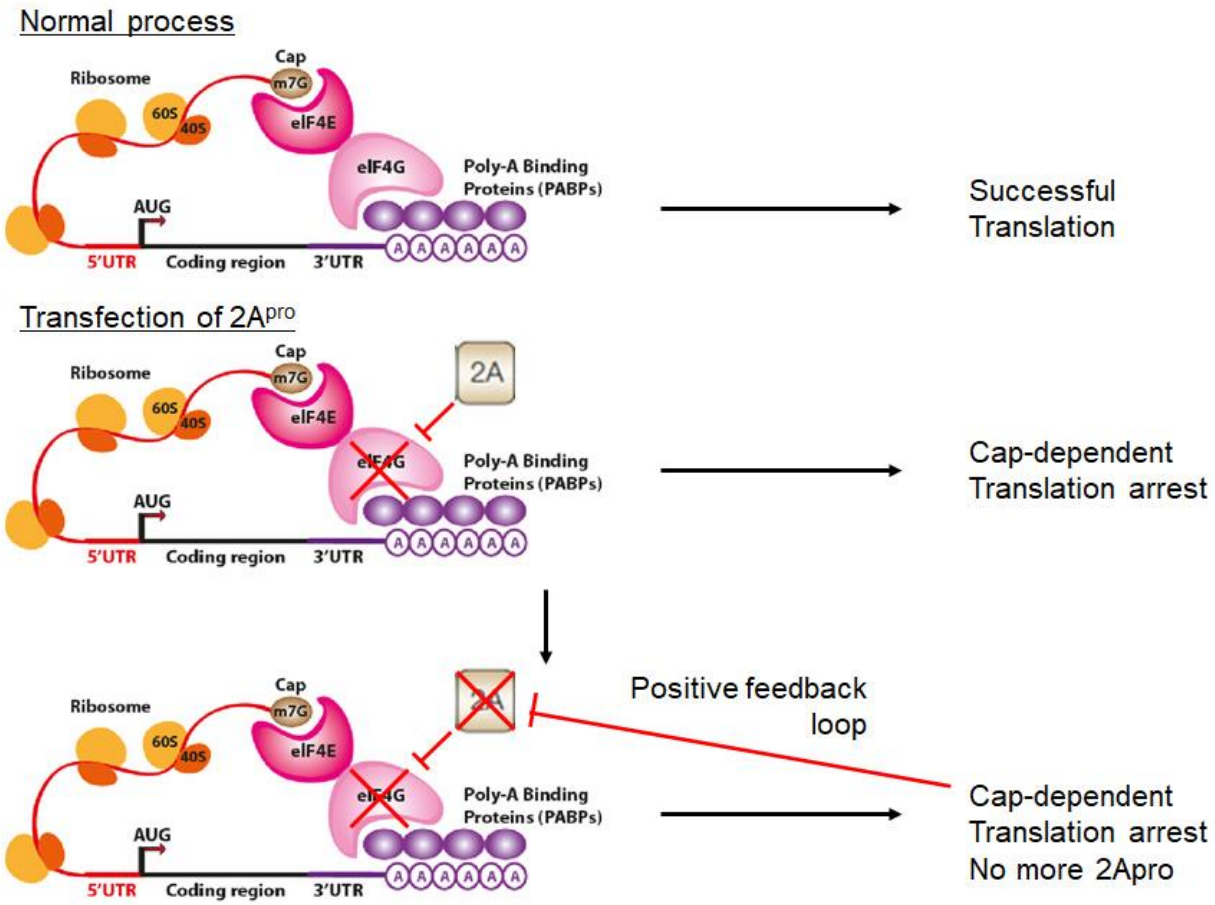

Figure 2.1. Expression of 2A^{pro} shuts down host translation, creating a protein expression-detection conundrum.
During normal cellular translation, eIF4G facilitates initiation by binding PABP and serving as a scaffold for other initiation factors. During expression of picornaviral 2A^{pro}, minute quantities of the translated protease rapidly degrade eIF4G, arresting cap-dependent translation. This blockage creates a feedback loop that prevents any additional translation of 2A^{pro}, limiting accumulation 2A^{pro} to undetectable levels. Adapted from Da Sacco et al, 2012[114].

2.1.1 Establishing cleavage assay as proxy for 2A^{pro} expression.

To confirm expression of wild type 2A^{pro}, we decided to use known cleavage targets of 2A^{pro} proteins as proxies. Nup98 and eIF4G are known 2A^{pro} degradation targets and are readily depleted within hours of protein expression[108]. Nup98 is cleaved almost entirely within 6 hours, while eIF4G cleavage can be detected by 6 hours, but is not complete until at least 12 hours (Fig. 2.2). It is important to note that this assay merely confirms expression of 2A^{pro}, but does not quantify degree of expression. 2A^{pro} is an extremely processive enzyme that readily cleaves all eIF4G and Nup98 prior to any detection of other virus components during infection[108]. As such, it is not surprising that even nominal amounts of produced protease are sufficient to cleave almost the entire cell's Nup98 and eIF4G within hours of initiating expression.

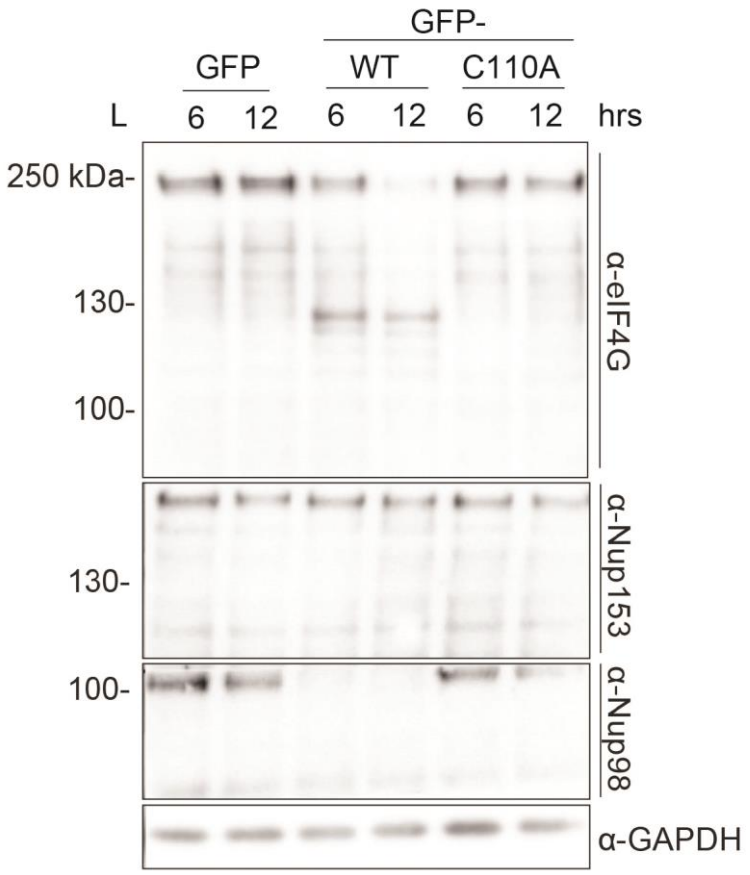

Figure 2.2. 2A^{pro} expression leads to rapid cleavage of known targets such as eIF4G and Nup98.

Tracking degradation of known cleavage targets like eIF4G and Nup98 serves to confirm successful protease expression. Inaccessible Nups such as Nup153, which is localized on the nuclear side of the NPC, are not cleaved. With larger cleavage targets and with relatively early time points, cleavage products can also be captured by immunoassays. eIF4G has a well characterized cleavage site[115], producing a cleavage product migrating at approximately 130 kDa. Similarly, Nup98 cleavage products can also be detected (data not shown)[109].

2.1.2 Defining transient transfection parameters

Much of our preliminary work, such as developing cleavage assays, establishing immunoblot conditions, lysis conditions, and initial immunoprecipitation conditions was performed using transient transfection and expression of proteases. Subsequent experiments to validate 2A^{pro} effects on nuclear transport were also facilitated with this established transfection protocol. Specifically, during transient transfection, plasmids with compatible promoters for eukaryotic protein expression were combined with specific kit reagents, often lipid-based micelle forming mixtures, to directly transport genes of interest into mammalian cells (Fig. 2.3)[116]. The plasmid DNA was transcribed by cellular machinery within the nucleus, and the resulting mRNA is translated into proteins of interest, such as 2AC110A[116].

We assayed several tissue culture transfection kits (Helafect, Lipofectamine, jetPRIME), before deciding to use jetPRIME transfection reagent kits (Polyplus Transfection) for our experiments. We assessed the kits on transfection efficacy, cellular toxicity, and ease of use (data

not shown). Helafect was relatively poor compared to jetPRIME for protein expression, whereas Lipofectamine and jetPRIME produced similar expression levels. However, Lipofectamine reagents were more toxic and required an additional time point post-transfection to refresh media for cells, whereas jetPRIME did not. Given similar results and improved ease of use, jetPRIME was a more favorable transfection reagent kit for our experiments.

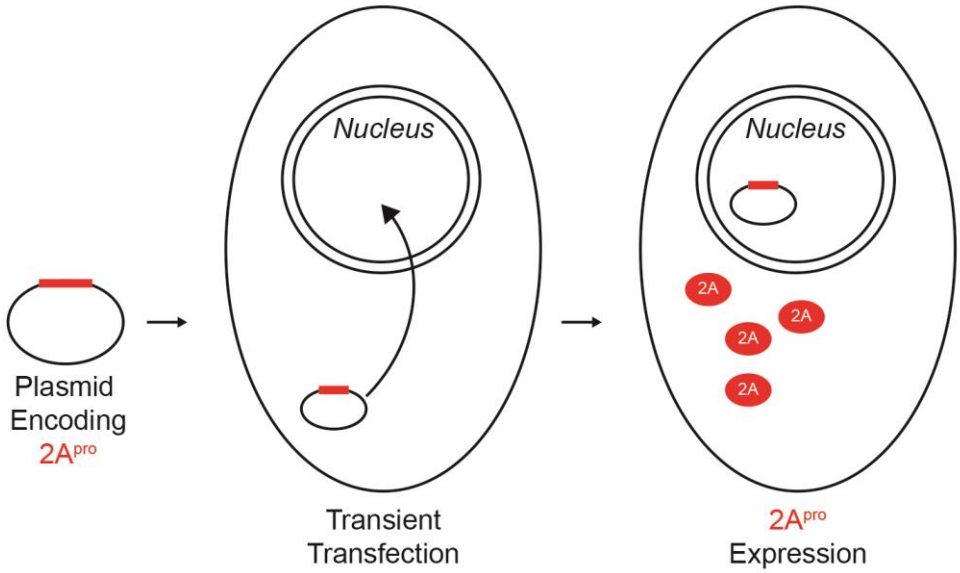

Figure 2.3. Schematic of transient transfection and protein expression in mammalian cell lines.
Plasmids containing genes of interest under the CMV promoter were transiently transfected into tissue culture cells following manufacturer protocols. Genes of interest, for example, encoding $2A^{pro}$, were subsequently transcribed and translated by cellular machinery.

2.1.3 Establishing stable cell lines with inducible protein expression

Once initial experimental conditions were established, we initiated preparation of stable cell lines with Doxycycline (Dox)-inducible protein expression of genes of interest[117]. There were a number of advantages stable cell lines offered over transient transfection: (1) No more need for preparative quantities of plasmid DNA or transfection reagents (which are relatively expensive compared to Dox), (2) antibiotic selection promoted more homogeneous protein expression by ensuring surviving cells at least retained the gene of interest, (3) cell growth can be easily scaled up for protein production (Fig. 2.4). Our collaborators from the Rice laboratory generously provided us genes of interest cloned in PiggyBac transposon vectors, which were suitable for stable cell line generation. The PiggyBac Transposon system utilizes inverted terminal repeats (ITRs) that flank a gene of interest under a Tet-off promoter and an antibiotic resistance gene for applying selective pressure after DNA integration[118]. The Super PiggyBac Transposase recognizes ITRs in transfected vectors and preferentially recombines the cassette into cell genomes at TTAA sites[119-121].

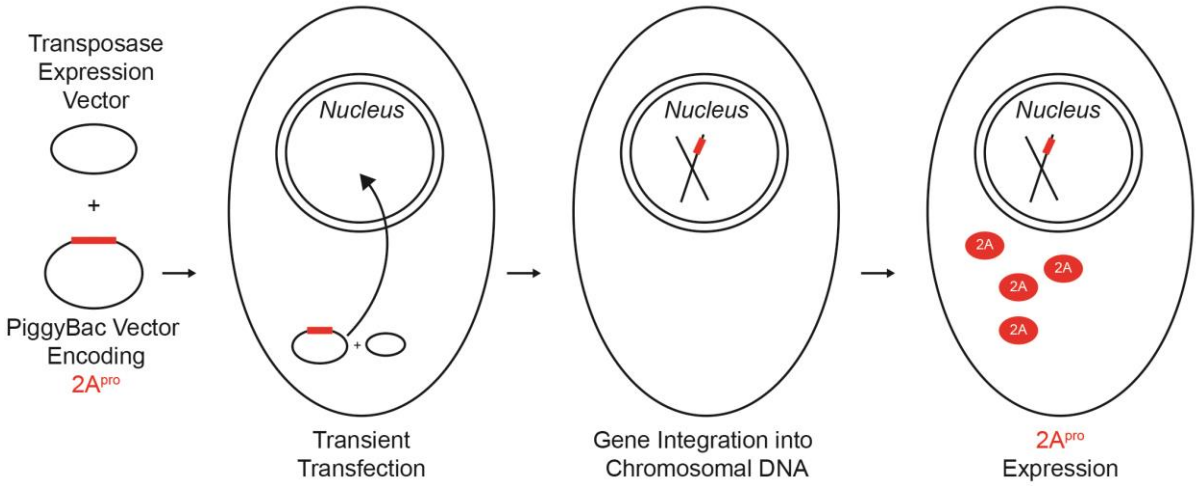

Figure 2.4. Schematic of stable cell line inducible protein expression in mammalian cell lines.
Stable cell lines provide a reliable and tunable inducible protein expression platform with several advantages over transient transfection protocols. Target cells are transfected with PiggyBac vectors containing a gene of interest and a Transposase expression vector. The genes of interest integrate into chromosomal DNA along with an antibiotic resistance gene, which makes large scale cellular expansion easier and cell populations more homogeneous. Genes of interest are placed under the expression control of an inducible promoter (Tet-off). Addition of Dox triggers protein production.

We transfected PiggyBac vectors carrying GFP, 2A^{pro}, and 2AC110A, into HEK293T and HeLa cell lines with the jetPRIME reagent kit, followed manufacturer guidelines for cell maintenance and antibiotic selection (Puromycin at 1 µg/mL), and obtained stable integrated cell lines with our genes of interest. Both cell lines expressing our genes of interest, with the exception of HEK293T cells expressing 2A^{pro}, survived antibiotic selection during culture maintenance and passaging (Fig. 2.5). Given it is not uncommon for inducible protein expression platforms to leak proteins[122], we suspected the HEK293T leaked 2A^{pro}, and triggered apoptosis in cells that had undergone successful genetic integration[123].

Cell line	GFP	GFP-2A	GFP-2AC110A
HEK293T	Alive	Dead	Alive
HeLa	Alive	Alive	Alive

Figure 2.5. Cell line integration of genes of interest and survival of antibiotic selection.
HEK293T and HeLa cells were transfected with PiggyBac vectors for expression of either GFP, GFP-2A, or GFP-2AC110A. Cells were maintained and underwent selective antibiotic pressure as per manufacturer protocol. All cell lines, other than HEK293T transfected with 2A^{pro}, survived selective pressure and were successfully passaged.

After passaging cell lines with integrated genes of interest, we assayed cells for protease expression levels with and without Dox. We wanted to establish the degree, if any, of proteins leakage during maintenance and growth of cells, and to determine protein production levels during Dox induction. We assayed a range of Dox concentrations (1-100 ng/mL) for inducing protein expression. With the help of the Rice laboratory, we established 100 ng/mL as a viable Dox concentration for induction of protease gene expression. Protein production can be tuned with lower Dox concentrations (data not shown), however, for our experimental applications, higher expression levels were beneficial to mimic the degree of uncontrolled protease biosynthesis during picornaviral infections.

GFP-, -2A, and -2AC110A protein synthesis in HEK293T and HeLa cells was assayed by immunoblot. Cells were grown in regular media or with growth media and 100 ng/mL Doxycycline for induction of protease production. GFP and GFP-tagged proteases were detected by anti-GFP antibody and by immunoblotting for Nup98 and eIF4G, as per established cleavage assay (Fig. 2.6). Nominal GFP and GFP-2AC110A protein expression was detected in 0 ng/mL Dox samples, confirming our initial suspicions of mild protein leakage under maintenance conditions. Dox induction resulted in significant expression of GFP and GFP-2AC110A in both HEK293T and HeLa cells. Nup98 and eIF4G were cleaved in HeLa cells producing wild type GFP-2A^{pro}, thus confirming successful protein biosynthesis. Interestingly, HeLa cells expressing GFP-2A (wild type) gene yielded protein bands in the GFP immunoblot that were larger than control GFP, but smaller than full-length GFP-2AC110A. Given that during picornaviral polyprotein translation, 2A^{pro} cleaves its N-terminal protein (VP4)[124], it is likely that this catalytic activity extended to the GFP tag. This result suggests that not only can we track 2A^{pro} gene expression through cleavage of a target protein, we may also be able to detect accumulation of GFP-2A self-cleavage products by immunoblot.

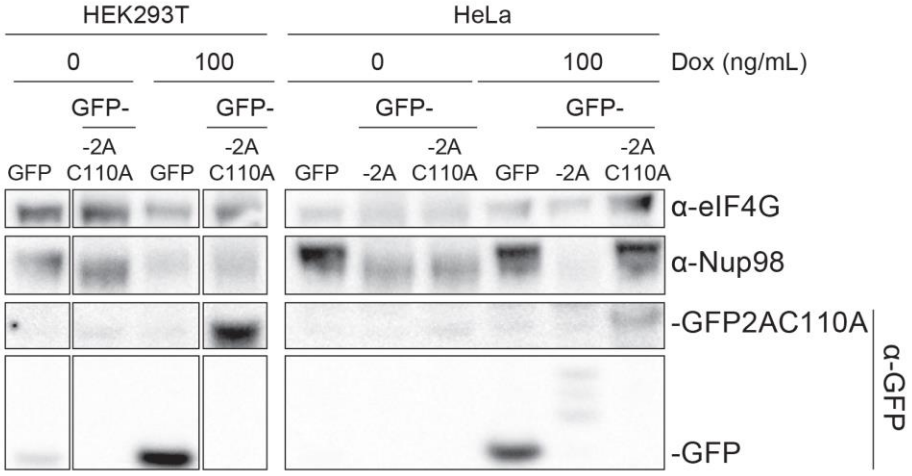

Figure 2.6. Immunoblot assaying protein levels with or without Doxycycline induction of expression.

HEK293T and HeLa stable cell lines were assayed for protein expression with and without Dox induction. Cells were incubated in regular growth media or media with 100 ng/mL Dox for 12 hours before cell collection and downstream processing. Lysates were analyzed by immunoblot for GFP levels to assay genes of interest expression, and Nup98 and eIF4G to track 2A^{pro} expression. Dox induction resulted in significant levels of protein expression, with even GFP-2A^{pro} self-cleavage products detected in low levels[124].

Given that $2A^{pro}$ production is known to be toxic to cells by triggering apoptosis[123], we sought out to quantify HeLa cell survival during GFP (control), 2A, and 2AC110A expression. To quantify cell viability during protease biosynthesis, we counted pre-seeded cells at 0, 12, 24, and 36 hours post-induction. GFP stable cells were also assayed without Dox to compare any effects the induction itself may have on cellular survival. It was immediately apparent that $2A^{pro}$ significantly deteriorated cell growth even within the first 12 hours of expression, with HeLa cell counts stagnating at pre-induction levels. It is likely that while some cells naturally underwent through their cell cycle and mitosis, an equal portion of the cell population died to apoptosis. By 24 hours of $2A^{pro}$ gene expression, we observed that almost 50% of the starting cell population had died, and with only ~25% remaining by 36 hours. Picornavirus infections typically last approximately 12 hours before cell death[108, 125], which is only a 2-3 fold faster death rate compared to the conditions of $2A^{pro}$ production.

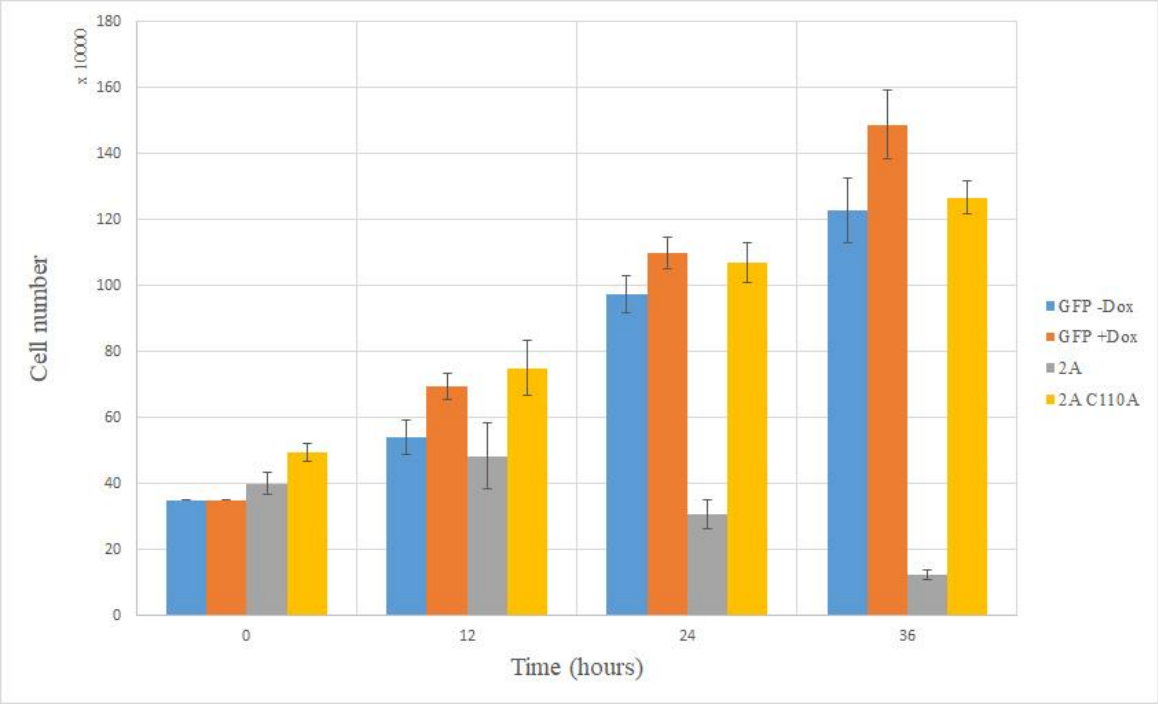

Figure 2.7. Cell viability and survival during protease expression.
We assayed HeLa cell line survival and growth during induction of protein expression over a time course of 36 hours, with time points every 12 hours. HeLa GFP cells were also assayed for growth with and without Dox to determine if any significant effects manifested as a result of induction. HeLa cells expressing GFP and 2AC110A genes both grew equally and without any issues (as compared to the non-induced cells). HeLa cells expressing $2A^{pro}$ failed to expand even by 12 hours, and 50% of cells died by 24 hours.

Conversely and somewhat unexpectedly, neither GFP nor 2AC110A production significantly altered cell growth and viability. By 24 hours, cell populations expressing GFP and 2AC110A genes both grew by ~150%, and another 100% by 36 hours. We had initially suspected that expression of 2AC110A would decrease cell growth over time compared to the control cell lines. Despite the lack of proteolytic activity, we hypothesized that the mutant protease would still

interact with target proteins (interfere with housekeeping activities) or trigger the cells' innate immune response. Indeed, we could visualize GFP-2AC110A localization around the nucleus with live cell fluorescence imaging (Fig 2.27), suggesting that the protease is likely interacting with its would-be cleavage target Nups. Under DIC, 2AC110A expressing cells looked more wrinkled and "sickly" than control cells (data not shown), somewhat similarly to $2A^{pro}$ producing cells. Nevertheless, despite these observations and their underlying causes, the effects turned out to be minor enough to not impact cellular growth.

2.2 Discovery and characterization of $2A^{pro}$ interacting partners and cleavage targets by proteomic analysis

One of our primary investigative aims was to identify and characterize the interacting partners of picornaviral proteases, especially $2A^{pro}$. While both proteases were reported to play roles in cleavage of cell factors, we focused our efforts on characterizing $2A^{pro}$ given its more rapid and dominant cleavage activity and downstream control of host gene expression. Furthermore, we focused our experimental efforts on the catalytically inactive 2AC110A. Given its lack of proteolytic activity, we rationalized that this mutant would be more likely to form stable interactions with its cleavage targets and/or binding partners in the absence of their subsequent proteolytic destruction and so loss of interaction. In addition, the mutant protease should not cleave eIF4G and shut down host protein expression, permitting us to accumulate the protein to biochemically relevant levels for immunoprecipitation trials.

2.2.1 Pilot immunoprecipitation experiments and establishing pulldown conditions

Initial immunoprecipitation trials were conducted on transiently transfected HEK293 and HeLa cells with GFP and GFP-2AC110A expression vectors. Following manufacturer protocols for the jetPRIME kit, we scaled up transfection of cells to 150 mm dishes, which would contain approximately 10-fold more cells. We collected cells, lysed cell pellets in several buffer conditions compatible for pulldowns[126], and immunoprecipitated GFP and GFP-2AC110A and associated proteins with magnetic Dynabeads conjugated with GFP specific antibodies[126]. We primarily assayed Tris and HEPES containing buffers to stabilize pH, NaCl to regulate osmolarity, and a detergent like Triton X-100 to gently dissociate cellular compartments (such as the nucleus)[127, 128]. We settled on two similar and promising pulldown lysis buffers (300 mM NaCl, 0.5% Triton-X 100, and either Tris-HCl, pH 8.0, or HEPES, pH 7.4) (Fig. 2.8), with which immunoprecipitation experiments yielded clean elution profiles. Specifically, we were looking for conditions where pulldown of GFP (control) yielded no detectable background, and GFP-2AC110A immunoprecipitation contained the handle and interacting partners.

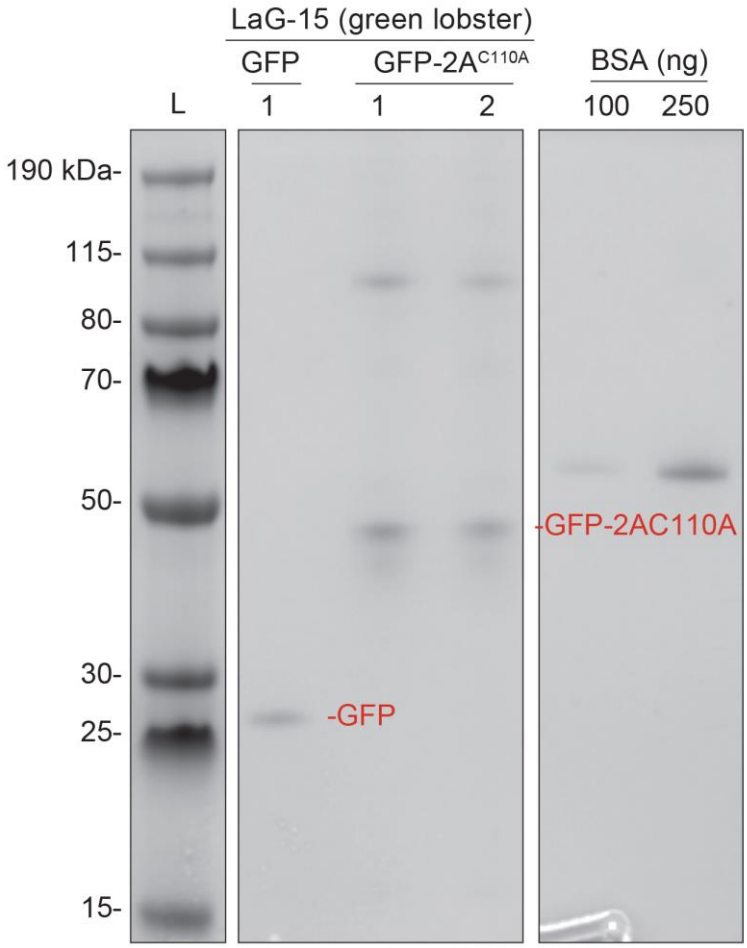

Figure 2.8. Preliminary assay of pulldown conditions for GFP-2AC110A.
We immunoprecipitated GFP and GFP-2AC110 in two similar lysis conditions and analyzed elution samples by SDS-PAGE and stained protein bands with Colloidal Coomassie. We identified one additional and nearly stoichiometric band in the GFP-2AC110A elution samples. This band was migrated at ~100 kDa, potentially corresponding to the molecular weight of Nup98. LaG-15 is an in-house generated anti-GFP antibody with high specificity. BSA samples were included in the gel as references for quantity of protein in nanograms.
Lysis buffers: 1 - 50 mM Tris-HCl pH=8.0, 250 mM NaCl, 0.5% Triton X-100, 5 mM EDTA.
2 - 20 mM HEPES pH=7.4, 300 mM NaCl, 0.5% Triton X-100

Immunoprecipitation of GFP in these buffers did not reveal any additional proteins other than a ~25 kDa band corresponding to the molecular weight of GFP, suggesting a relatively clean pulldown (Fig. 2.8). Pulldowns of GFP-2AC110A in both buffer conditions revealed a nearly identical elution profile: one protein band correlating to the molecular weight of GFP-2AC110A (~45 kDa) and another band at ~100 kDa. In collaboration with the Chait laboratory, we analyzed the elution samples by Mass Spectrometry (MS) to identify any potential interacting partners ermerging in our immunoprecipitation experiment (Table 2.1). After data normalization and curation, we identified Nup98 as one of the top interacting partners of 2AC110A (Table 2.1). We also identified Rae1 in nearly stoichiometric quantities as Nup98. Rae1 (also known as Gle2) is a known interacting partner of Nup98 and plays an integral role in nuclear-cytoplasmic transport of

mRNA and mRNPs[129, 130]. Rae1 contains four WD40 motifs, which tightly bind the Nup98 GLEBS domain and facilitates formation of the Nup98-Rae1 complex[130, 131].

Table 2.1. Mass Spectrometry analysis of preliminary GFP-2AC110A pulldowns.

Protein	# PSMs	# Unique Peptides
RAE1 mRNA export factor	68	11
Nup98-Nup96	64	28
GFP	49	6
Nup93	36	22
2AC110A	31	4
Nup155	29	14
Nup205	26	18
Nup 210	18	11
E3 SUMO-protein ligase RanBP2	16	11
Isoform 3 Nup153	15	10
Nup107	15	9
Nup160	14	10
NUP188 homolog	13	9
Importin subunit beta-1	10	7
eIF 3 subunit L	10	6

We analyzed immunoprecipitated GFP and GFP-2AC110 samples by MS to identify any interacting partners. Output data was normalized by the control GFP sample to eliminate background and non-specific proteins. The final list was curated to remove known contaminants. Identified interacting proteins are ranked by the number of Peptide Spectral Masses (PSMs)[132]. A higher number PSMs generally correlates with larger quantities of protein in the sample. The number of unique peptides for each sample was included in the table and to indicate diversity in PSM sequences.

Aside from Nup98-Rae1, most of the remaining interacting partners identified in the 2AC110A IPs were associated Nups and transport proteins. These proteins were identified with 2-6 fold lower number of PSMs than Nup98-Rae1, indicating that these proteins were likely second order interacting partners of Nup98 (since Nup98 associates within the NPC) and not direct binding partners of 2AC110A. Surprisingly, we did not detect any eIF4G in the MS data despite its prevalence as one of the key cleavage targets of $2A^{pro}$. However, we instead observed EIF3L in the pulldown data. eIF3L is a component of eIF3, a 13-protein complex that plays roles in nearly every step of translation initiation[133]. However, given the preliminary nature of these pulldowns and how much room for improvement remained, we did not make additional interpretations into the absence of eIF4G (possibly the binding interaction was too transient even with the catalytically inactive 2AC110A) or presence of eIF3L.

2.2.2 Large scale preparation of cell material for immunoprecipitation experiments

There are many parameters to improve immunoprecipitation results and downstream MS analysis of the eluates. It is desirable to assay different buffer and lysis conditions, different beads, different antigen-specific antibodies or nanobodies, increase the quantity of starting material, and

scale up pulldown reactions[127, 128]. One of the methods the Rout laboratory pioneered to improve immunoprecipitation experiments and respective yields is cell cryolysis (Fig. 2.9)[134]. This method depends on large-scale expansion and preparation of cell material such as yeast cells[128], mammalian cell lines[134], and Trypanosomes[135]. After collection of cell material as a cell pellet, it is pushed through a syringe directly into liquid N_2, forming "noodles" or small pellets of cell materials[134]. This flash freeze preserves protein and nucleic acids within their respective complexes and facilitates the subsequent step, cryolysis. Frozen cell pellets/noodles are ground into powder with steel balls in a rapidly rotating Teflon jar under constant exposure to liquid N_2. The resulting cell powder is homogeneous, can be stored in -80ºC freezers, and can be weighed out into tubes during immunoprecipitation experiments[134]. The homogeneity of the starting material provides consistency during experiments, especially over long periods of time, and ease of use. Cryolysis is also a superior alternative to other known cell lysis methods, such as harsh buffers (RIPA), sonication, and mechanical cell homogenization[134]. Cell powder forgoes the need for several mandatory buffer parameters in traditional cell lysis protocols, permitting experimental exploration of a wider variety of buffer conditions[134].

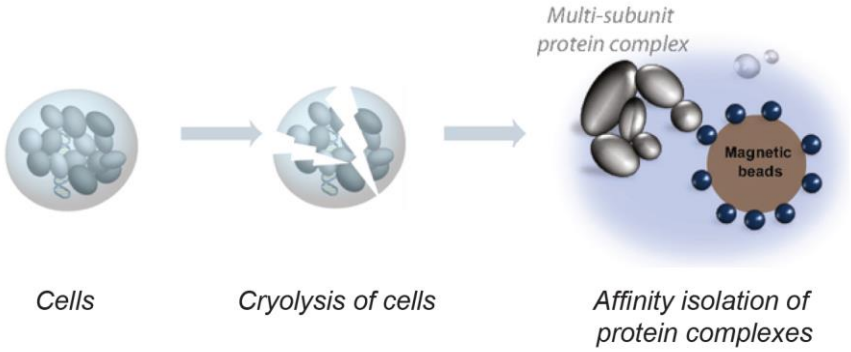

Figure 2.9. Schematic of cellular cryolysis pipeline.
Cells are grown in preparatory scale and prepared for collection. Collected cells are flash frozen with liquid N_2, and subsequently cryolysed with steel balls and a Teflon jar. The resulting frozen cell powder can be used for immunoprecipitation experiments. Cryomilled cell powder has several advantages over traditional cell lysis methods. The powder is stable at -80ºC for long term storage, is homogeneous, and can be accurately weighed out consistently for experiments. Adapted from Xiang et al, 2020[136].

We expanded our established HeLa and HEK293T stable cell lines producing GFP, GFP-2A (HeLa only), and GFP-2AC110A into large scale preparations. After inducing protein synthesis overnight, we harvested the cells, flash froze the cells into noodles, and cryomilled the material into fine powder. We subsequently assayed the cell powder for proper expression of our proteins of interest by immunoblot (Fig. 2.10). GFP bands matched the predicted molecular weights of our proteins of interest and we even detected GFP-2A self-cleavage products in the immunoblot. Furthermore, Nup98 and eIF4G were found cleaved, validating $2A^{pro}$'s proteolytic activity. After validating the cell powder for presence of our tagged handles, we utilized it for immunoprecipitation experiments.

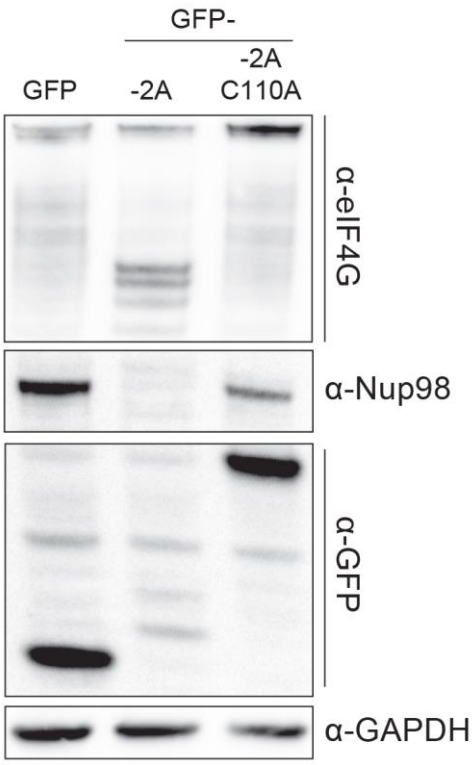

Figure 2.10. Western blot analysis of cryomilled powder.
Cell powder prepared for our HeLa stable cell lines was lysed, clarified, and the supernatant analyzed by immunoblot for protein expression. We assayed for presence of GFP, as well as cleavage of Nup98 and eIF4G.

2.2.3 Affinity capture of GFP-2AC110A and interacting proteins

With validated cryomilled cell powder from our stable HeLa and HEK293T cell lines, novel and improved Dynabeads conjugated with GFP-specific nanobody (LaG 94-10, Peter Fridy, Rout Laboratory), and established lysis buffer conditions, we initiated another round of immunoprecipitation experiments. LaG 94-10 were utilized for their ease of preparation and purification, as well as for their high affinity for GFP. Large scale conjugation of nanobodies to magnetic Dynabeads facilitated affinity capture experiments by minimizing batch variation. GFP-2AC110A was successfully pulled down with significantly more interacting proteins than the GFP control or GFP-2A^{pro}, as seen by Silver Stain (Fig. 2.11). Notably, we were able to affinity capture some of the wild type GFP-2A^{pro}, however the protein levels of the handle and co-precipitating proteins were considerably lower.

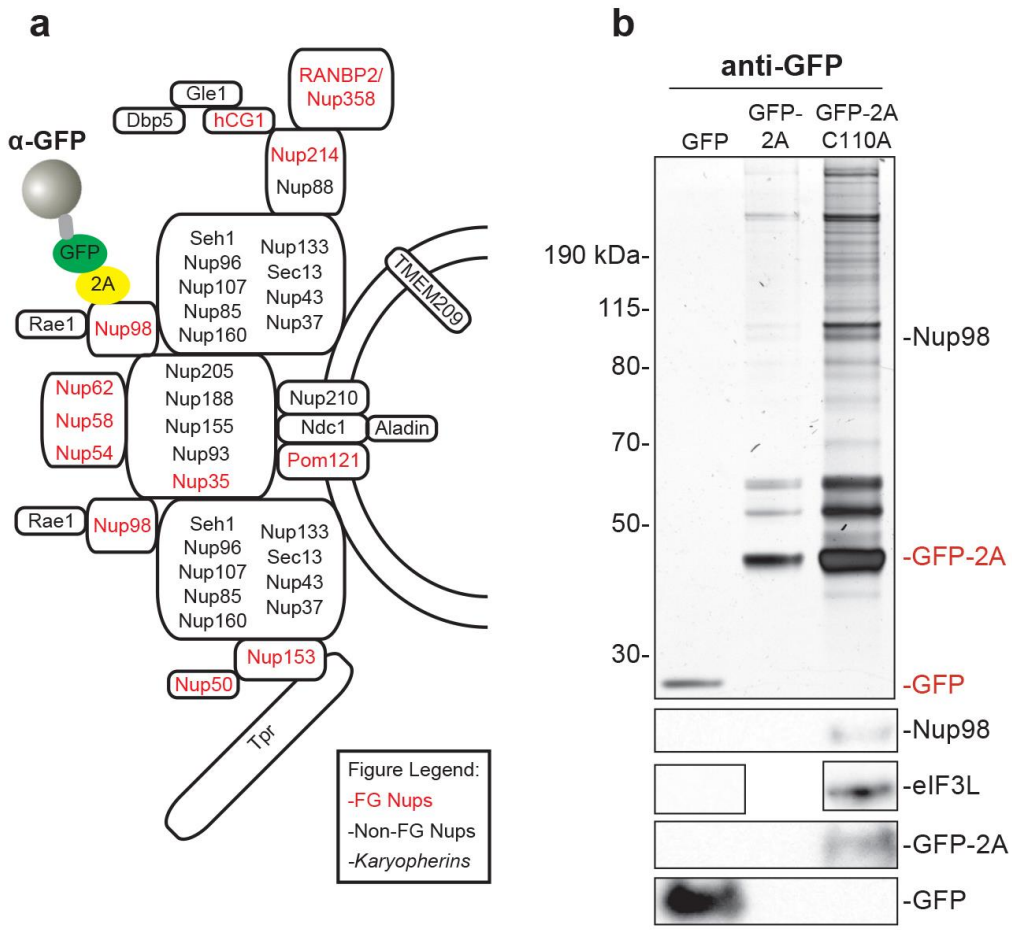

Figure 2.11. HeLa cell powder GFP immunoprecipitation experiments.
GFP, GFP-2A, and GFP-2AC110A pulldowns with cryomilled HeLa cell powder analyzed by SDS-PAGE and Silver Stain. **a**, GFP-2AC110A was predicted to bind Nup98 and pulldown other interacting NPC components. GFP affinity capture was done with anti-GFP nanobody (LaG 94-10) conjugated to magnetic Dynabeads. **b**, a variety of interacting proteins can be detected with GFP-2AC110A. Immunoblotting confirmed the presence of GFP-2AC110A, eIF3L, and Nup98. 100 mg of cryomilled powder was lysed in 20 mM HEPES, pH 7.4, 300 mM NaCl, 0.5% Triton X-100.

We assayed the eluate by immunoblot to validate the presence of GFP/GFP-2AC110A, Nup98, and eIF3L in GFP-2AC110A elutions. We subsequently analyzed the pulldown data by MS in triplicate. Another layer in assaying the efficacy of our immunoprecipitation experiments was confirming the pulldown efficiency. We prepared aliquots of the various stages of an affinity pulldown experiment: resuspended and sonicated protein pellet post-clarification, clarified supernatant, post-IP flowthrough, and the final IP elution. We analyzed each sample aliquot from all three pulldowns by immunoblotting and tracked changes in the amount of GFP and GFP-2AC110A between stages (Fig. 2.12). Unsurprisingly, we detected some of the expressed proteins in the pellet, likely as part of insoluble proteins sedimented through high-speed centrifugation[137]. We compared GFP and GFP-2AC110A signal intensities between the Supernatant (prior to IP) and Flowthrough stages (which is immunodepleted sample) and observed a nearly complete disappearance of signal in the Flowthrough samples. This experiment indicated that we had a

greater than 90% efficiency at capturing available handle during our pulldown experiments. This result validates the efficacy of our affinity capture conditions and suggests that the captured proteins are quantitatively representative of the interactions formed *in vivo*.

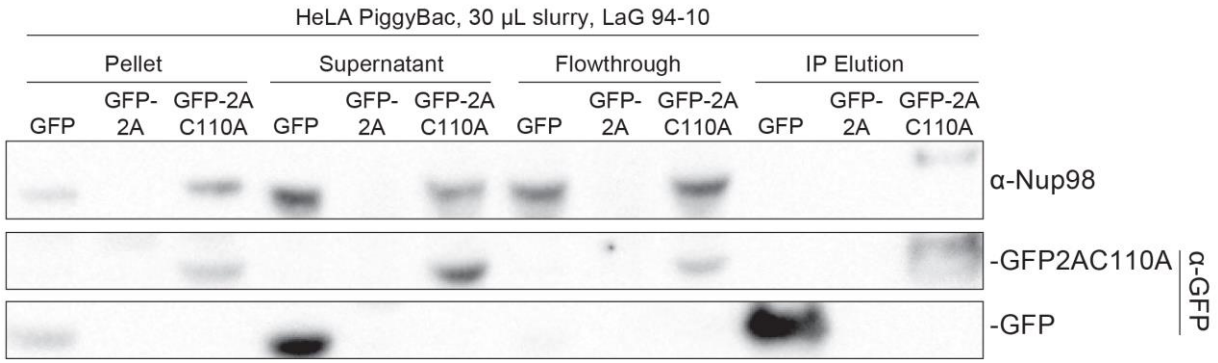

Figure 2.12. Assaying immunoprecipitation efficiency.
We analyzed samples from every key stage of a standard immunoprecipitation experiment by immunoblot. We sought to track the level of GFP signal in pre-IP Supernatant samples and how much it was depleted in the resulting Flowthrough samples during affinity capture. We observed nearly complete immunodepletion of GFP and GFP-2AC110A, signifying above 90% pulldown efficiency within our operating conditions.

Mammalian cell lines can often have potentially major differences in biological characteristics, such as morphology, and can also differ at an Omic level, with variance in protein and RNA expression paradigms[138, 139]. To prevent cell line bias within our data, we believed it was important to confirm our proteomic data with material obtained from another cell line. As such, we repeated our immunoprecipitation experiments with HEK293T cell powder with GFP and GFP-2AC110A gene expression. We observed similar elution profiles as in the HeLa experiments, albeit with relatively lower protein content (Fig. 2.13). We suspect that cell line based differences account for this discrepancy. Nevertheless, the pattern of interacting protein bands in the GFP-2AC110A IP detected by SDS-PAGE is similar to what was observed in HeLa cells, suggesting that the protease's interactome, or at the least the most abundant proteins, are similar in both HeLa and HEK293T cell lines. Unfortunately, due to the coronavirus outbreak and the MS data analysis pipeline prioritized for Covid-19 related research, the HEK293T pulldowns (n=3) have not yet been analyzed by MS, and additional data is not available.

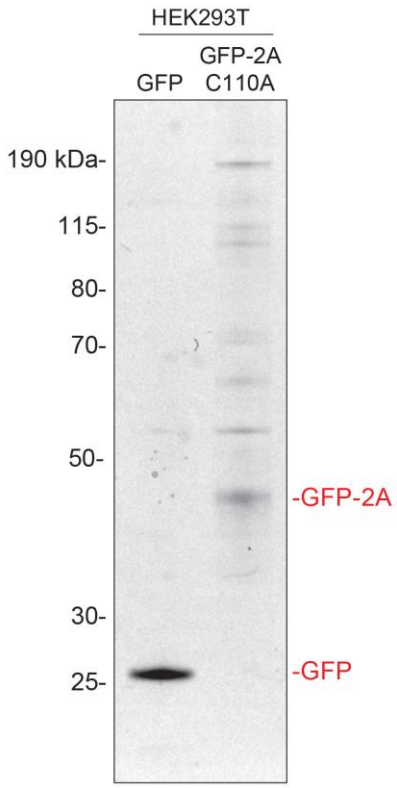

Figure 2.13. HEK293T cell powder immunoprecipitation experiments.
GFP and GFP-2AC110A pulldowns with cryomilled HEK293T cell powder analyzed by SDS-PAGE and stained with colloidal coomassie. A variety of interacting proteins can be detected with GFP-2AC110A. 100 mg of cryomilled powder was lysed in 20 mM HEPES, pH. 7.4, 300 mM NaCl, 0.5% Triton X-100.

2.2.4 Analysis of 2A^{pro}C110A interacting partners

After MS analysis of our affinity capture experiments and transformation of raw data into a readable output, we sought to establish a non-biased data analysis pipeline (Fig. 4.10). We started with a list of proteins identified by MS analysis, averaged the data set (since it was originally done in triplicate), and sorted the list by number of unique peptides. We trimmed the list to retain only proteins with three or more unique peptides based on recommendations of our collaborators in the Chait laboratory. We normalized the new set of proteins by peptide quantity of the GFP data set. This step removed or significantly decreased representation of common well-known contaminants found across all data sets, such as Keratins, filament proteins, Heat Shock proteins, among many others[140]. After normalization, we removed any proteins found in the CRAPome database for GFP affinity capture experiments, a publicly available repository for pulldown experiment data to facilitate identification of background contaminations in a variety of immunoprecipitation conditions (Table 4.2)[141]. This was a crucial analysis step to reveal the most likely bona fide interacting partners of 2A^{pro} and 2AC110A.

Raw MS analysis identified 435 proteins in the GFP-2AC110A dataset, and after the aforementioned normalization and curation steps, only 202 proteins remained in the list. We then ranked proteins by peptide quantity (assessed by Proteome Discoverer software, Thermo Fisher Scientific) (Fig. 2.14), determined fold enrichment of proteins between data sets (Fig 2.15b), and compared peptide quantities and fold enrichments of proteins found in both 2A^{pro} and 2AC110A

data sets (Figs. 2.16, 2.17). Given the various issues with the GFP-2A^{pro} data, namely decreased expression yield, lower likelihood of stable interaction formation due to remaining proteolytic activity, and the self-cleavage and dissociation of the catalytically active protease from its own GFP tag, we focused the majority of our efforts on the GFP-2AC110A data. We plotted the top ~40 interacting proteins by raw peptide quantity, which is a proxy for "amount" of the protein found by MS analysis (Fig. 2.14). Identified proteins were broken down into three categories, Nups (red), translation initiation factors (purple), and cytoskeletal and other proteins (gray). The top groups of interacting proteins were Nup98-Rae1 and almost the entire eIF3 complex. As with our pilot pulldowns, Nup98-Rae1 were detected with an approximately 1-to-1 protein stoichiometric ratio. Given this data, it is likely that 2AC110A is binding one of these two proteins during affinity capture. Given Nup98 is a direct cleavage target, we suspect 2AC110A is forming a 'direct' interaction with this Nup, prior to cleaving it (Fig. 2.15a). Considering the strong affinity between the GLEBS domain of Nup98 and WD40 motifs of Rae1[131], it is likely that Rae1 is pulled down with Nup98, as an 'indirect' binder of 2AC110A (Fig. 2.15b).

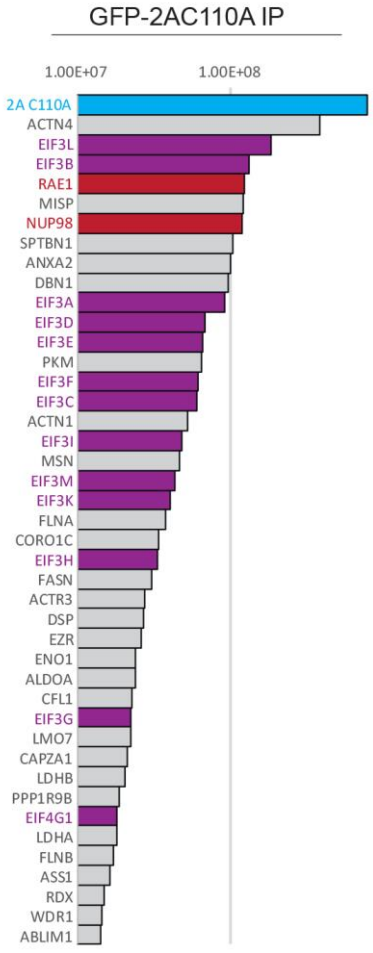

Figure 2.14. Top GFP-2AC110A interacting partners.
Processed GFP-2AC110A pulldown data where identified interacting proteins were ranked by total peptide quantity (top 40). Identified proteins were broken down into four categories: 2A protease (cyan), Nups (red), translation initiation factors (purple), and cytoskeletal and other proteins (grey).

Interestingly, we also observed comparably high levels of eIF3L and eIF3B in the MS data analysis, as well as marginally lower levels of other eIF3 complex proteins. In all, we detected 12 out of 13 proteins that form the eIF3 complex[133], and these proteins were almost entirely in the top 20 most prevalent proteins of a 2AC110A pulldown. eIF4GI, one of the primary cleavage targets of $2A^{pro}$, was detected as well, but at a 10-fold lower level than eIF3L. We considered if the cellular ratio of eIF3 proteins was greater than eIF4G and kinetically driving the observed ratios of proteins in our pulldowns. However, internal MS analysis of cell lysates (Data not shown) and published work[142] suggests there may be 2-3 fold as much eIF4G as eIF3L and other eIF3 proteins, suggesting this possibility is less likely.

Given the interactomic data, specifically the high levels of eIF3 proteins compared to eIF4G, and the predominance of eIF3L in multiple rounds of pulldowns, we tentatively formed a hypothesis that eIF3L forms a binding site for $2A^{pro}$, from where the protease cleaves eIF4G during translation initiation. This idea is based on our immunoprecipitation data reproducibly showing eIF3L as the most commonly and predominantly found eIF3 component (Figs. 2.14, 2.19b, 2.20). While we tentatively propose eIF3L to be the primary piggyback site for $2A^{pro}$, it is not implausible, and even likely, that the protease makes additional interactions with other eIF3 complex components *in vivo* (Fig. 2.15c).

In addition to Nup98-Rae1 and the eIF3 complex, we also detected a number of cytoskeletal proteins, such as filament forming proteins, motor proteins, and LIM-domain containing actin binding proteins[143]. Curiously, these proteins were not curated by the CRAPome non-specific background list of proteins, suggesting they may be bona fide interacting partners. Furthermore, our collaborators from the Chait laboratory remarked that they have never seen LIM-domain actin binding proteins (LIMA1[144, 145], ABLIM1[146], LMO7[147]) in MS data of other experiments, which reinforced our suspicion that these are genuine interactions. However, it is unclear what biological relevance these cytoskeletal proteins may have. There is no literature tying the 2A or 3C proteases to any function with the cytoskeleton. We suspect $2A^{pro}$ may associate with cytoskeletal proteins as a method of transport throughout the cell to localizations of use, such as the NPCs. Another hypothesis suggests a role for $2A^{pro}$ in cytoskeletal rearrangement, similar to picornaviral 2C protein, which rearranges vesicles in infected cells[148]. However, it is also plausible that $2A^{pro}$ is merely "stickier" and attracts a wider range of contaminants.

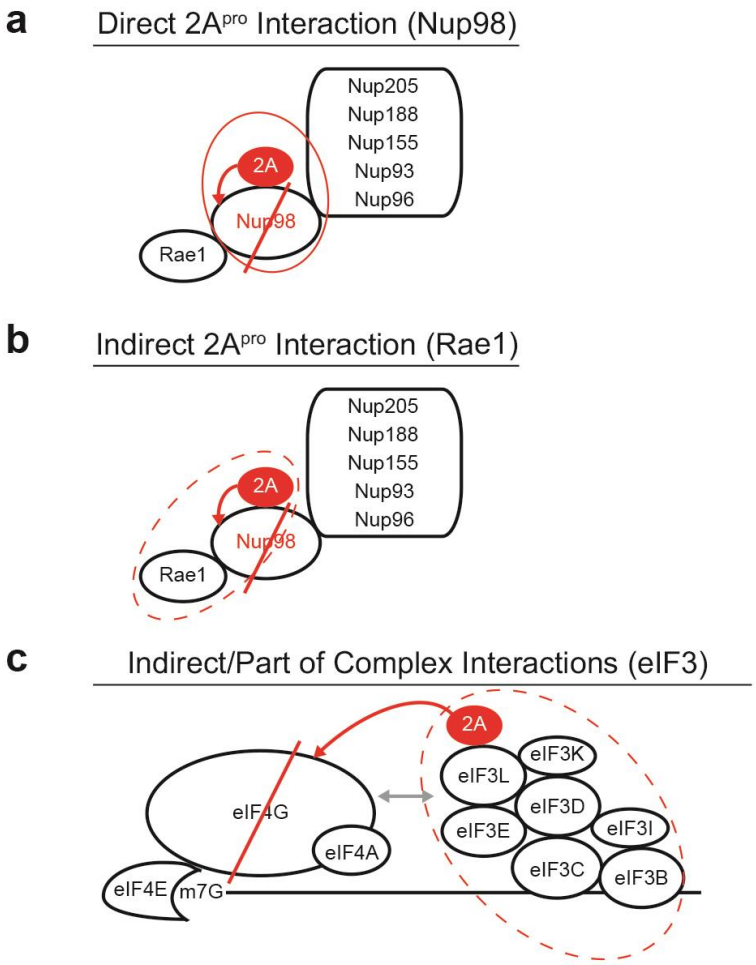

Figure 2.15. Types of 2AC110A interacting partners.
Based on proteomic data analysis, we started formulating soft definitions for the various types of interacting partners identified in our pulldowns. **a**, Nup98 is a known cleavage target and is predicted to be a direct interacting partner of 2AC110A. **b**, Rae1 is a strong binding partner of Nup98 and is likely an indirect interactor of 2AC110A during immunoprecipitation experiments. **c**, the eIF3 complex is predicted to be a targeting platform for $2A^{pro}$ mediated cleavage of eIF4G. While eIF3L is a likely binder of $2A^{pro}$ in this scenario, it is also plausible other eIF3 complex proteins play a role in this potentially indirect interaction.

Despite limitations with the wild type $2A^{pro}$ affinity capture experiment, we can nonetheless glean useful data from it. One key limitation was the generally decreased level of the handle and interacting proteins. We accounted for this issue through normalization of the GFP-2AC110A data by GFP levels (based on fold difference) of the GFP-$2A^{pro}$ pulldown. We subsequently plotted the normalized top ~40 proteins of both pulldowns by peptide quantity (Fig. 2.16a). We observed similar peptide levels of a number of proteins, such as the cytoskeletal interacting proteins: ACTN4, SPTBN1, FASN, LMO7, ABLIM1, and FLNA. Nup98 was not detected in the $2A^{pro}$ dataset, almost certainly because nearly all Nup98 is cleaved within cells expressing the protease. Rae1 was not detected in $2A^{pro}$ affinity capture data either, suggesting it is only present in the 2AC110A data as the primary interacting partner of Nup98. Absence of other

Nups from the 2A^{pro} affinity capture data is not surprising, as they were second and third order interactors of Nup98. Some of the eIF3 complex proteins can be detected in the 2A^{pro} MS data, but not all. In addition, all eIF3 proteins that are detected in the 2A^{pro} pulldown data have much lower peptide quantity levels. This result suggests 2A^{pro} is capable of direct interactions with eIF3L and some fraction of the eIF3 complex in spite of its proteolytic activity. We plotted the top 20 most enriched proteins in the 2AC110A dataset compared to 2A^{pro} MS data (Fig. 2.16b), and they unsurprisingly comprise of almost entirely NPC and eIF3 components.

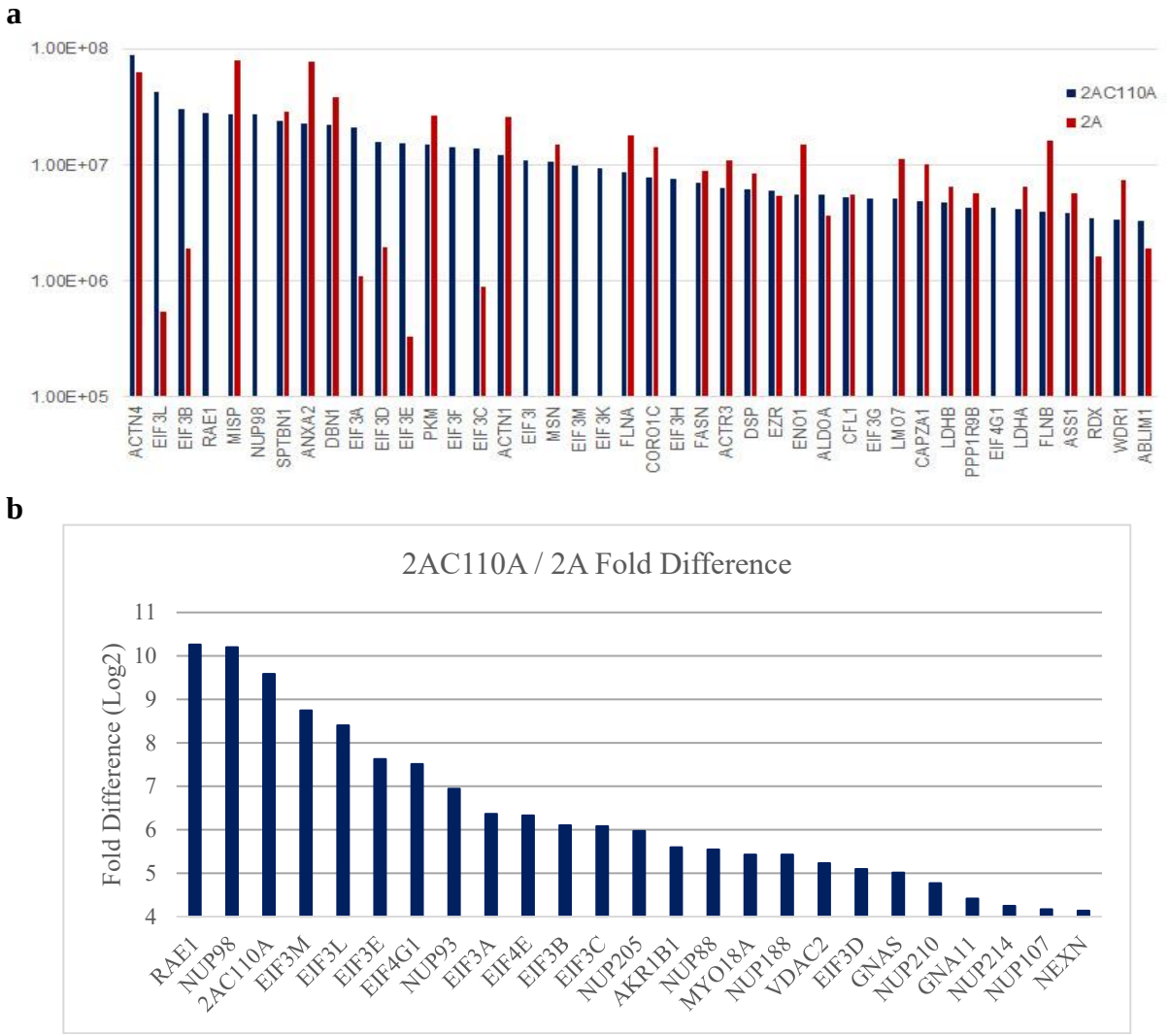

Figure 2.16. Variation in 2A^{pro}C110A and 2A^{pro} interacting partners visualized
a, 2A^{pro} and normalized 2AC110A MS data ranked by peptide amount and plotted side by side for direct comparison. Many of the top 40 proteins have similar peptide levels in both datasets. However, the Nup98-Rae1 complex is entirely absent from 2A^{pro} pulldown data. Similarly, eIF3 complex members are either absent or relatively depleted in the 2A^{pro} data. 2A^{pro} are represented by red bars, 2AC110A data is represented by blue bars. **b**, Fold enrichment of 2AC110A over 2A^{pro} proteins. We plotted proteins by fold enrichment (peptide quantity of 2AC110A/2A^{pro} datasets), and transformed the final enrichment by Log2. The top 20 most enriched proteins in the 2AC110A data set are almost entirely NPC and eIF3 components.

We filtered the 2A^{pro} and 2AC110A MS data to retain only proteins found in both datasets and plotted representative proteins based on peptide quantity in each pulldown (Fig. 2.17). The X-Axis of the resulting scatterplot was peptide quantity in the 2AC110A pulldown, while the Y-Axis was peptide amount of proteins in the 2A experiment. Comparing the datasets in this manner permits us to make an interpretation about which proteins stand out in the pulled down fractions of either affinity capture experiment. For instance, eIF3 complex proteins (specifically eIF3L, A, C, D, E) can be found in both pulldown datasets, albeit in much lower quantities for the 2A^{pro} pulldown. This discrepancy was present despite normalization of datasets to GFP levels, as the 2A^{pro} pulldown would have less handle to immunoprecipitate due to limitations of protease expression and accumulation. Nup98-Rae1 are only present in the 2AC110A pulldown data (Fig. 2.17), suggesting the catalytic cleavage of Nup98 during 2A^{pro} immunoprecipitation trials disperses Rae1 as well.

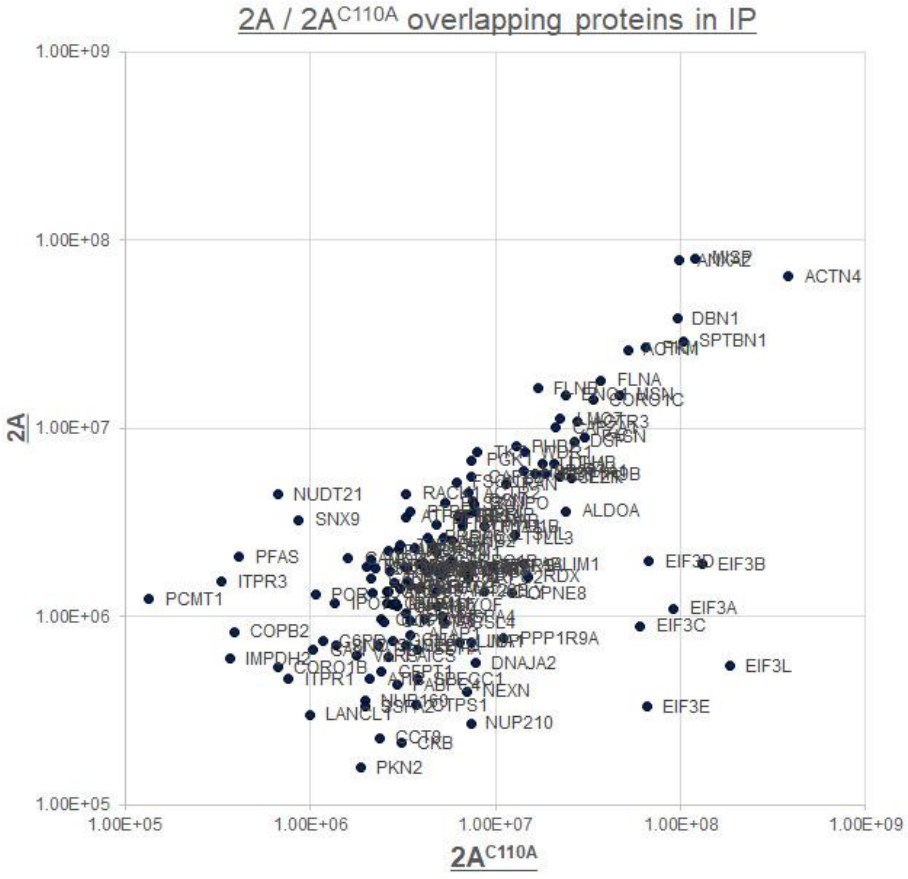

Figure 2.17. Protein level comparison in 2A^{pro}C110A and 2A^{pro} shared proteome.
Comparison of normalized shared proteins between both GFP-2A^{pro} and GFP-2AC110A immunoprecipitation experiments. The X-Axis represents the peptide quantity of 2AC110A associated proteins, while the Y-axis represents interacting proteins of 2A^{pro}. Some proteins, such as Nup98 and Rae1, are only found associated with 2AC110A. Some eIF3 components can be detected in both pulldowns, but massively depleted in 2A^{pro} pulldowns. Cytoskeletal and associated proteins (ACTN4, LIM proteins, Myosins) can be detected at nearly equal peptide levels in both pulldowns.

A large number of cytoskeletal and associated motor proteins (such as ATN4) can be found in both pulldown datasets, at equal or similar ratios, suggesting similar association of these proteins to both wildtype and mutant 2A (Fig. 2.16). Finally, some proteins such as NUDT21 and PFAS (Fig 2.17) are observed to be enriched in the $2A^{pro}$ dataset, but we cannot explain their function related to picornavirus infection, and notably, they are not identified as cleavage targets[108].

2.2.5 Assessing $2A^{pro}$ cleavage of proteins of interest

We sought to further investigate observations made from our MS data, specifically the fact that Nup98-Rae1 was totally absent from the $2A^{pro}$ pulldown. To determine whether Rae1 was being cleaved similarly to Nup98, we assayed HeLa cell line lysates by immunoblot (Fig. 2.18). $2A^{pro}$ expression led to nearly total depletion of Nup98, but nominal, if any, cleavage of Rae1. Since Rae1 is not proteolytically degraded by $2A^{pro}$, we hypothesize that Rae1's absence from $2A^{pro}$ affinity capture data is due to depletion of Nup98 and subsequent lack of primary binding partner for Rae1. Meanwhile, 2AC110A immunoprecipitation experiments can bring down Nup98 bound to the catalytically inactive protease, with Rae1 bound to Nup98.

We analyzed a number of other proteins by immunoblot to answer other biological questions. For instance, is the $2A^{pro}$ specifically cleaving Nup98, or are other NPC components being proteolysed as well? Assaying 8 Nups by immunoblotting, we observed that $2A^{pro}$ did not affect other NPC components tested, suggesting a high degree of specificity to Nup98. eIF3L was also assayed by immunoblotting and was not found to be degraded. Since endogenous eIF3L levels are not affected by $2A^{pro}$ catalytic activity, this suggests that decreased levels of eIF3 components in the $2A^{pro}$ pulldown data are likely caused by other factors, such as tertiary complex destabilization. This situation differs from Nup98-Rae1, whereby eIF3 proteins are not completely absent from affinity capture with wild type $2A^{pro}$. We believe the observed difference is due to the catalytic activity of $2A^{pro}$, resulting in lack of stability with the eIF3 complex.

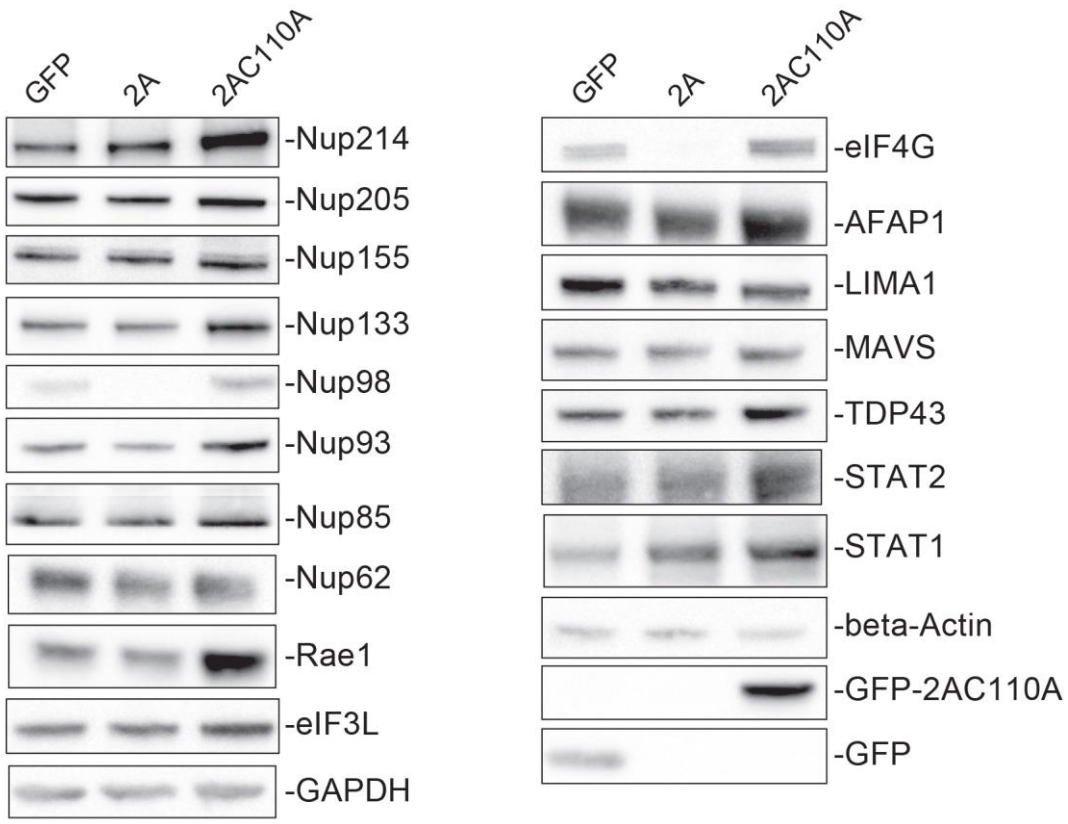

Figure 2.18. Western Blot analysis of lysates from HeLa stable cell lines expressing 2A and 2AC110A.
Stable HeLa cell lines were induced to express GFP-, -2A^{pro} and -2AC110A, with cells collected 16 hours post induction. Cells were lysed in the same buffer conditions as our immunoprecipitation experiments, and the clarified lysates were subsequently analyzed by immunoblot. We assayed a number of proteins of interest, with a keen focus on whether protein levels were depleted during 2A^{pro} expression.

Cytoskeletal proteins detected in both 2A^{pro} and 2AC110A pulldowns, such as LIMA1, AFAP1[149], and LMO7 (data not shown), were also found intact during 2A^{pro} expression. This result eliminates suspicion of a direct 2A^{pro} role in cleaving cytoskeletal components. Nevertheless, we continue to suspect a non-direct role, such as binding and assisting with cytoskeletal remodeling or piggybacking on actin binding proteins to traverse the cell. Some published 2A^{pro} cleavage targets, specifically TDP43[99] and MAVS[89], were also assayed by immunoblot to cross-validate our data with published work. Despite literature suggesting that these two proteins are cleavage targets, we were unable to detect any 2A^{pro} mediated cleavage. However, we do not interpret this data as inconsistency between published work and our own. It is established that during picornaviral infection, certain protein targets are cleaved hours ahead of others (Fig. 3.4)[125]. For instance, eIF4G and Nup98 are cleaved 3-4 hours post-infection, while other targets, such as Nup62 (in the case of Rhinovirus), are cleaved ~6 or more hours post-infection[125]. Picornaviral infection results in exponential production of viral components, which would correlate with significantly slower timelines for cleavage of lower tier proteins within ectopic expression systems. Effectively, we suspect that we do not detect MAVS or TDP43 cleavage in our lysates due to lack of 2A^{pro}

accumulation, at least relative to the state of an infected cell. Such an interpretation would also suggest that our expression systems are tuned to capture the earliest stages of $2A^{pro}$ function during picornaviral infections.

2.3 Proteomic analysis of Nup214 interactome during $2A^{pro}$ expression

The Rout laboratory is dedicated to studying components of the NPC through broad scope of methods and techniques. One of our strengths is cutting edge expertise with discovering and developing nanobodies specific to a wide scope of antigens, such as receptors on cell surfaces, cytoskeletal components, and Nups[150]. The Rout laboratory developed Nup214 nanobodies (Peter Fridy, unpublished data) that are highly effective for affinity capture experiments. This development presented an especially useful experimental situation, whereby we could immunoprecipitate Nup214 and associated NPC proteins from cell powder producing viral proteases. Such methodology would enable us to interrogate the effects of $2A^{pro}$ on the NPC from a totally different angle. Furthermore, Nup214 was shown to be unaffected by $2A^{pro}$ expression in our cell line systems, and 2AC110A pulldown MS data barely detected Nup214, suggesting that we could link the datasets.

2.3.1 Nup214 affinity capture during expression of 2A protease

Nup214 nanobodies were conjugated to Dynabeads for affinity capture experiments with HeLa cell line powder producing our proteins of interest. The goal was not to pulldown GFP-2AC110A or GFP-$2A^{pro}$ directly, but rather reverse pulldown by targeting Nup214, which would bring down NPC components such as Nup98. We would also be able to observe any NPC proteins or transport proteins depleted due to $2A^{pro}$ expression and cleavage. Nup214 affinity capture eluates were assayed by SDS-PAGE and immunoblotting to track presence of GFP-2AC110A and Nup98 depletion (Fig. 2.19).

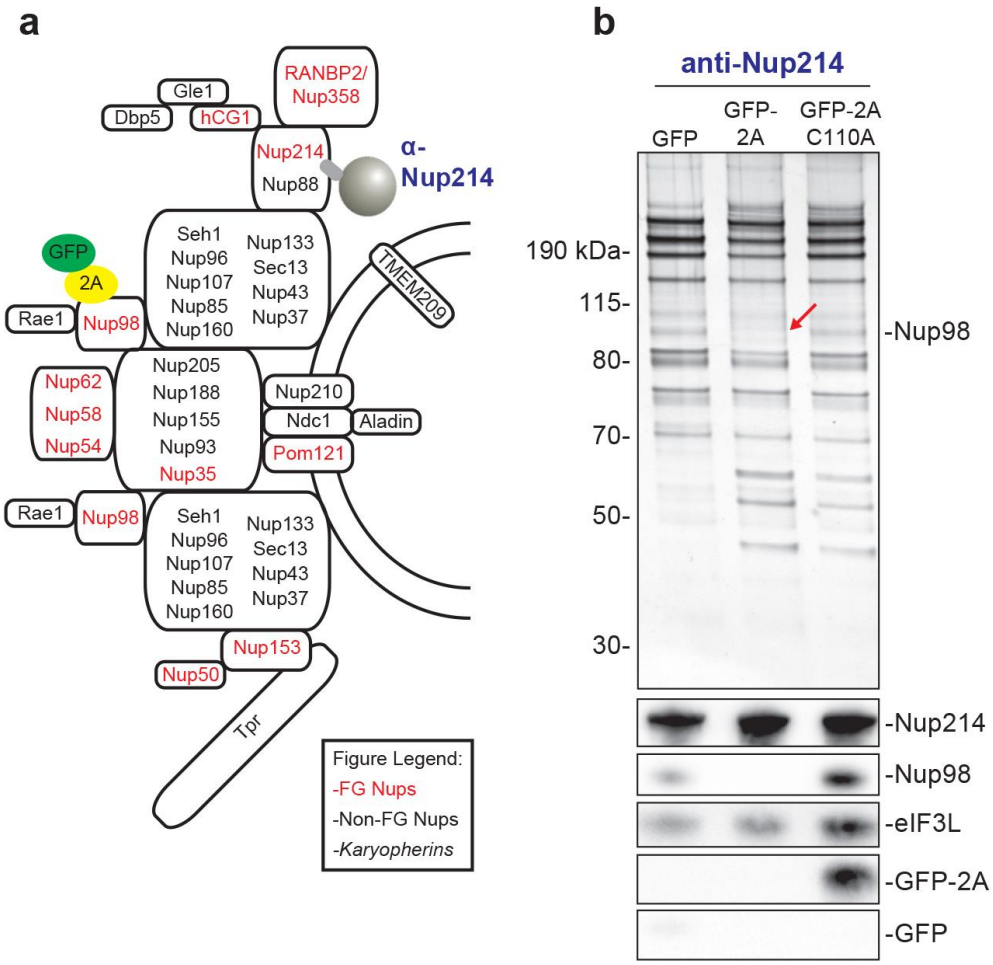

Figure 2.19. Nup214 pulldowns during protease expression.
a, Nup214 nanobodies were utilized to immunoprecipitate whole NPC in cell powder from HeLa stable cell lines producing our proteins of interest. **b**, Eluates were assayed by SDS-PAGE (top gel) and immunoblot (GFP, Nup98, eIF3L, Nup214). Nup98 is depleted from Nup214 pulldowns during $2A^{pro}$ expression. Nup214 pulldowns also have elevated levels of lower molecular weight protein background than the control (GFP cell powder). GFP-2AC110A is detected by immunoblot, but not GFP itself, further validating Nup98 as a direct 2A binder. eIF3L levels are elevated in pulldowns with 2AC110A present. 100 mg of cryomilled powder was lysed in 20 mM HEPES, pH. 7.4, 150 mM NaCl, 0.5% Triton X-100.

Nup214 pulldowns with wild type and catalytically inactive proteases both showed elevated levels of interacting partners with lower molecular weight (Fig. 2.19b). Immunoblots demonstrate Nup98 is pulled down during Nup214 affinity capture and that Nup98 is missing during $2A^{pro}$ expression due to proteolytic degradation. Furthermore, GFP signal was only present during GFP-2AC110A expression, validating the direct interaction between 2AC110A and Nup98. eIF3L was detected in all three pulldowns, but was detected at elevated levels with $2A^{pro}$, and further enriched with 2AC110A gene expression. eIF3L level increases correlated with the associated pulldown of 2AC110A, validating the 2AC110A-eIF3L interaction. Nup214 pulldowns were repeated in triplicate for subsequent MS/MS analysis.

2.3.2 Quantitative analysis of Nup214 interactors during protease expression

MS analysis of Nup214 immunoprecipitation experiments followed a modified $2A^{pro}$ analysis pipeline (Fig. 4.11), in which the data sets were not normalized to the pulldown in presence of GFP. Proteins identified by MS analysis were nonetheless interrogated by the CRAPome database, and we were left with 372 of 839 putative interacting proteins. Protein interactors were ranked by peptide quantity, and unsurprisingly data analysis revealed many NPC and transport proteins as top Nup214 binders (Fig. 2.20). Additionally, Nup98 was ranked 5th, so as expected, GFP-2AC110A was detected in the top 40 Nup214 interacting partners. This reverse pulldown confirms the direct interaction formed between Nup98 and the $2A^{pro}$. Surprisingly, we also detected eIF3 complex proteins with relatively similar peptide quantities as 2AC110A. This data further supports the 2AC110A-eIF3L interactions, since a Nup214 affinity capture can pulldown Nup98 bound to 2AC110A, which is bound to eIF3L and associated proteins.

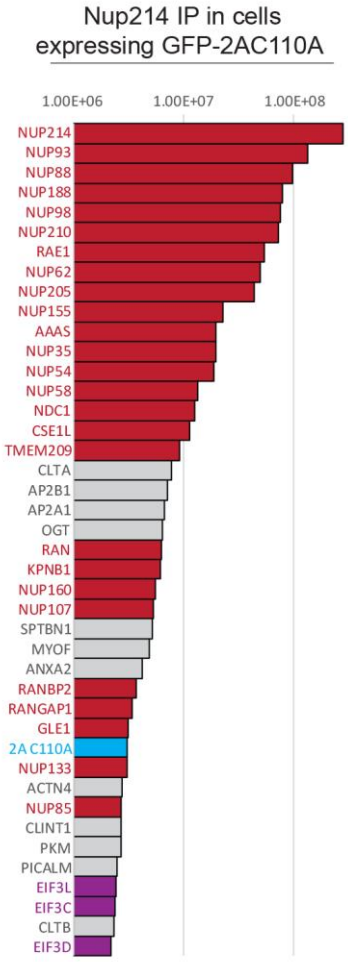

Figure 2.20. Nup214 interacting partners during $2A^{pro}$C110A expression.
Nup214 affinity capture elutions were analyzed by MS and through the previously established data workflow. Top Nup214 binders during 2AC110A expression were plotted by most abundant peptide quantity. Nups and transport proteins were unsurprisingly the most prevalent, however 2AC110A and eIF3L and other eIF3 complex proteins were also detected within the top 40 binders. Identified proteins were broken down into four categories: 2A protease (cyan), Nups (red), translation initiation factors (purple), and cytoskeletal and other proteins (grey).

We compared Nup214 affinity capture datasets under $2A^{pro}$ and 2AC110A production to investigate interactomic profiles and look for any outlier protein enrichment (Fig. 2.21). We utilized a volcano plot to show the data, with the X-axis showing Log2 transformed fold-difference between data sets, and the Y-axis measuring statistical significance. The right side of the volcano plot are proteins enriched in the 2AC110A pulldown (relative to $2A^{pro}$), while $2A^{pro}$ enriched proteins are on the left side. A number of proteins were found to be 3 or more fold enriched in the 2AC110A pulldown dataset, such as Nup98, Rae1, eIF3L, and eIF3K, among others. It is not surprising that Nup98-Rae1 were multiple fold enriched in the 2AC110A dataset compared to $2A^{pro}$ data, given that $2A^{pro}$ degrades and depletes Nup98. However, it was surprising to detect enrichment of eIF3 complex proteins given these would effectively be 4^{th} order interactions: Nup214-Nup98-2AC110A-eIF3. This observation is also a testament to the degree eIF3 proteins, especially eIF3L, favor binding to 2AC110A.

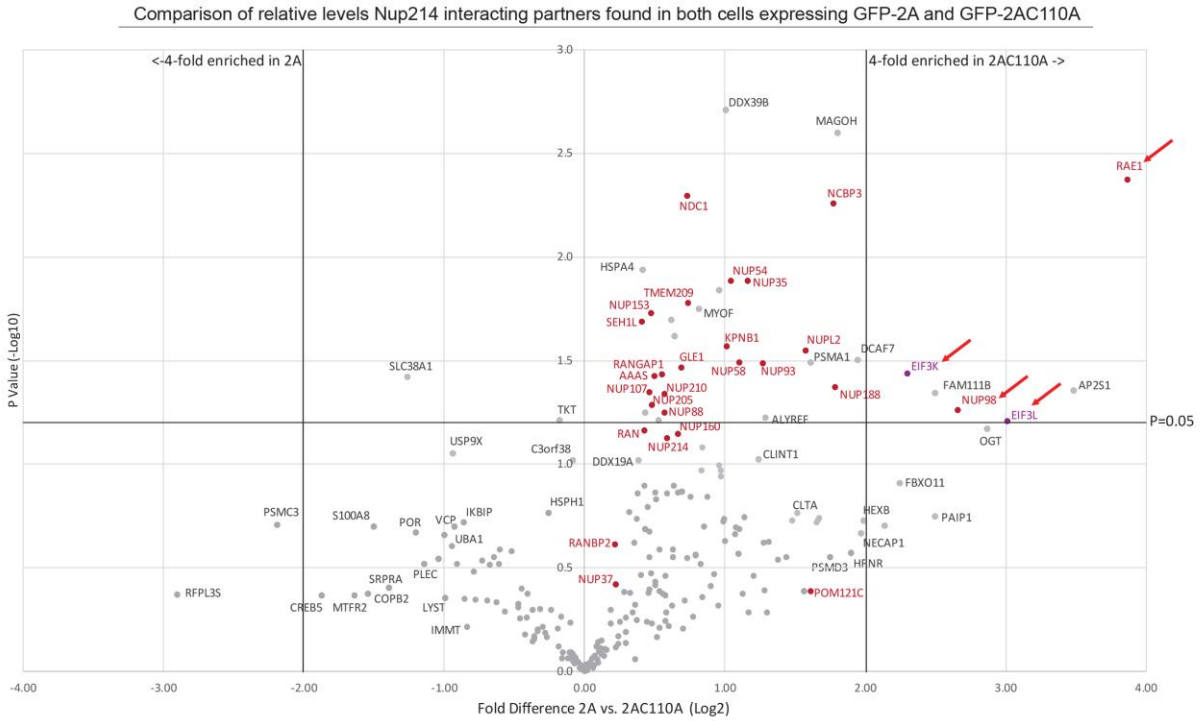

Figure 2.21. Comparison of relative levels of Nup214 interacting partners during protease expression.
MS data for Nup214 pulldowns during $2A^{pro}$ and 2AC110A were compared for relative fold enrichment (X-axis, Log2 transformed) and statistical significance (Y-axis, -Log10 transformed). We added vertical bars representing greater than 3-fold enrichment on both sides of the plot, as well as a horizontal bar representing statistical significance of at least p=0.05. Identified proteins were broken down into three categories, Nups (red), translation initiation factors (purple), and cytoskeletal or other proteins (grey).

A variety of other proteins were also found enriched to a lesser degree in the 2AC110A data set, most of them Nups (red). This observation can be explained by $2A^{pro}$ mediated depletion of Nup98 potentially destabilizing the Nup214 complex we are pulling down, and lose some associated Nups. Globally, our data reveals that CVB3 $2A^{pro}$ does not immediately attack many

Nups, nor significantly alters the structure of the NPC, and instead focuses on surgically depleting only Nup98.

2.3.3 Analyzing 2A^{pro} cleavage specificity for Nup98 over other NPC components

To determine if NPC enrichment in Nup214 pulldowns with 2AC110A was due to complex destabilization as we predicted (Fig. 2.21) or due to cleavage of Nups by 2A^{pro}, we analyzed depletion of peptides identified by MS analysis. Proteome Discoverer software is normally used to output MS data for identified proteins. All peptides identified during MS runs are collated into total peptide quantities for each unique protein. Nup98 is normally produced as a bicistronic fusion protein that is separated into individual components by an autoproteolytic domain (APD) at the C-terminus of Nup98 (Fig. 2.22)[131, 151]. Nup98 and Nup96 form a binding interaction through the SLIM domain of Nup98, which is located in the unstructured region of Nup98 (Fig. 2.22). This direct interactions tethers Nup98 to the NPC as part of the Y-complex[152]. Furthermore, since Nup98-96 is a fusion, these proteins are not discriminated as individual proteins by Proteome Discoverer. The easiest way to determine presence or absence of Nup96 within the Nup214 pulldowns would be to analyze all Nup98-96 peptides. Nup96 was confirmed to be present in Nup214 MS data, but at very low levels (data not shown). By analyzing depletion of Nup98-Nup96 peptides, we can also gain insights into how specific 2A proteolytic activity is, or whether it could spread to neighboring Nups.

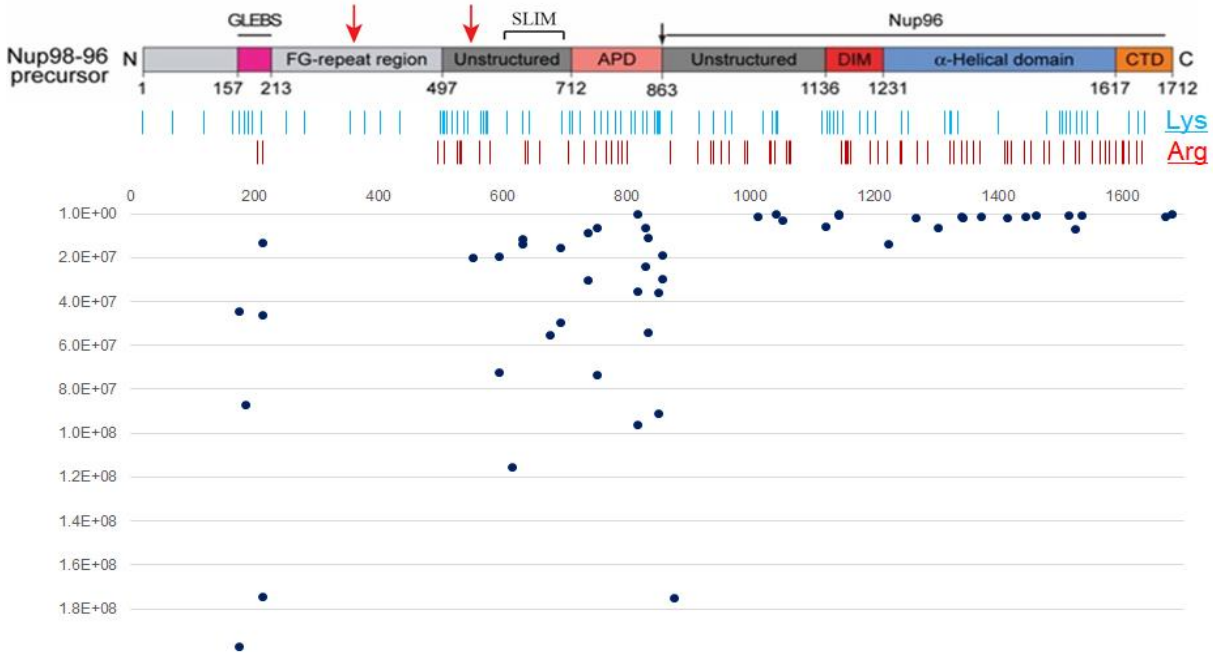

Figure 2.22. Nup98-96 peptides plotted against secondary structure and assessed for depletion during 2A^{pro} expression

Nup98 is translated as a bicistronic fusion with 96 and separated into individual proteins by the autoproteolytic domain (APD). We plotted all identified Nup98-96 peptides along the secondary structure of the fusion protein (X-Axis), and observed depletion of Nup98 peptides during 2A^{pro} expression as measured and plotted along Y-axis, peptides located further down are more depleted). Nup98 peptides identified by MS localized to the major structured regions of Nup98. Red arrows indicate putative cleavage sites for 2A^{pro}[109]. Adapted from Ren et al[131].

Once we organized the Nup98-96 peptide data, we plotted all identified peptides along the length of the fusion protein. We transformed the data by averaging Nup98-96 peptides from Nup214 pulldowns with GFP and 2AC110A, and assessing peptide depletion within the $2A^{pro}$ expressed dataset (Fig. 2.22). We observed that Nup98 peptides were localized at discrete regions that overlap with structured domains, the GLEBS motif, the APD, as well as the C-terminal "unstructured" region that is responsible for Nup98 binding to the NPC[153]. Such peptide localization was likely due to Trypsin preferably cleaving Lys/Arg residues in more structured parts of Nup98. We also detected enormous depletion of Nup98 peptides within Nup214 pulldowns in the presence of $2A^{pro}$. Nup96 peptide levels were unaffected, which is in line with $2A^{pro}$ performing surgical and specific cleavages against solely Nup98 and not neighboring NPC components despite their proximal availability.

2.4 FG-Nup affinity capture with Dynabeads conjugated to polyclonal antibodies

In a similar manner to the Nup214 pulldown, we also assayed 2AC110A association to Nup98 during FG Nup affinity capture experiments. mAB414 are polyclonal antibodies specific to FG repeats, normally utilized for immunoblot or immunofluorescent detection of Nups[154]. mAB414 were conjugated to magnetic Dynabeads (Samson Obado, Michael Rout, unpublished data) and used for an immunoprecipitation experiment (n=1). Nup98 was found depleted by SDS-PAGE and immunoblot (Fig 2.23b) during $2A^{pro}$ expression. 2AC110A, but no other GFP signal, was observed associating with FG Nups, reiterating the interaction affinity of the 2A protease for Nup98. Unfortunately, due to the coronavirus outbreak and prioritization of the MS data analysis pipeline for Covid-19 related research, we did not attempt additional replicates of the FG Nup pulldowns.

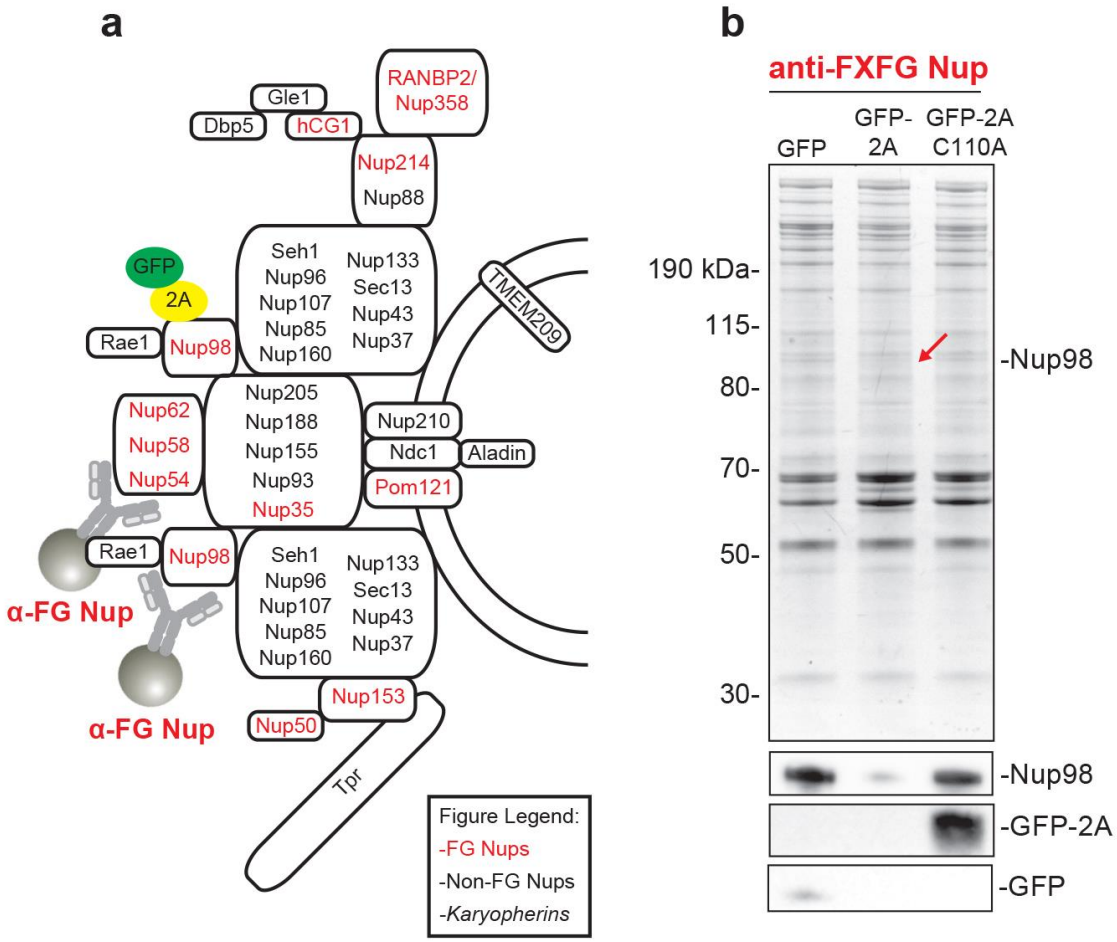

Figure 2.23. FG Nup pulldowns during protease expression.
a, mAB414 polyclonal antibodies were utilized to immunoprecipitate FG Nups in cell powder from HeLa stable cell lines expressing our proteins of interest. **b**, Eluates were assayed by SDS-PAGE (top gel) and immunoblotting (GFP, Nup98). Nup98 is depleted from FG Nup pulldowns during $2A^{pro}$ expression. GFP-2AC110A is detected, enormously enriched over GFP, further supporting $2A^{pro}$ and 2AC110A as direct Nup98 binders. 100 mg of cryomilled powder was lysed in 20 mM HEPES, pH. 7.4, 300 mM NaCl, 0.5% Triton X-100.

2.5 Efforts to validate interactomic data through biochemistry and cell biology

We sought out to further validate our interactomic data and identified 2AC110A interacting partners through a diverse array of experiments. We assayed cell culture and biochemical methodology, such as putative chemical inhibitors (Section 2.5.1) of $2A^{pro}$ catalytic activity, chemical crosslinking to identify residues involved in binding interactions (Section 2.5.2), as well as siRNA knockdowns of eIF3L to assay any measurable effect on eIF4G cleavage (Section 2.5.3). These efforts unfortunately did not pan out, but are nonetheless important to discuss as they present promising methodology to pursue.

2.5.1 Assaying $2A^{pro}$ peptide inhibitor

From the onset of our project, we were keen on assaying a $2A^{pro}$ chemical inhibitor, if one existed. Many such small chemical and peptide inhibitors have been identified for $3C^{pro}$, but

efficient compounds against $2A^{pro}$ are scarce[72, 155]. A $2A^{pro}$ inhibitor would also be interesting by helping determine whether $2A^{pro}$ catalytic activity played a role in the discrepancy between datasets in eIF3 protein accumulation, among many applications in cell culture experiments. zVAM.fmk was reported as an inhibitor of HRV2, -14, and -16 $2A^{pro}$, as measured by decreased viral replication, lack of caspase inhibition, and decreased eIF4G depletion[156]. zVAD.fmk is a known Caspase-9 inhibitor often utilized in picornavirus research to reduce Caspase mediated cleavage[88, 108, 157]. The fluoromethyl ketone (fmk) group facilitates cellular incorporation of the tri-peptide inhibitor and improves targeting[158].

Unfortunately, zVAM.fmk was not commercially available, so we commissioned the Proteomics core facility (Henry Zebroski III, The Rockefeller University), to chemically synthesize it. It was prepared and purified by HPLC to 97% purity (data not shown). We induced protease production in our HeLa stable cell lines expressing $2A^{pro}$ and $2A^{pro}$ after addition of zVAM.fmk (dissolved with DMSO to a stock concentration of 200 μM prior to addition to cell culture) to assay whether the peptide could inhibit eIF4G or Nup98 cleavage as reported (Fig. 2.24). Unfortunately, our *in vivo* assay showcased nominal reduction in eIF4G cleavage, suggesting zVAM.fmk is unlikely to be useful during immunoprecipitation experiments designed to capture wild type $2A^{pro}$ binding partners.

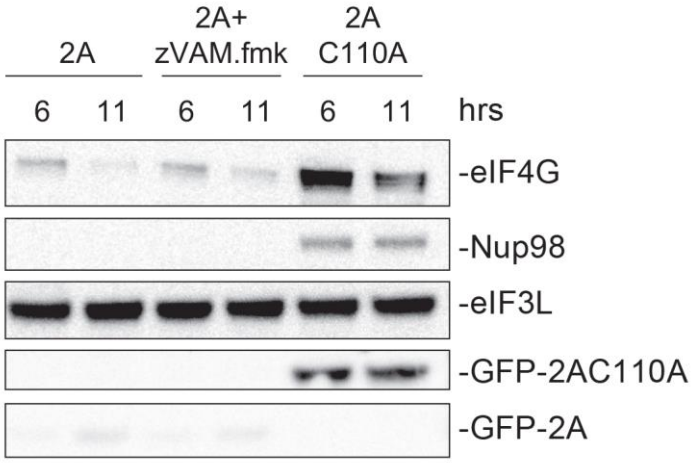

Figure 2.24. Assaying reduction of $2A^{pro}$ cleavage with peptide inhibitor zVAM.fmk. zVAM.fmk was assayed as a putative peptide inhibitor of $2A^{pro}$. HeLa stable cell lines were seeded, and induced for protease production. 2 hours prior to induction, z.VAM.fmk was added to cell culture to incubate and absorb the peptide inhibitor. Cells were collected and lysed at 6 and 11 hours post-induction and lysates were assayed by immunoblot. Unfortunately, eIF4G cleavage was barely, if at all, abrogated by addition of the peptide inhibitor.

2.5.2 Attempting to validate GFP-2AC110A interactions with eIF3 and Nup98 through chemical crosslinking

To validate direct interactions between catalytically inactive 2A protease and its purported binding partners within the eIF3 complex, we assayed on-bead chemical crosslinking during affinity capture experiments. Disuccinimidyl suberate (DSS) is an established crosslinker utilized by the Chait and Rout groups for interactomic studies[159]. DSS is composed of an 8-carbon spacer arm, with N-hydroxysuccinimide (NHS) groups on both ends that react with primary amines on amino acids (such as Lysine or Arginine side chains). We conducted crosslinking during affinity

capture experiments with GFP-2AC110A with three orders of magnitude of DSS in an attempt to capture 2AC110A-eIF3L/Nup98 complexes (Fig. 2.25a). Any putative complexes would be analyzed by MS and subsequently characterized to identify putative amino acids located closely to the molecular interface involved in complex formation. Eluates were assessed by SDS-PAGE and immunoblotting to track depletion of the handle and interacting protein. Even at the lowest concentration of DSS, we saw significant depletion of interacting proteins in the eluate, which can be interpreted as a change in migration due to those proteins forming complexes that are too large to be detected in the gel at assayed molecular weights. Such a result is generally expected for crosslinking experiments. However, we also observed relatively low depletion of 2AC110A itself, prior to using the highest concentrations of DSS (Fig. 2.25a). This is not entirely unprecedented, given DSS crosslinking depends on exposed amine groups, of which $2A^{pro}$ has relatively few.

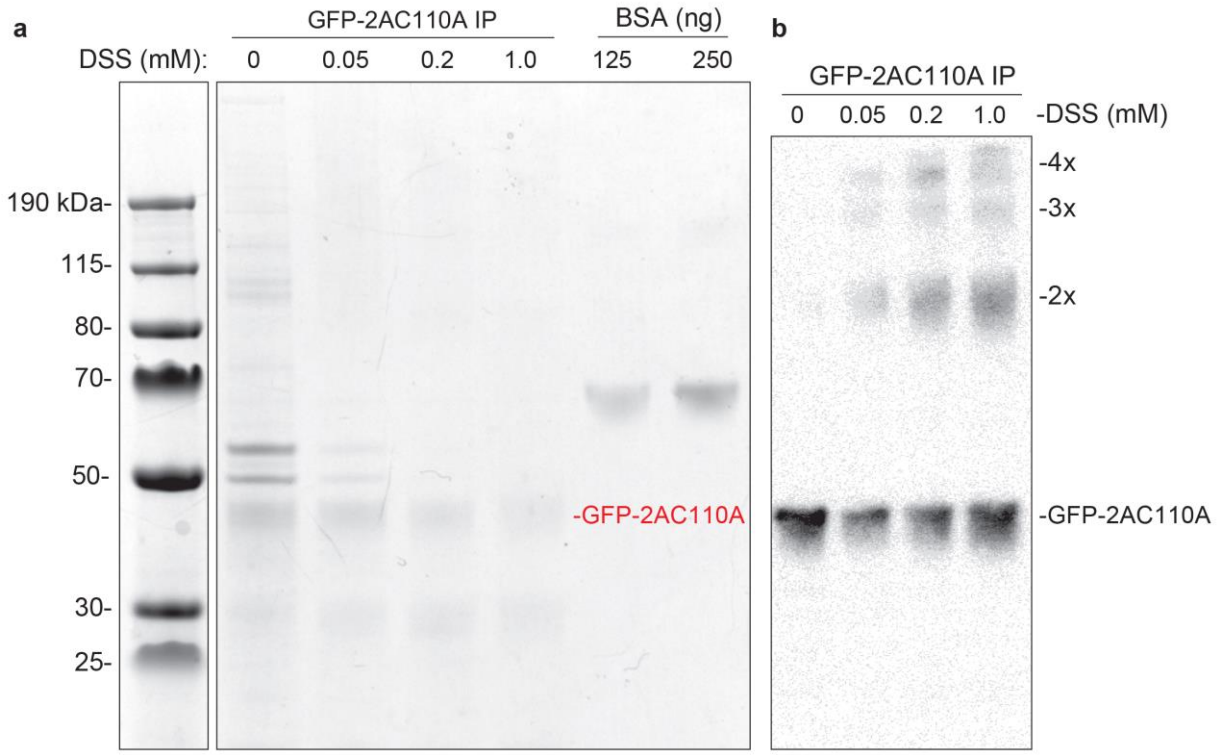

Figure 2.25. Assaying DSS crosslinking during GFP-2AC110A pulldowns.
GFP-2AC110A pulldowns combined with DSS crosslinking to assay direct interactions between the protease and binding partners. **a**, Interacting proteins disappear from detectable range of the SDS-PAGE during DSS crosslinking as a result of formation of large complexes. However, 2AC110A itself does not seem to deplete as rapidly as other proteins despite DSS concentration increases. **b**, immunoblot analysis of GFP signal of the same samples reveals minimal depletion of 2AC110A, as well as potential oligomerization of 2AC110A from self-crosslinking.

We also assayed DSS mediated crosslinking and protein depletion from detectable range by immunoblot, with antibodies targeting GFP-2AC110A (Fig. 2.25b). The immunoblot data correlated with observable SDS-PAGE results. GFP-2AC110A levels dropped only marginally, despite increasing concentrations of DSS. Interestingly, during DSS crosslinking, GFP immunoblotting detected bands corresponding in molecular weight to oligomerization of GFP-2AC110A (~90 kDa, ~135 kDa, ~180 kDa). There is some evidence that 2AC110A can

dimerize[160], supporting the potential idea that DSS crosslinking facilitates 2AC110A oligomerization. Altogether, SDS-PAGE and immunoblot analysis suggest that 2AC110A may not be easily incorporated into crosslinked complexes. That is not to suggest that 2AC110A crosslinking by DSS does not result in covalent bonds formed between 2AC110A and interacting partners (at highest DSS concentrations). However, direct crosslinks would be expected to be few in number, necessitating a significant scale up in immunoprecipitation and crosslinking. I previously attempted scaled-up pulldowns on 500 mg cell powder (100 mg is the usual), with poor results (data not shown), suggesting scale-ups of pulldowns can be problematic. In addition, such experiments would use up an enormous quantity of precious cell powder, for potentially little gain. As such, we did not pursue larger scale DSS crosslinking experiments to assay residues involved in direct binding to 2AC110A.

2.5.3 Analysis of siRNA knockdown of eIF3L on 2A^{pro} cleavage activity

We aimed to further prove the hypothesis of eIF3L and the eIF3 complex serving as a piggybacking site for 2A^{pro}-mediated cleavage of eIF4G. We reasoned that if we could decrease eIF3 complex formation or prevent translation initiation functions, we might be able to decrease eIF4G cleavage. We initially aimed to achieve this inhibition through small compounds, but unfortunately, none were available specifically for eIF3. Chemical screens that lowered picornaviral replication and infection yielded a variety of inhibitors, almost all of which targeted MAPK signaling further upstream of translation initiation[161].

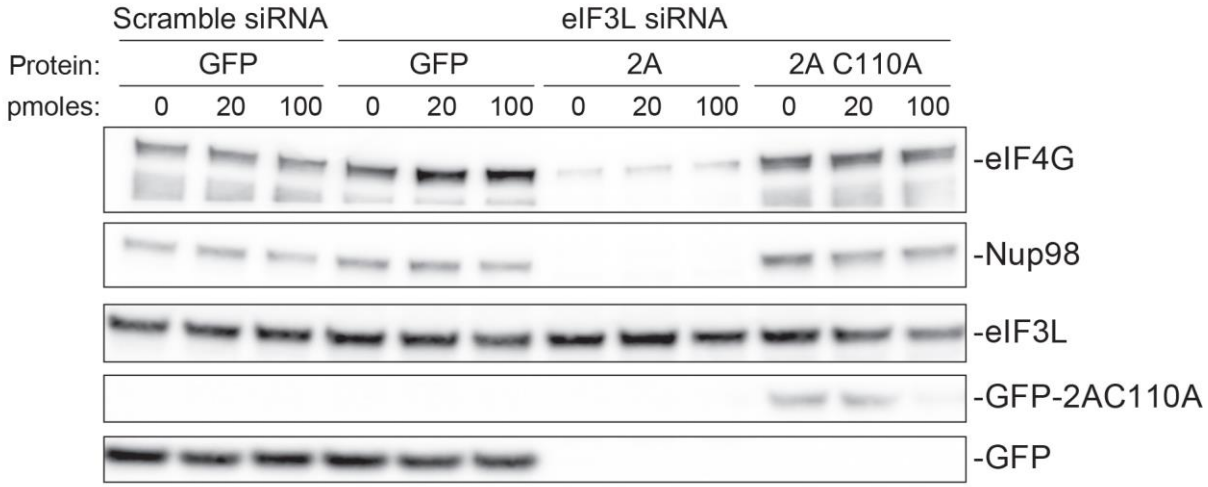

Figure 2.26. Western Blot analysis of siRNA knockdown of eIF3L and downstream effects on 2A^{pro} mediated cleavage of Nup98 and eIF4G.
Stable HeLa cell lines were transfected with either scramble or eIF3L siRNA cocktails (0, 20, or 100 pmoles of RNA) to investigate whether depletion of eIF3L would mitigate eIF4G 2A^{pro} mediated degradation. After completing the RNAi protocol as per Dharmacon instructions, we induced expression of our proteins of interest, collected cells, and prepared lysates for analysis by immunoblot. We assayed protein levels of GFP, eIF3L, Nup98, and eIF4G.

Without any chemical compounds available for use, we instead elected to decrease eIF3L levels through siRNA knockdowns of the gene. We ordered an siRNA cocktail from Dharmacon, as well as scrambled siRNA controls which were conjugated to Cy3 to function as transfection

controls. We transfected siRNAs with Dharmafect 4, as per manufacturer instructions, at three concentrations. After siRNA transfection and 72 hours of RNAi, we validate transfection efficiency by checking cells with Scramble siRNA-Cy3 under fluorescence microscopy. Almost all cells fluoresced at the Cy3 channel, confirming the efficacy of our siRNA transfection protocol (data not shown). We subsequently induced expression of our proteins of interest for 12 hours, and collected cell material for preparation of lysates for immunoblotting (Fig. 2.26).

Immunoblot analysis suggested that eIF3L proteins levels decreased by ~20-50% (Table 2.2) with the highest assayed siRNA amount (100 pmoles) in each assayed cell line. However, this protein level decrease was not as high as we were anticipating. We can detect a minor decrease in $2A^{pro}$ mediated degradation of eIF4G in $2A^{pro}$ expressing cells under maximum eIF3L knockdown (eIF4G protein nearly doubles in 100 pmoles sample compared to 20 pmoles of siRNA). However, we also observed a decrease in GFP and GFP-2AC110A expression in 100 pmole siRNA transfected samples, which suggested that knocking down eIF3L protein levels lowers translation of proteins. Presumably, lower protein translation levels resulting from eIF3L knockdown would further decrease the already barely detectable $2A^{pro}$ translation. Even if eIF4G degradation was mitigated by lack of eIF3L, it would be challenging to attribute this observation to a decreased availability of eIF3L piggybacking sites for $2A^{pro}$ since, alternatively, depletion of a key initiation factor could lower translation of $2A^{pro}$.

Table 2.2. Quantification of eIF3L protein amounts after siRNA mediated knockdown of expression.

Cell line	siRNA	pmoles siRNA	Fraction of eIF3L
GFP	Scramble	0	100%
GFP	Scramble	20	101%
GFP	Scramble	100	109%
GFP	eIF3L	0	100%
GFP	eIF3L	20	93%
GFP	eIF3L	100	80%
2A	eIF3L	0	100%
2A	eIF3L	20	113%
2A	eIF3L	100	87%
2AC110A	eIF3L	0	100%
2AC110A	eIF3L	20	76%
2AC110A	eIF3L	100	56%

We quantified eIF3L protein depletion during siRNA knockdowns utilizing ImageJ software. eIF3L protein levels decrease only with eIF3L-specific siRNA cocktails; marginally during 20 pmole RNA transfections, and more significantly during transfection of 100 pmoles of RNA.

2.6 Studying localization changes during $2A^{pro}$ expression

It is well established that during the course of picornavirus infection, $2A^{pro}$ expression directly affects nuclear-cytoplasmic protein and RNA transport[106, 109, 162]. The underlying hypothesis is nuclear-localized proteins that promote picornaviral replication, such as by facilitating formation of an IRES for translation, need to relocalize to the cytosol. This relocation is driven through specific cleavage of NPC components, such as Nup98[163, 164]. To investigate picornaviral mediated protein relocalization, we developed a cellular fractionation technique that

can accurately and effectively separate the nuclear and cytoplasmic fractions of mammalian cell lines.

2.6.1 Nuclear and cytoplasmic fractionation of HeLa cells during $2A^{pro}$ expression

HeLa stable cell lines integrated with the $2A^{pro}$ and 2AC110 were grown in 100 mm dishes and induced to overexpress proteins overnight. Cells were fractionated as per provided protocol (Fig. 4.12) and fractions were assayed by SDS-PAGE and immunoblotting (Fig. 2.27). In this experiment, we only separated cells into Cytoplasmic and Nuclear fractions. By SDS-PAGE, samples looked very similar, aside from minor accumulation of a lower molecular weight protein in the cytosol of $2A^{pro}$ expressing cells. Within nuclear fractions, between 10-15 kDa molecular weight, one can also observe Histones (Fig. 2.27a). By immunoblotting several biological replicates of fractionation experiments, we assayed and analyzed the localization state of a number of proteins during $2A^{pro}$ mediated cleavage of Nup98, such as other NPC components, cell fraction markers, translation factors, transcription factors, and other proteins (Fig. 2.27b).

Our experiments confirmed that a cytosolic control protein, GAPDH[165], does not contaminate the nuclear fractions, while also confirming equal gel loading. Two other proteins can serve as nuclear markers. The first is Lamin A/C, is a filamentous protein that localizes to the inner face of the nuclear envelope (and maintains nuclear structure there)[166]. The second is ASH2L, a Histone Lysine Methyltransferase[167]. That said, while minor levels of Lamin A/C are normally observable in cytoplasmic fractions due to the extreme sensitivity of the antibody used during immunobloting, $2A^{pro}$ expression seems to significantly increase Lamin A/C accumulation in the cytosol. Such cytoplasmic accumulation of Lamin is can be explained in two ways. It is possible that a small fraction of $2A^{pro}$ producing cells underwent apoptosis, or are sufficiently far along the apoptotic signaling pathway, such that the cells' nuclei leak Lamins[123, 168].

Alternatively, it is possible that $2A^{pro}$ mediated cleavage of Nup98 has inhibited specific transport pathways, such as Importin-α/β, that mediate the passage of newly translated Lamin A/C proteins to the nucleus. Similar cytoplasmic accumulation can also be observed with H3, which is predicted to be shuttled by Importin- α's, but mostly IPO4[169, 170]. While the idea that apoptosis increases nuclear protein accumulation in the cytosol is plausible, it should also be reflected by consistent and even distribution of other nuclear-localized proteins in the cytosol[168]. However, Nups85, 153, 205, and 214 can be observed to barely accumulate in any of the cytoplasmic fractions, suggesting that cytoplasmic build up in $2A^{pro}$ producing cells is more likely to be mediated through Nup98 degradation and downstream effects on import pathways. Potentially, targeted depletion of Nup98 may lead to a limited breakdown of the passive diffusion barrier, which is exacerbated during cellular fractionation and its effects more prevalent with smaller molecular weight proteins diffusing out of the nuclear fraction[35, 38]. However, passive diffusion across the NPC is limited to proteins with MWs of ~40-kDa or smaller[38], and Lamin A/C migrates at ~60-70 kDa. Given our data, we suspect that Nup98 depletion has a minor but significant impact on nuclear import, resulting in some nuclear-localized proteins, such as Lamin A/C and Histones H3 and H2A.Z, accumulating in the cytoplasmic fraction during translation.

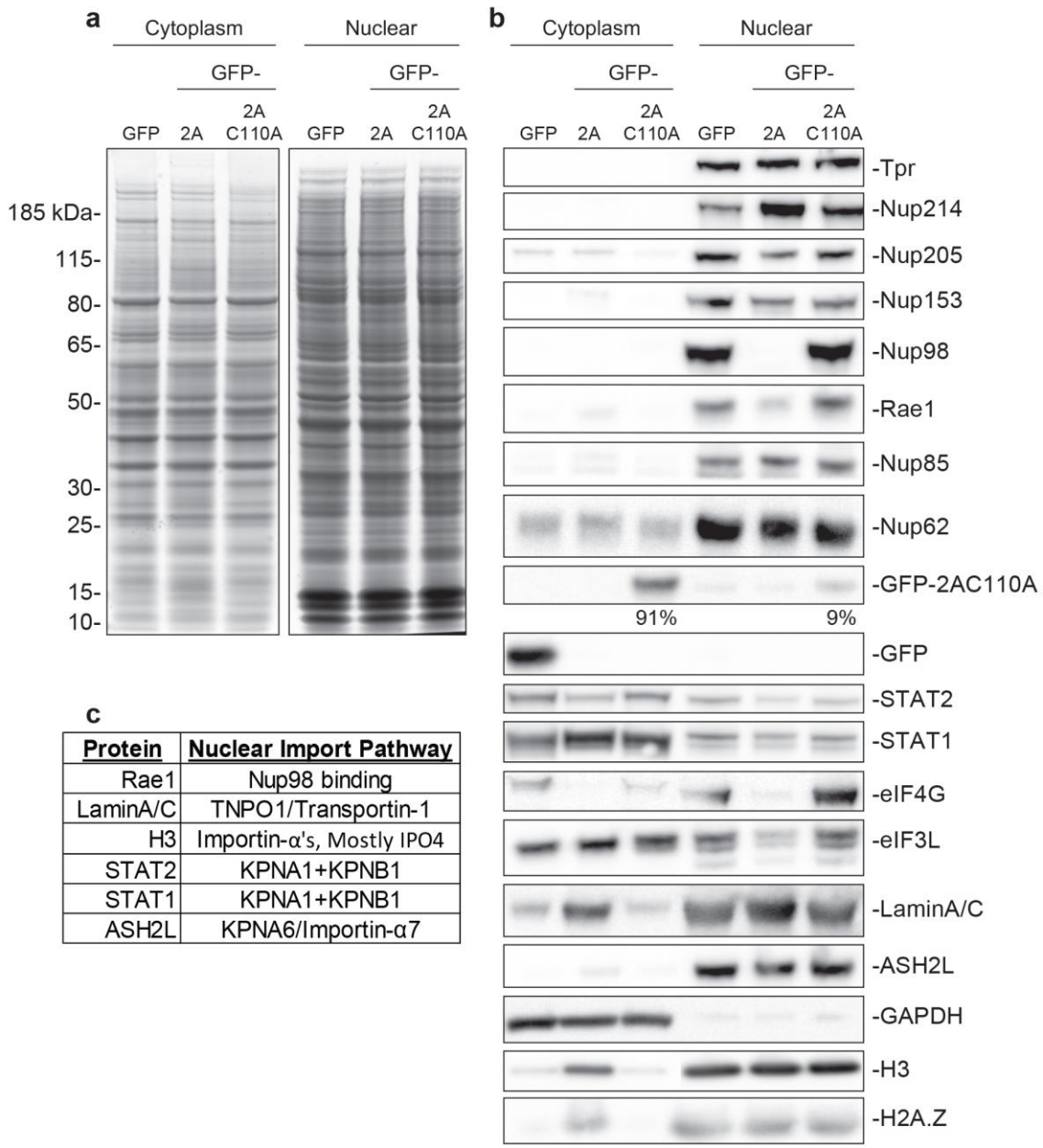

c

Protein	Nuclear Import Pathway
Rae1	Nup98 binding
LaminA/C	TNPO1/Transportin-1
H3	Importin-α's, Mostly IPO4
STAT2	KPNA1+KPNB1
STAT1	KPNA1+KPNB1
ASH2L	KPNA6/Importin-α7

Figure 2.27. Biochemical fractionation of cells expressing 2A^{pro} and 2AC110A.
HeLa stable cell lines induced to produce proteases of interest were biochemically fractionated into nuclear and cytoplasmic fractions and assayed by SDS-PAGE (**a**) and Western Blot (**b**). **a**, coomassie staining of both fractions, from each cell line, revealed global similarity between fractions under ectopic protein expression. **b**, immunoblot analysis revealed nominal changes to Nup localization. We can observe 2A^{pro} mediated cleavage of Nup98 resulted in Rae1 depletion from the nuclear fraction and subsequent accumulation in the cytosol. Furthermore, we can detect 2AC110A localization in the nuclear fraction, likely through direct interactions with Nup98. **c**, curated list of proteins observed more noticeably enriched in the cytoplasmic fraction in response to 2Apro catalytic activity. Rae1 specifically associates with Nup98 and localizes in the NPC through direct reside interactions. Other proteins are predicted to shuttle through the NPC by a variety of import proteins predicted to be related to Nup98[163, 169-171].

NPC components assayed by immunoblot largely remained in the nuclear fraction. However, Nup98 is observed as totally degraded during $2A^{pro}$ expression, which unsurprisingly led to relocalization of Rae1 from the nuclear fraction to the cytosol. We can observe a portion of total 2AC110A localizing to the nucleus, likely due to direct interactions formed between 2AC110A and Nup98; regular GFP signal was entirely localized to the cytoplasm. We can also observe a decrease of eIF3L in the nuclear fraction of $2A^{pro}$ producing cells, and a corresponding increase in the cytoplasm, matching a similar pattern of de-localization observed with Rae1. While the majority of eIF4G is found associated with translation units and ribosomes along the ER, some can be detected in the Nuclear Fraction from ribosomes localized to the cytoplasmic surface of the Nucleus[172]. eIF4G is cleaved during $2A^{pro}$ expression, and we can observe a total depletion of any nuclear localized eIF4G; we suspect a depletion of eIF4G in the nuclear fraction results in mislocalization of associated translation factors, such as eIF3L. Finally, we observe $2A^{pro}$ mediated relocalization of STAT1 to the cytosol, which is in-line with previously published literature on SARS-Cov-2 Orf6 hijacking Nup98 function and similarly blocking STAT nuclear import[173]. STAT2 levels decreased during $2A^{pro}$ expression in both fractions, suggesting there may be a mechanism during picornaviral infections to reduce this signaling pathway. Abrogating STAT1 and STAT2 localization to the nucleus, and subsequently affecting their function as transcription factors, is yet another strategy employed by viruses to prevent host cells from responding to infections[163, 173]. STAT1 and STAT2 play a key regulatory role in signal transduction of genes normally activated through the interferon pathway. Shutting off STAT signaling by preventing nuclear import provides picornaviruses with yet another mechanism of subverting host response to infection.

2.7 Analysis of protease induced changes on nuclear-cytoplasmic transport in HeLa cells

Cellular fractionation is a useful tool for studying $2A^{pro}$ induced wholesale changes between cytoplasm and nuclear fractions, for example, which proteins are enriched in the cytoplasm during $2A^{pro}$ expression. We supplemented our studies of nuclear-cytoplasmic localization of proteins with more specific assays designed to interrogate the actual transport mechanics during $2A^{pro}$ mediated cleavage of Nup98 and disruption of associated transport pathways. This task was accomplished with the use of fluorescent-NLS/NES tagged reporters[70, 174]. Some canonical NLS and NES tags are sufficiently well characterized that we know which transport factors mediate their transport. However, there are many non-canonical localization signals that are interesting to interrogate with our stable cell line system.

2.7.1 Localization of expressed proteins of interest in HeLa stable cell lines

We initiated fluorescence imaging experiments by establishing localization of our ectopically expressed proteins in HeLa stable cell lines. We induced protein production, and after overnight induction we observed GFP fluorescence by live cell imaging (Echo Revolve Microscope). GFP production and localization was unsurprisingly ubiquitous and without any cellular stress, GFP spread across the entire cell (Fig. 2.28). GFP-2AC110A was observed in the cytosol, with elevated intensity at the edge of the nucleus, reminiscent of the 2AC110A enrichment to Nup98 at the NPC. GFP-$2A^{pro}$ did not localize anywhere in the cell, with signal focused on small speckle-like dots throughout cells. Published literature would suggest these speckles to possibly be P-bodies[175, 176]. Furthermore, it is challenging to interpret this localization because

immunoblot analysis reveals that GFP-2A^{pro} undergoes self-cleavage, with GFP being excised off the fusion protein.

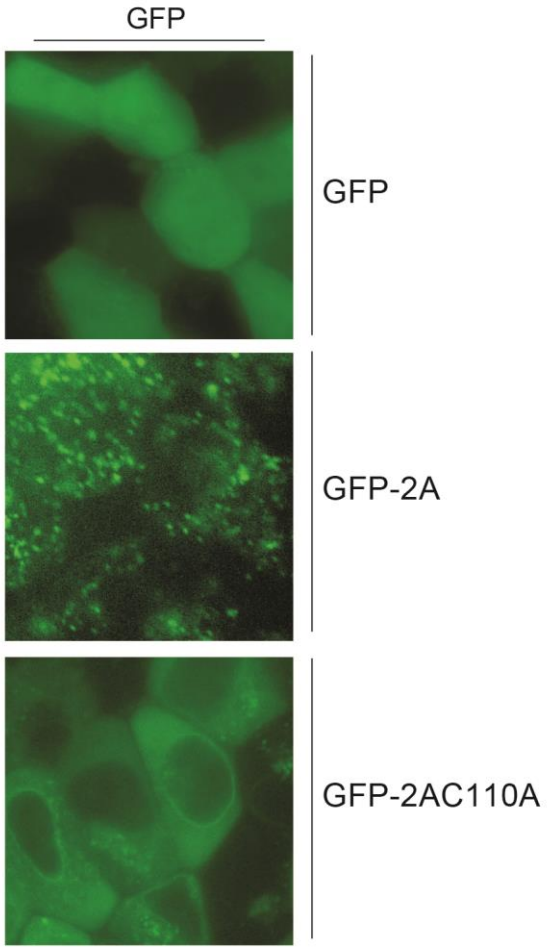

Figure 2.28. Localization of 2A^{pro} and 2A^{pro}C110A during protein expression.
GFP, GFP-2A, and GFP-2AC110A are inducibly expressed in HeLa stable cell lines and cells are imaged under GFP fluorescence (as live cells). GFP signal distributes evenly across a cell. GFP-2A^{pro} forms small speckles that may be P-bodies or stress granules[176]. GFP-2AC110A localizes to the cytoplasm and enriches on the rim of the nucleus, presumably via Nup98-2AC110A interactions.

2.7.2 2A^{pro} induces localization changes of mRNA

Rae1 is well characterized as a shuttling mRNA export factor directly bound to Nup98 through WD40-GLEBS motif interactions[130]. Given its predominant role in RNA export, we expected 2A^{pro} mediated cleavage of Nup98 and subsequent mislocalization of Rae1 to have significant and observable effects on mRNA localization in cells. We used a published protocol to develop a poly-T Fluorescent *in situ* hybridization (FISH) stain to assay 2A^{pro} mediated effects on mRNA localization[163] (Fig. 2.29).

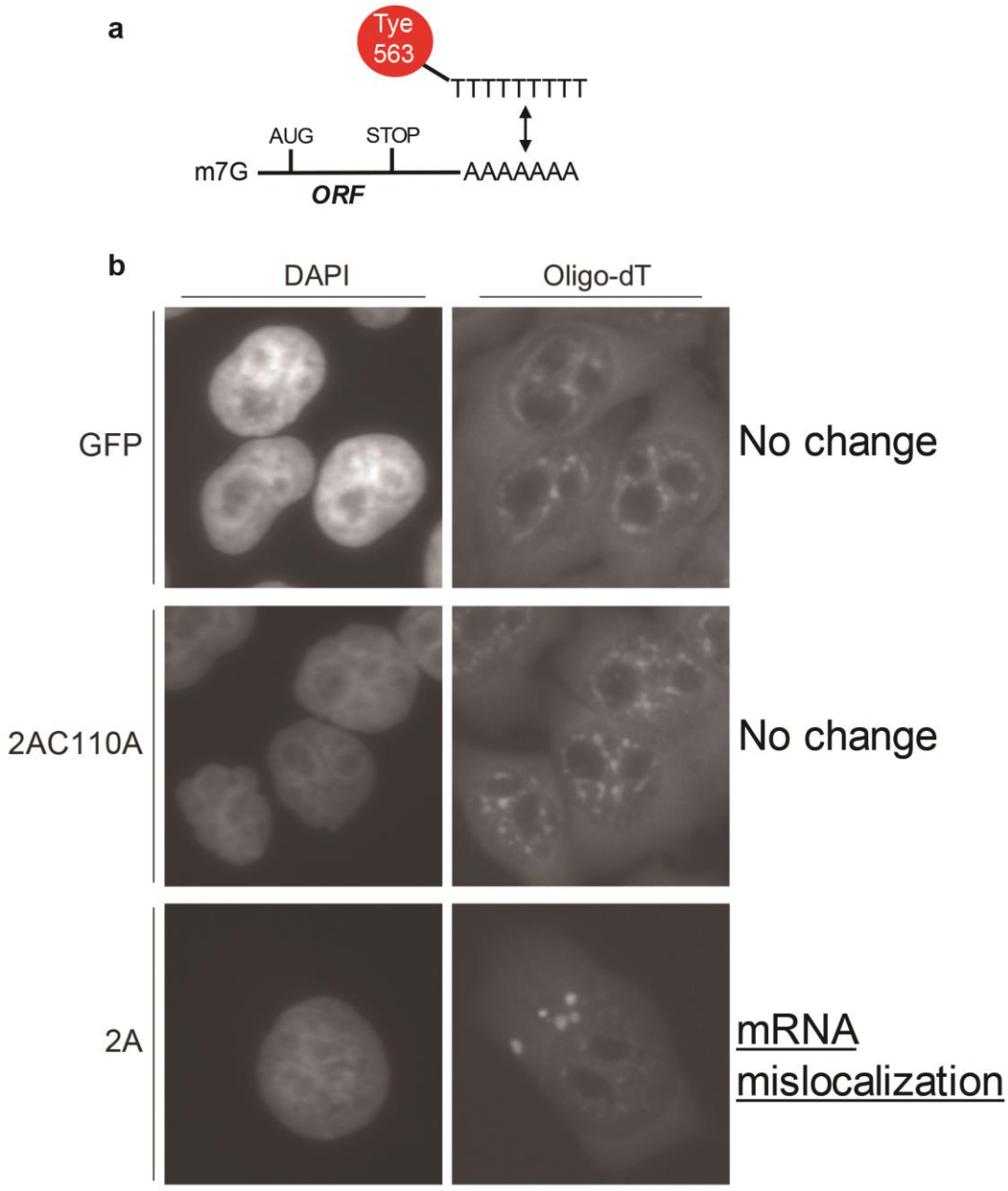

Figure 2.29. 2A^{pro} induces localization changes of mRNA.
HeLa stable cell lines were induced to express our genes of interest, and cells were subsequently processed through the poly-T FISH protocol to assay mRNA localization. **a**, probes with ~30 Thymidines and a 5'-Tye563 dye were chemically synthesized by IDT. These probes bind directly to the poly-A tail of mRNA, allowing us to visualize mRNA localization in cells. **b**, mRNA localization was unchanged during GFP or GFP-2AC110A expression, but was significantly impacted during 2A^{pro} expression. Poly-T FISH signal is slightly decreased in during 2A^{pro} expression and a major change in mRNA localization can be observed.

Indeed, expression of GFP or GFP-2AC110A had no effects on RNA localization, with the majority of signal localizing throughout the cytosol, and as small speckles surrounding the

perimeter of the nucleus. Meanwhile, $2A^{pro}$ production and cleavage activity has a major impact on mRNA localization, with poly-T FISH signal forming fewer, but slightly larger speckles reminiscent of P-bodies or stress granules[175, 177]. Smaller speckles of signal normally distributed throughout the nucleus mostly disappear. $2A^{pro}$ expression also seems to have some effect on overall mRNA signal, with preliminary quantifications showing a ~15% reduction compared to GFP and 2AC110A expressing cells. Signal reduction was assessed by measuring the signal per cell, and comparing the average signal levels (n=5, analyzed with ImageJ, data not shown).

2.7.3 $2A^{pro}$ induces localization changes in GFP_2 reporters

SV40 NLS is transported to the nucleus by Importin α/β, while the PKI NES operates through Crm1/Exportin-1[178]. In published literature, both of these export and import pathways were demonstrated to be impacted by $2A^{pro}$ production and catalytic activity[70]. We assayed stable HeLa cell lines constitutively expressing GFP_2-NLS/NES fusion proteins to validate published literature describing $2A^{pro}$ mediated relocalization of such reporters with transient transfection of GFP-$2A^{pro}$ and GFP-2AC110A (Fig. 2.30). Note, that while both sets of signals are "GFP" and otherwise emit light on the same wavelength, the GFP_2 reporters are Enhanced GFP (eGFP), while the proteases' tagged GFP is the original fluorescent protein. The eGFP signal output is over 50-fold greater than regular GFP[179]. Side-by-side comparisons demonstrated GFP production did not interfere with the eGFP reporter protein signals (data not shown), thus allowing us to use these validated reporters.

GFP_2-NES normally localizes to the cytosol with higher intensity fluorescent signal around the nuclear rim. However, during $2A^{pro}$ expression we observed a significant signal increase in the nucleus as the GFP fusion more evenly distributed throughout the cell (Fig. 2.30). 2AC110A production had no impact on localization of the GFP reporter, confirming that the catalytic activity of $2A^{pro}$ triggered relocalization of the NES reporter. Nup98 is a cofactor for Crm1 dependent protein export, so it is expected that Nup98 depletion by $2A^{pro}$ leads to inhibition of Crm1 export of the GFP_2-NES reporter[180].

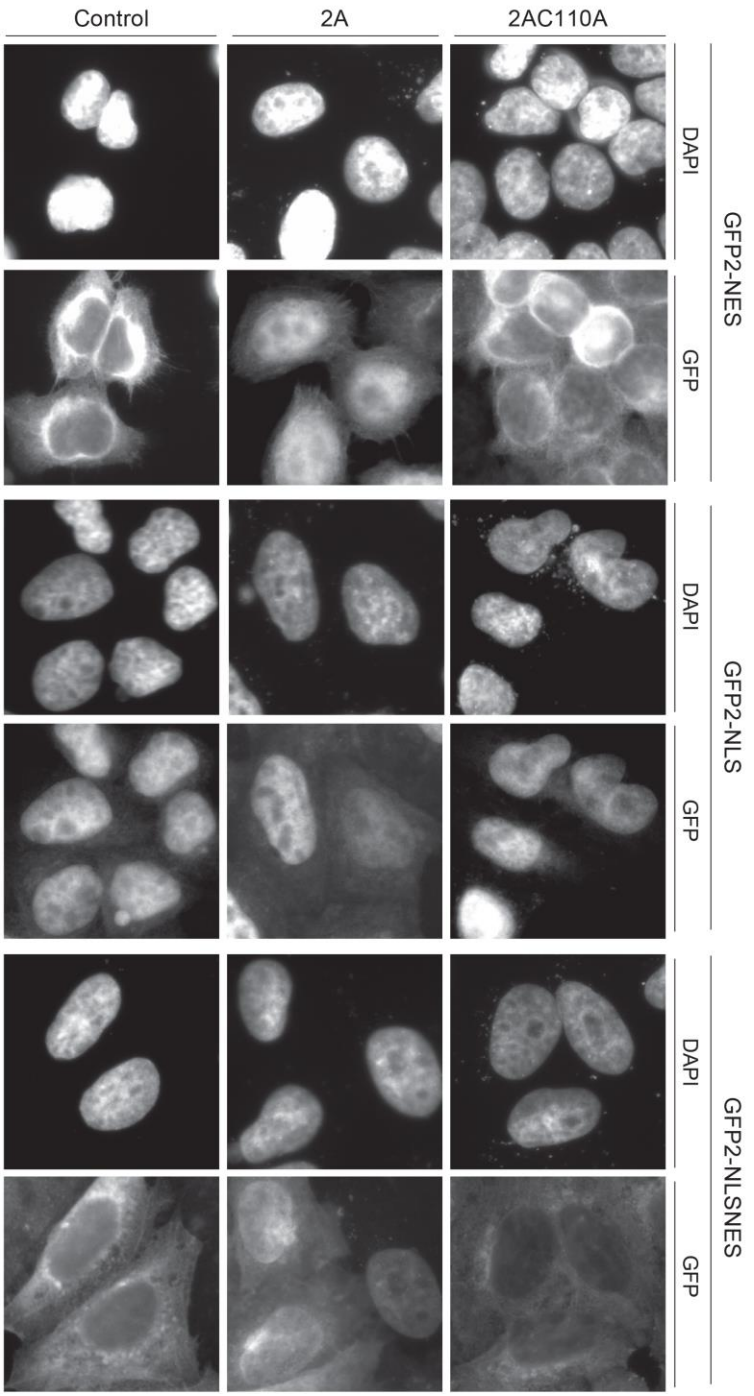

Figure 2.30. 2A^{pro} cleavage of Nup98 mediates relocalization of NLS and NES reporters. GFP_2-NLS/NES/NLSNES protein fusions are constitutively expressed in a HeLa stable cell line. GFP-2A and GFP-2AC110A were transiently transfected, expressed overnight (~14 hrs), and cells were subsequently treated as per immunofluorescence protocol. Control cells are untransfected cells to demonstrate the unperturbed signal. Cells were imaged under DAPI or FITC filters, with DAPI showcasing nuclear localization, and FITC demonstrating GFP_2 reporter localization during various protease production contexts.

GFP_2 with the SV40 NLS normally localizes to the nucleus, with weak GFP signaling detected in the cytoplasm. However, the non-nuclear GFP signal became marginally increased upon production of $2A^{pro}$, thus validating published data that Nup98 cleavage disrupts Importin α/β function and initiates relocalization of NLS reporters[70]. It is also observable that in this cell line and experimental context, the relocalization is not as rapid or intense as observed with NES mislocalization, within the timeline of the assay. A similar distribution pattern was also be observed with the GFP_2-NLSNES fusion reporter. Normally, this fusion protein localizes mostly to the cytosol, but it was found more in the nucleus during $2A^{pro}$ production, signifying to its import pathway being affected less than its export pathways by Nup98 depletion. This result is especially interesting because it supports the notion that $2A^{pro}$ activity does not disturb all transport pathways equally, but rather has differential targeting of particular pathways and potentially staggered temporal effects[70]. Based on our data, we propose that $2A^{pro}$ catalytic activity affects Nup98 mediated protein export more significantly than protein import.

2.7.4 $2A^{pro}$ mediated cleavage of Nup98 impacts localization of NLS-mCherry-LacZ reporters.

We were keen on further characterizing the effects of $2A^{pro}$ on nuclear-cytoplasmic transport and searched for relevant materials in published studies. In line with our idea, the Bieniasz laboratory reported on transport pathways affected during overexpression of an interferon-related protein. This laboratory was generous to share with us fluorescent reporters carrying non-canonical NLS sequences driving nuclear and cytoplasmic reporter localizations to different levels (Table 2.3)[181]. These fluorescent reporters contain an NLS-mCherry-LacZ fusion and are designed to be unaffected by passive diffusion because of to their larger size (~120 kDa, Fig. 4.6)[181].

Table 2.3. NLS constructs and expected localizations.

NLS	Localization
C-Myc	Nuclear
Nucleopasmin	Nuclear
HTLV-1 Rex	Cytoplasm/Nuclear
MX2	Nuclear

We utilized fluorescent reporters to determine localization during $2A^{pro}$ catalytic activity. This table presents used NLSs and their localization as seen in according to published literature[181].

We prepared new fusion proteins by replacing eGFP with an mCherry tag for fluorescent compatibility and utilized these reporters in transport assays. We transiently transfected our HeLa stable cell lines with each reporter and induced protease production to track $2A^{pro}$ dependent localization changes (Fig. 2.31). Given varied motif promiscuity towards Importins[182] and diverse NLS mechanisms, determining exact import and export mechanisms for each NLS reporter is extremely difficult. Nonetheless, this assay can detect and track changes in localization in response to $2A^{pro}$ catalytic activity.

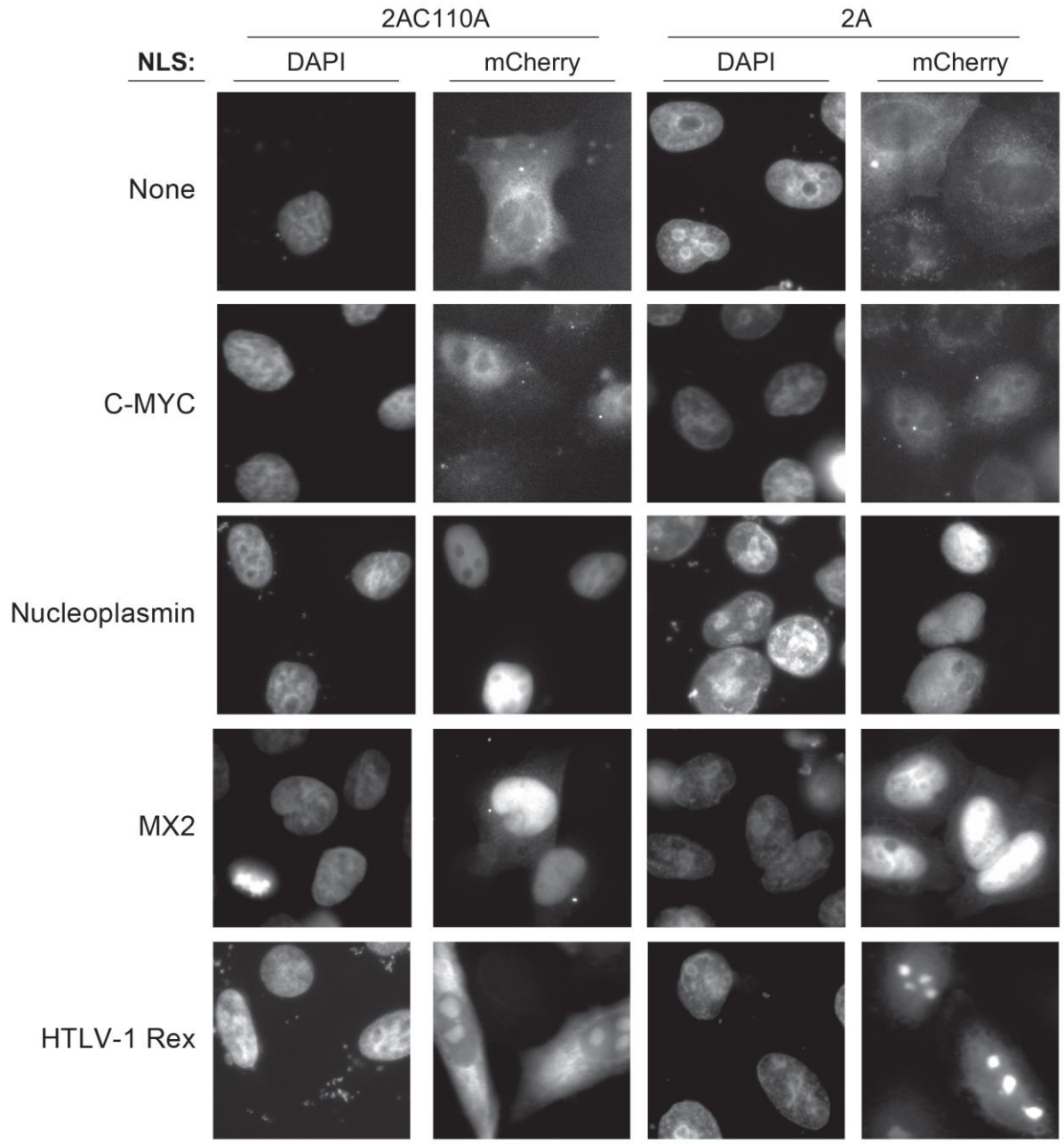

Figure 2.31. Localization of NLS-mCherry-LacZ reporters during 2A^{pro} production. Stable HeLa cell lines synthesizing GFP-2AC110A and GFP-2A^{pro} were transiently transfected with NLS-mCherry-LacZ reporters to characterize non-classical transport mechanisms. After 12-16 hours of reporter production, cells were induced to biosynthesize 2A^{pro} for 12-16 hours before ceasing cellular metabolism by fixing cells with formaldehyde[183]. Each NLS utilized in the assay is marked on the left side of the image. Both cell lines were imaged with DAPI for nuclear staining and mCherry for the fusion protein.

In our experiments, the mCherry control fusion protein lacking an NLS was found in the cytoplasm throughout the entire cell, but was not observed in the nucleoplasm (Fig. 2.31). This result was expected since the protein lacked a localization signal and was too large to passively

diffuse through the NPC. Addition of C-Myc NLS, predicted to bind Importin-α3[184], localized mCherry reporters to the nucleus. $2A^{pro}$ production did not affect the C-Myc reporter localization. Similarly, as expected from the published work[181], the Nucleoplasmin NLS localized reporters tightly to the nucleus. $2A^{pro}$ biosynthesis did not induce relocalization of the reporters, suggesting that Nucleoplasmin NLS-dependent import is also not affected by Nup98 degradation. Another NLS was derived from Human myxovirus resistance 2 (MX2). This protein is an interferon-induced inhibitor of HIV-1 infection that localizes to the nuclear envelope and blocks nuclear import of viral cDNAs[181, 185]. The N-terminus of MX2 contains an NLS-like motif that matches consensus of Proline-Tyrosine (PY) NLS sequences[186]. As expected, MX2 NLS-tagged reporters localized to the nucleus. $2A^{pro}$ gene expression did not affect localization, suggesting that Nup98 depletion has no impact on MX2 NLS localization.

The last NLS originated from Human T-cell leukemia virus type 1 (HTLV-1) Rex protein, a viral protein produced during infection of cells. Rex is a regulatory protein that promotes viral replication by exporting viral mRNA from the nucleus to the cytoplasm, where it is translated to produce HTLV-1 proteins[187]. The HTLV-1 Rex protein retains an NLS motif that localizes it to the nucleus, where the same NLS motif functions as an RNA binding domain (RBD) for the Rex-responsive element (RxRE) located at the 3' end of HTLV-1 mRNAs[188]. Rex NLS-tagged reporters were observed both in the cytosol and nucleolus of cells.[181] Given the Rex NLS's dual-function, these results can be explained by Rex NLS reporter predominantly binding endogenous mRNA. $2A^{pro}$ production breaks down reporter export and relocalizes the tagged fusion protein more predominantly to the nucleus.

$2A^{pro}$ mediated cleavage of Nup98 had nominal effect on the import of SV40 NLS (Fig. 2.30), and no effect on the import of C-Myc, Nucleoplasmin, and MX2 NLS reporters (Fig. 2.31). However, export of PKI NES reporters, as well as the HTLV-1 Rex NLS, was majorly impacted by protease mediated depletion of Nup98. This observation was further accentuated with the combined NLS and NES eGFP reporter (SV40 and PKI motifs), which was observed localized in the cytoplasm until $2A^{pro}$ mediated export breakdown drove the fusion protein into the nucleus. Together, our experiments with import and export reporters suggest that CVB3 $2A^{pro}$ surgically cleaves Nup98 to alter specific, predominantly export related nucleocytoplasmic transport pathways. Thwarting export of various proteins prevents infected cells from mounting a response to picornavirus infection through interferon or innate immune pathways. Our data further highlight that Nup98 mediated export is a convergent target among different viruses, with VSV[129], SARS-CoV2[163, 173], and Influenza viruses[189] all evolving unique ways to sabotage these transport pathways.

CHAPTER 3. Discussion

Picornaviruses is a large family of viruses evolved to target different hosts including humans. A genus of Picornaviruses called Enteroviruses is primarily responsible for most human-disease causing infections. According to the CDC (cdc.org), clinical symptoms and infection rates vary significantly. Milder respiratory infections, such as common cold associated symptoms, are typically caused by rhinoviruses, with infection rates numbering in millions annually across the world. Other picornaviruses, such as Coxsackievirsues and Echoviruses, are less common but, nevertheless, can cause significant breakouts, especially among children. Given the clinical importance of picornaviruses and their unique biological properties, these viruses pose an attractive research target to characterize replication and host subversion mechanisms.

Picornaviruses are intracellular parasites with an RNA genome and a replication cycle in the cytoplasm of infected host cells[14]. Picornaviruses, like many other viruses, evolved unique strategies to subvert host detection of the virus, mount an immune response, hijack host cellular machinery, and to promote viral replication[14]. Picornaviruses shut down many host functions including endogenous translation, innate immune responses, and import and export of proteins, RNA, and RNPs. Practically all of these effects are achieved through the catalytic activity of two viral proteins, the 2A and 3C proteases[4, 70]. The $2A^{pro}$ is especially crucial to picornaviral subversion of cellular machinery as it directly cleaves eIF4G[29, 80-85], a critical component of translation initiation, and Nup98[29, 106], a key FG-Nup and protein mediating mRNA export across the NPC.

Picornaviruses and their proteases are well characterized, however many important questions about $2A^{pro}$ targeting mechanisms and cleavage target selection remain unanswered. Furthermore, given the established role $2A^{pro}$ plays in cleavage of Nups and abrogation of nuclear import and export, we were especially interested to study $2A^{pro}$ and develop it as a tool for characterizing transport across the NPC. As per our investigative aims, we established a tunable protease expression platform in mammalian cell lines. We utilized this platform for two primary purposes, to biochemically characterize the interactome of $2A^{pro}$ to glean additional insights into its function, and to assay nuclear-cytoplasmic trafficking.

3.1 $2A^{pro}$C110A preferentially binds Nup98 and directly cleaves it

Affinity capture experiments and MS analysis revealed that Nup98 and eIF3L were the top interacting partners of the catalytically inactive $2A^{pro}$. While eIF3L is involved in translation initiation (see next section), Nup98 is a key player in nuclear and cytoplasmic trafficking of proteins and mRNA. Nup98 is a mobile FG Nup, detected on both cytoplasmic and nuclear sides of the NPC. Nup98 forms tight binding interactions with Rae1 through its GLEBS motifs, facilitating Rae1 localization to the NPC, where it serves as an mRNA export factor[130].

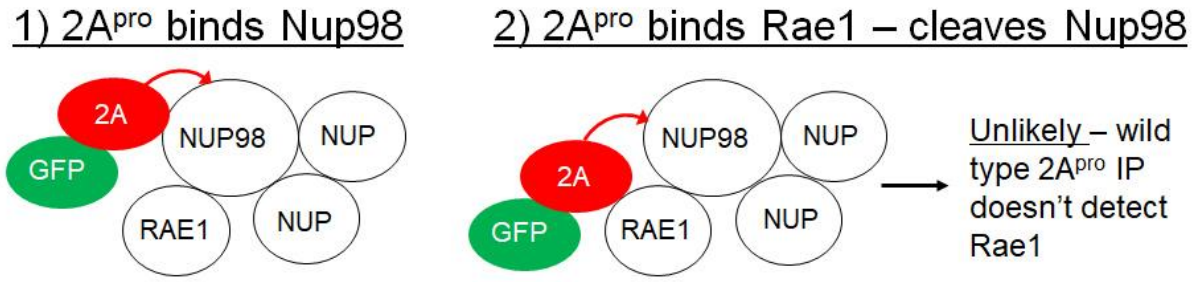

Figure 3.1. $2A^{pro}$ directly binds and cleaves Nup98.
Based on 2AC110A immunoprecipitation data, we can predict two possible Nup98 targeting and cleavage mechanisms for the wild type protease. (**1**) $2A^{pro}$ can bind and cleave Nup98 directly. Or (**2**) $2A^{pro}$ binds Rae1, which interacts directly with Nup98, and trans-cleave Nup98. The $2A^{pro}$ pulldown data, where neither Rae1 nor Nup98 are present, suggests direct Nup98 cleavage. If $2A^{pro}$ bound Rae1 directly, we would detect it during MS analysis.

By comparing pulldown data with the catalytically active $2A^{pro}$, we can propose two parallel mechanisms employed by $2A^{pro}$ to target and degrade Nup98. The 2AC110A pulldown data detected both Nup98 and Rae1, at 1-to-1 stoichiometric levels, while the $2A^{pro}$ pulldown data did not detect either protein. Solely based on the data from the catalytically inactive $2A^{pro}$ affinity

capture experiment, we would not be able to definitively ascertain if $2A^{pro}$ can bind to Nup98 and cleave it directly (Fig. 3.1 – 1), or if $2A^{pro}$ can bind to Rae1 as a staging platform to then attack and degrade Nup98 (Fig. 3.1 – 2). However, since we did not detect Rae1 in the wild type $2A^{pro}$ affinity capture data, it is a reasonable assumption that Rae1 is not a binding target for $2A^{pro}$ and is merely detected during 2AC110A pulldowns as part of the complex with Nup98. This conclusion is further supported by the $2A^{pro}$ cleavage assays, which revealed no detectable degradation of Rae1 during production of catalytically active $2A^{pro}$.

3.2 $2A^{pro}$ likely interacts with eIF3L during infection to as a mechanism of facilitating target selection and cleavage of eIF4G

Eukaryotic translation initiation depends on initiation factors, such as eIF4G, eIF4E, as well as 40S ribosomal subunit bound to eIF3[190-192]. These factors form scaffolds that facilitate correct ribosomal attachment to mRNA, loading of tRNAs[193], as well as form focal points for cellular regulation of translation[19, 20]. The eIF3 complex was predominant in the 2AC110A pulldowns and was also detected at lower levels in the $2A^{pro}$ affinity capture data. In the 2AC110A pulldown, eIF3L and eIF3B are detected in equal stoichiometry to Nup98-Rae1, with all the other components of the eIF3 complex in the top 20 most enriched proteins. Indeed, 12 of the 13 eIF3 components were identified in our 2AC110A pulldown[133, 192], with eIF3J as the only missing component, possibly because it folds into the ribosomal decoding center[194]. Meanwhile, eIF4G, one of the top cleavage targets for the $2A^{pro}$, was detected at 10-fold lower levels than eIF3L.

Analyzing this data, we hypothesized that eIF4G cleavage was mediated through a different mechanism than Nup98. One would normally expect the $2A^{pro}$ to directly bind its target eIF4G, however our immunoprecipitation data suggested this interaction was not direct. In fact, with eIF4G detected at 10-fold lower levels, we suspect it is a 2^{nd} order interaction, with the eIF3 complex forming the first order binding interaction to $2A^{pro}$/2AC110A (Fig. 3.2). Given 2AC110A's affinity for eIF3L and associated complex proteins, we propose a novel cleavage mechanism. We posit that $2A^{pro}$ binds the eIF3 complex by interacting directly with eIF3L and possibly with other eIF3 components. These interactions would constitute a platform from where $2A^{pro}$ can cleave eIF4G during translation initiation (Fig. 3.2 – 1).

Based on our MS data, it is unclear if 2AC110A makes a single binding interaction with eIF3L, or if the protease wedges itself between several eIF3 components. The presence of eIF3 complex proteins in the $2A^{pro}$ MS dataset, but not eIF4G, further reinforces our proposed indirect cleavage mechanism of eIF4G. If eIF4G was degraded during direct binding interactions by $2A^{pro}$, in a similar manner to Nup98, then we should have detected considerably greater peptide quantity levels of eIF4G during pulldown and MS analysis. Finally, reverse pulldowns via affinity capture of Nup214 revealed a significant enrichment of eIF3L, but not eIF4G. eIF3L was detected as a 4^{th} order interaction from the original target handle, further validating the affinity between 2AC110A and eIF3L, as well as the existence of a 2^{nd} binding site on $2A^{pro}$ for interactions with eIF3L. For us to obtain such a result, 2AC110A would need to simultaneously bind Nup98 and eIF3L. An alternative explanation could be dimerization of 2AC110A. Some evidence of 2AC110A dimerization does exist in the literature[160] and our chemical crosslinking experiments suggest potential oligomerization of GFP-2AC110A may be possible (Fig 2.24).

Whether $2A^{pro}$ binds the eIF3 complex to cleave eIF4G as a monomer or dimer does not take away from the overall hypothesis of eIF3 serving as a targeting platform for the protease. eIF3 is a stable complex associated with the 40S ribosomal subunit. It does not fall apart and reassemble between translation cycles, and based on published cryo-EM data of the translation initiation

complex, eIF3L is proximal to eIF4G during translation initiation[195]. Given the stability of the eIF3 complex between rounds of translation and eIF3L's spatial proximity to eIF4G[195], the eIF3 complex is a viable piggybacking site to promote eIF4G degradation by $2A^{pro}$.

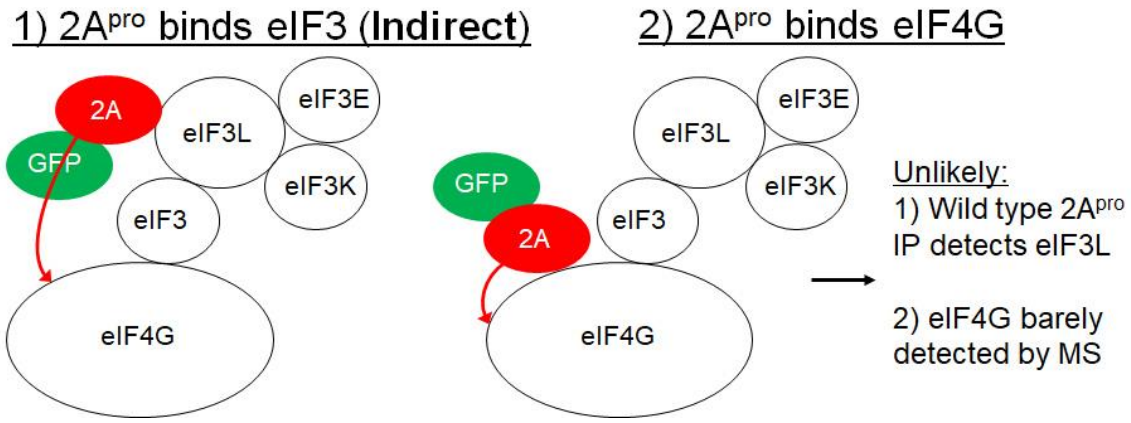

Figure 3.2. $2A^{pro}$ piggybacks on eIF3L and cleaves eIF4G.
Immunoprecipitation data analysis suggests an alternative mechanism for cleavage of eIF4G. MS data analysis reveals a predominance of eIF3 complex proteins in 2AC110A pulldowns, and the presence of half of the eIF3 components during affinity capture of $2A^{pro}$. eIF4G is detected during 2AC110A pulldowns, but the peptide quantity is an order of magnitude lower than eIF3L or eIF3B, suggesting a degree of separation between 2AC110A and eIF4G. As such, we can predict two possible eIF4G targeting and cleavage mechanisms. (**1**) $2A^{pro}$ binds the eIF3 complex, likely with eIF3L as a critical focal point, and cleaves eIF4G indirectly. Alternatively, (**2**) $2A^{pro}$ binds eIF4G and cleaves it directly. Since eIF3 proteins are abundant during both $2A^{pro}$ and 2AC110A pulldowns while eIF4G levels are 10-fold lower, we favor variant 1 as the cleavage mechanism of eIF4G.

We attempted to functionally validate our hypothesis that $2A^{pro}$ has a novel and different cleavage mechanism for eIF4G that relies on eIF3L as a piggybacking and binding site. We envisioned that a simple experimental assay would have been to add small molecule inhibitors of eIF3 during $2A^{pro}$ synthesis and check the eIF4G and Nup98 degradation. Literature searches revealed a number of small chemical compounds that interfere with binding to the 40S ribosomal subunit or prevent eIF4G engagement. However, none of several tested inhibitors worked in our assay (data not shown).

Therefore, we resorted to siRNA-driven knockdown of eIF3L but did not observe any major effects on eIF4G cleavage, possibly due to insufficient decrease in eIF3L production or interference with the translation process itself. While we observed a decrease in eIF4G cleavage during eIF3L knockdown, we could not decisively confirm whether the proximal lack of eIF3L as a piggybacking protein was the cause. Indeed, a decrease of any translation or initiation factor concentration could negatively affect cellular translation, which would have a similar output of the decreased target degradation in our assay.

Finally, we employed chemical crosslinking during 2AC110A immunoprecipitation experiments. The goal was to identify residues between 2AC110A and its interacting partners such as Nup98 and eIF3L to validate and map their direct binding. We tested DSS concentrations in a broad range, but did not observe sufficient 2AC110A crosslinking to pursue this methodology

further. DSS covalently binds free amine groups on side chains of amino acids, so it is possible there were no exposed amine groups on 2AC110A that were usable for crosslinking.

We considered alternative hypotheses for the predominance of eIF3 in our $2A^{pro}$ and 2AC110A immunoprecipitation data. Picornaviral Type I-IV IRESes utilize various host machinery to promote viral polyprotein translation. Cleaved eIF4G, eIF3, other initiation factors, and various nuclear localized proteins such as splicing factors and RNA binding proteins are all implicated in the formation of picornaviral IRESes[22]. Some components, such as eIF3, are present in all four types of IRES[22]. This raised the question: if instead of utilizing eIF3 as a piggybacking site for cleavage of eIF4G, can $2A^{pro}$ instead be recruiting the eIF3 complex to picornaviral RNA IRES sites to promote IRES-driven translation? No published evidence exists to suggest that $2A^{pro}$ facilitates or drives recruitment of protein complexes. Furthermore, a small ~20 kDa protease like 2A can only have a few protein-facing functional sites. It has an exposed catalytic site and presumably an eIF3L binding site, irrespective of which hypothesis is more likely (Fig. 3.2). If $2A^{pro}$ facilitated or promoted recruitment of eIF3, it would require either the catalytic site or yet another domain or motif to play a role in target selection to drive $2A^{pro}$-eIF3 to picornaviral RNA. A similar hypothesis is that the $2A^{pro}$ facilitates formation of an $eIF4G^{cp}$-$2A^{pro}$-eIF3L complex, which exploits a different mechanism of recruitment to the IRES.

We also considered the possibility of enhancement of WD40 domain binding through Nup98, similar to how we detected Rae1 (a WD40 domain protein) binding[130]. eIF3B was detected at nearly stoichiometric levels to eIF3L, but is relatively distal from eIF3L in the eIF3 complex[133, 196]. While eIF3L is located near eIF4G[195], eIF3B is separated from it by several proteins. eIF3B plays a key role as a scaffolding protein linking components of eIF3 together into a large 13 protein complex[197]. eIF3B contains nine WD40 motifs, compared to Rae1's four motifs[196, 198], raising the alternate possibility that 2AC110A binding of Nup98 leads to direct interactions with the eIF3 complex through Nup98-eIF3B. However, this hypothesis fails to explain eIF3L's affinity to 2A and 2AC110A, as eIF3L does not contain WD40 domains. eIF3I also contains seven WD40 motifs[199], but is detected at much less peptide quantity than either eIF3L or eIF3B. During Nup214 immunoprecipitation experiments, we detected eIF3L enriched with 2AC110A, but not eIF3B. If the WD40 domains of eIF3B were indeed driving the interaction, we should have observed its enrichment. Finally, Nup98 and Rae1 were identified at a ~1:1 stoichiometric ratio, suggesting there should not be any free Nup98 available to bind other proteins via a GLEBS domain. Despite these alternative functional implications and possibilities for targeting eIF3 by $2A^{pro}$, we believe that our work supports our primary hypothesis that eIF3L serves as a docking site for $2A^{pro}$, from where it cleaves eIF4G.

3.3 $2A^{pro}$ mediated degradation of Nup98 and eIF4G are the first host cleavage events that occur during picornaviral infection

Picornaviral proteases, particularly $2A^{pro}$, are reported to engage cellular targets early during infection (Fig. 3.3). Protease production during picornaviral infection can be measured by cleavage of established targets such as eIF4G. As early as two hours post-infection (h.p.i.), one can detect eIF4G cleavage during RV[125] and CVB3 infection[108]. At two h.p.i. with CVB3[108] and four h.p.i. with RV[125], Nup98, another early cleavage target, is observed to become degraded. Protease mediated degradation of other proteins eventually also occurs later during infection, at five h.p.i. and onwards. Between different picornavirus species there is striking overlap in the timing of target degradation. eIF4G is always targeted first, well before any viral proteins (including viral coat proteins) are even detected by immune-based assays with mechanisms for

signal amplifications[125]. From an evolutionary perspective, shutting down host translation would be a key step in preventing a mounted innate immune response. Similarly, abrogating steady-state nuclear import and export through Nup cleavage would further attenuate host response, in addition to relocalizing nuclear proteins involved in IRES mediated picornaviral translation.

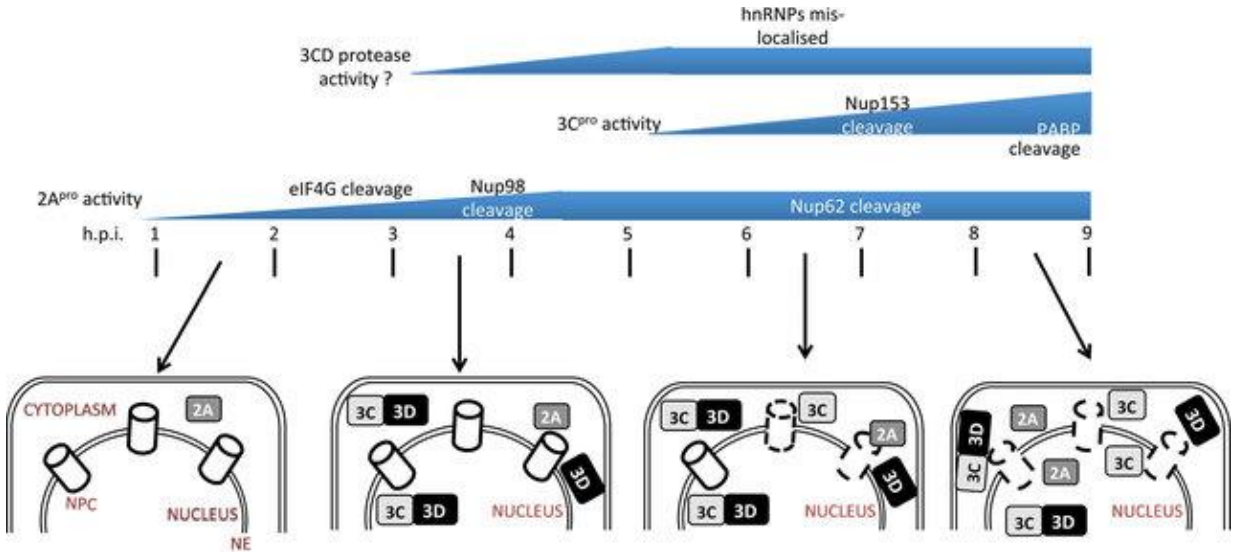

Figure 3.3. Timeline of protease activity during picornaviral infection.
Rhinovirus infections will cause eIF4G cleavage very early during viral replication.[125] Other key targets, such as Nups, will be targeted by $2A^{pro}$ early on to further prevent host immune response and relocalize key nuclear proteins that promote picornaviral IRES based translation. While eIF4G cleavage by $2A^{pro}$ can be detected as early as 2-3 h.p.i., $3C^{pro}$ mediated cleavage of Nups is significantly slower at ~7 h.p.i.. Adapted from Walker et al[125].

It is established that picornaviral infection of mammalian cell lines results in cleavage of Nup98 and eIF4G as early as two h.p.i.[125] (Fig3.4a, b). By this point in the infection, one cannot detect any viral protein accumulation. Despite lack of detectable viral proteins, there are sufficient quantities of $2A^{pro}$ to degrade eIF4G, shutting off host cell translation, and Nup98, affecting import of proteins and export of mRNA (Fig. 3.4b). However, the vast majority of other characterized $2A^{pro}$ cleavage targets are not degraded until hours later. Picornavirus protein production and replication within cells occurs at an exponential growth, suggesting orders of magnitude more of $2A^{pro}$ available 4-6 h.p.i to cleave other protein targets. Based on published literature, one can deduce that eIF4G and Nup98 are higher priority cleavage targets for the $2A^{pro}$. Such precise targeting has to be facilitated by a general $2A^{pro}$ "preferred affinity" for eIF4G and Nup98. Molecular mechanisms for such affinity are still not completely elucidated, though it is likely the $2A^{pro}$ has evolutionarily adapted to bind either the target proteins or a proximal piggybacking protein complex.

Our protease expression platforms and immunoprecipitation experiments shed light on the affinity of $2A^{pro}$ for Nup98 and eIF4G. Using stable mammalian cell lines as a model system, we observed the $2A^{pro}$ degrading these two key cleavage targets, albeit slower than during viral infection (Fig. 3.4c). The difference in time frame is not surprising as during picornaviral infection, protease production is tied to the IRES-driven translation systems, whereas our ectopic expression systems depend on the very host machinery depleted after $2A^{pro}$ translation. In addition, to our $2A^{pro}$ production systems mirror the cleavage patterns observed during the first two hours after

picornaviral infection, we were able to isolate Nup98 and eIF3 during affinity capture experiments with the catalytically inactive protease 2AC110A. The lack of catalytic activity promoted stable production of the protease, which subsequently served as a platform for direct and indirect immunoprecipitation experiments.

Direct pulldowns of 2AC110A revealed Nup98-Rae1 and eIF3L and the remaining eIF3 complex as predominant interactors. Reverse pulldowns with Nup214 during 2AC110A production revealed an enrichment of eIF3L, but not eIF4G. This suggested that 2AC110A was capable of directly interacting with Nup98 while also binding eIF3L. Some questions may remain about whether this dual binding is achieved with 2AC110A as a monomer or dimer, with some evidence suggesting $2A^{pro}$ dimerization is possible[111]. However, the endogenous oligomerization status of $2A^{pro}$ does not detract from our hypothesis that eIF3L-eIF3 serves a targeting platform for the cleavage of eIF4G.

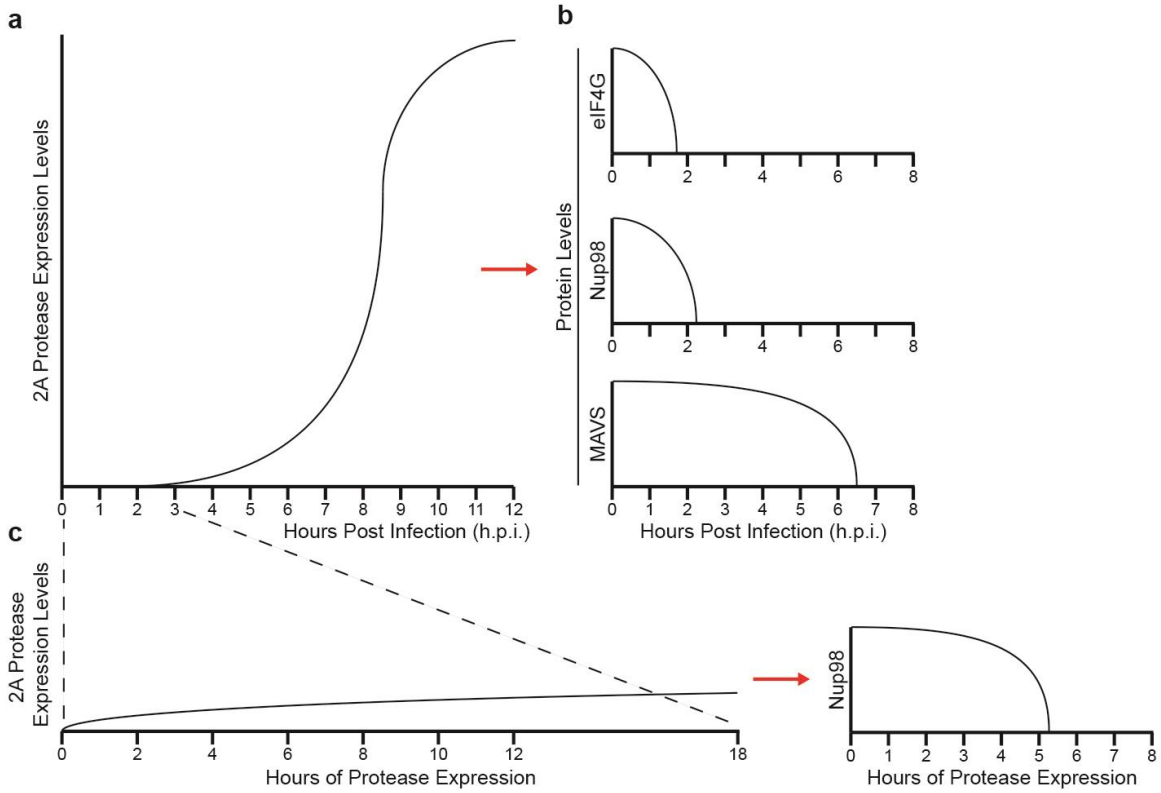

Figure 3.4. Ectopic protease production matches early stages of infection, prior to exponential production of picornaviral components.
During picornaviral infection, polyprotein translation can occur uninhibited due to viral IRES sequences of the RNA genome. **a**, Polyprotein translation and proteolytic processing can result in an exponential growth in the production rate of additional viral proteins. **b,** This pattern of protease synthesis results in several stages of cleavage target depletion, with Nup98 and eIF4G as the first cleavage targets, and other proteins such as MAVS or TRIF as later targets. Cleavage of late protease targets is driven through the exponential accumulation of proteases in an infected cell. **c**, Based on available data, we speculate that our ectopic protease expression systems are aligned with the first 2-3 hours of a viral infection.

Overall, we believe our protease expression platforms capture $2A^{pro}$ function and binding affinities during the earliest stages of picornaviral infection, before exponential viral protein production kicks in. We suspect that our expression systems do not produce sufficient $2A^{pro}$ to drive secondary or tertiary proteolytic cleavages as observed during 4-6 h.p.i., with proteins such as MAVS, Dystrophin, and TRIF. We identified a strong affinity of 2AC110A for Nup98 and eIF3L during pulldowns, which further supports our overarching hypothesis that the $2A^{pro}$ performs surgical strikes on Nup98 and eIF4G during the initial stages of a picornavirus infection. Our ectopic expression systems, particularly our stable cell lines with inducible protease expression, present themselves as useful tools to study specific cellular effects induced through $2A^{pro}$ mediated cleavage as well as serve as a model for $2A^{pro}$ function during the first few hours of viral infection.

3.4 $2A^{pro}$ inhibits nuclear protein transport driven by Nup98 and Rae1 mediated mRNA export

Nup98 is a critical player in protein transport and mRNA export. Nup98 is a dynamic FG Nup that can be detected on both nuclear and cytoplasmic sides of the NPC and mediates protein import through FG-based interactions with a number of importins (such as Importin-α/β, Transportin-1, Importin-7) and export through Crm1[57,58,70]. In addition, Nup98 is a key binding and localizing partner for the RNA export factor Rae1 through interactions between the Nup98 GLEBS domain and Rae1 WD40 motifs[130].

Interfering with Nup98-Rae1 function is not a unique viral strategy for controlling host RNA trafficking. VSV M protein and SARS-CoV-2 ORF6 both target Nup98-Rae1 to disrupt nuclear transport of their infected cells[66, 129, 163, 173]. While M protein and ORF6 disrupt normal Nup98 function by directly binding it and Rae1, picornaviruses evolved to cleave Nup98 through the catalytic activity of the $2A^{pro}$. Utilizing HeLa stable cell lines, we can study $2A^{pro}$'s effects on Nup98 mediated transport across the NPC. Specifically, we can degrade Nup98 on command through inducible production of $2A^{pro}$, and subsequently assay NLS-NES based reporters to elucidate transport mechanisms, or assay mRNA localization via Poly-T FISH.

During our cellular fractionation experiments, we observed that depletion of Nup98 through $2A^{pro}$ mediated cleavage delocalizes Rae1 from the nucleus into the cytosol. In parallel, Poly-T FISH analysis of cells expressing $2A^{pro}$ and 2AC110A reveals a striking difference in mRNA localization, as visualized by changes in intensity and signal distribution of mRNA speckles in response to $2A^{pro}$ catalytic activity. Putting these data together, we suspect that picornaviruses affect mRNA localization by inducing cellular stress responses and through delocalization of Rae1 and Nup98 degradation. This is consistent with published work with M protein[129] and ORF6[163] mediated mRNA export interference, reinforcing the observable convergent evolution of RNA viruses on targeting Nup98-Rae1.

Nup98 mediates a number of protein transport pathway by serving as a docking site for Kaps[58]. We were keen on utilizing our stable cell lines expressing $2A^{pro}$ to further characterize transport pathways dependent on Nup98 by abrogating its function. We developed two sets of fluorescent reporters fused with NLS and NES tags to study nuclear import and export. We started by validating published data on how $2A^{pro}$ affected transport pathways[70]. GFP_2 reporters fused with PKI NES, SV40 NLS, and their NLS-NES combination, were assayed under $2A^{pro}$ and 2AC110A expression conditions. PKI NES is exported by Crm1[200], and we observed mislocalization of the NES-tagged fusion reporter into the nucleus as a function of the $2A^{pro}$ catalytic activity. On the other hand, the SV40 NLS reporter was predominantly localized to the

nucleus. While we did observe some mislocalization during $2A^{pro}$ production, it was to a much lower degree than with PKI-NES reporters.

A likely explanation for this difference is that these transport pathways are affected at different rates. This idea is supported by Nup98 depletion of GFP reporters with the NLSNES tag. Under control conditions, this reporter predominantly localizes to the cytoplasm, supporting evidence that Crm1 mediated export of the PKI NES is more dominant than import of the SV40 NLS. In response to Nup98 depletion, however, the reporter relocalizes to the nucleus. Thus, $2A^{pro}$ affects the Crm1-mediated export to higher degree than the Nup98-driven import.

We developed a second set of fluorescent transport reporters to supplement our localization experiments with PKI NES and SV40 NLS. These reporters consist of an NLS fusion to mCherry and LacZ, specifically designed to be unaffected by passive diffusion[181]. We assayed these reporters during $2A^{pro}$ or 2AC110A production and were keen on detecting changes in reporter localization in response to Nup98 depletion. With our mCherry reporters, we assayed the C-Myc, Nucleoplasmin, MX2, and HTLV-1 Rex NLSs. C-Myc, Nucleoplasmin, and MX2 NLS tagged reporters all localized to the nucleus under control conditions and did not mislocalize during production of $2A^{pro}$, indicating that Nup98 degradation did not affect these import pathways.

In contrast, the cytosol and nucleolus localization of the HTLV-1 Rex NLS reporter was significantly changed by the $2A^{pro}$ catalytic activity. $2A^{pro}$ abrogated export of the Rex NLS reporter so that it was relocalized to the nucleus. This mislocalization can be explained by dissociation of Rae1 from the NPC and possible blockage of mRNA export, since HTLV-1 Rex NLS also engages viral RNA prior to export[187]. Altogether, we demonstrated the $2A^{pro}$ catalytic activity and cleavage of Nup98 to be primarily responsible for affecting nuclear export (PKI NES, HTLV-1 Rex NLS) (Fig. 3.5). Although nuclear import was also affected, as evidenced by cytoplasmic accumulation of Lamin A/C and Histones (Fig. 2.27b) and SV40 NLS mislocalization (Fig. 2.30), the effects were relatively minor compared to the changes observed with nuclear export (Fig. 3.5). More major transport changes during picornaviral infection likely occur due to the expression and production of the 3C protease, which has also been shown to cleave NPC components[201], as well as the exponential production of both proteases during infection. Nevertheless, our data suggest that one of the major functions of $2A^{pro}$ is to disrupt efficient nuclear export of host cell proteins (Fig. 3.5).

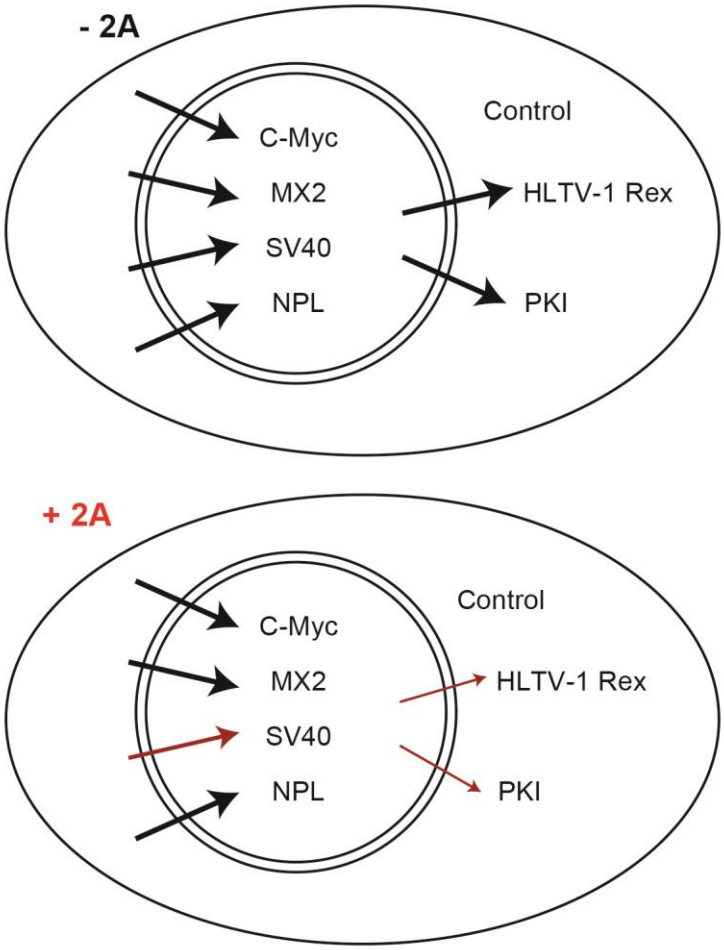

Figure 3.5. Transport reporter localization changes in response to $2A^{pro}$ catalytic activity. Nuclear import and export changes in response to $2A^{pro}$ production were assayed with NLS and NES tagged fluorescent protein reporters. NLS reporters denoting import were signified by black arrows going into the nucleus. NLS or NES tagged reporters representing export were shown by black arrows aiming out of the nucleus and into the cytoplasm. $2A^{pro}$ catalytic activity (red) slightly impacted the import of SV40 NLS reporters, but had a major impact on export of HTLV-1 Rex and PKI tagged reporters. C-Myc, MX2, and Nucleoplasmin (NPL) were unaffected by $2A^{pro}$ activity.

Fluorescent reporters with import and export signals, as well as our protease expression platforms, provided us with valuable tools to elucidate complex transport pathways across the NPC. Indeed, we applied both expression platforms to successfully interrogate a number of NLS and NES motifs. Some of these motifs and transport pathways were previously interrogated by other research groups with other picornaviruses. Our observations with the SV40 NLS and PKI NES[70] were not only experimental validation of published work, but also presented convergent data on picornavirus mediated abrogation of protein transport. Our expression platforms also revealed new data about other NLS motifs (C-Myc, Nucleoplasmin, MX2, Rex NLSs) and their dependence on Nup98 mediated transport. Given these preliminary insights, our expression platforms are poised to be further developed as molecular tools to interrogate nucleocytoplasmic trafficking. Our inducible stable cell lines can serve as the basis for alternative cell lines prepared

with a diverse array of viral proteins that target NPC components. For example, Rhinovirus 3C protease[201], VSV M protein[66, 129, 202], SARS-CoV-2 Orf6[163, 173], or Influenza NS1 protein[189], are all amongst the many viral proteins that abrogate normal host transport. Such novel cell lines can be combined with additional NLS reporters, forming an NPC-NLS-Kap matrix to intimately characterize protein and nucleic acid transport across the NPC.

In addition to combining NLS reporters with viral protein expression platforms, we can add a third degree of analysis to the matrix by genetically manipulating putative target proteins. Genetic editing techniques, such as CRISPR/Cas9 and TALENs, have advanced significantly since their discovery and initial development, currently featuring even in the clinic[203, 204]. With these advanced gene editing methodologies, we can edit putative target proteins and make them immune to the activities of viral proteins. For instance, since we can tentatively predict $2A^{pro}$ cleavage sites of Nup98[109], we could hypothetically develop a cell line with mutated Nup98 that is resistant to $2A^{pro}$ mediated cleavage. The use of Nup98 cleavage resistant mutants combined with $2A^{pro}$ production platforms and NLS/NES reporters would enable us to further elucidate the roles Nup98 plays in nucleocytoplasmic trafficking.

3.5 Unified model of $2A^{pro}$ mediated cleavage and downstream effects during early stages of infection

Based on published literature and our studies, we formulated a unified model of the initial stages (first 2-3 hours) of picornaviral infection, as pertaining to $2A^{pro}$ (Fig. 3.6). The Picornaviral RNA genome is expressed as a polyprotein and proteolytically processed by $2A^{pro}$ and $3C^{pro}$ into individual components.

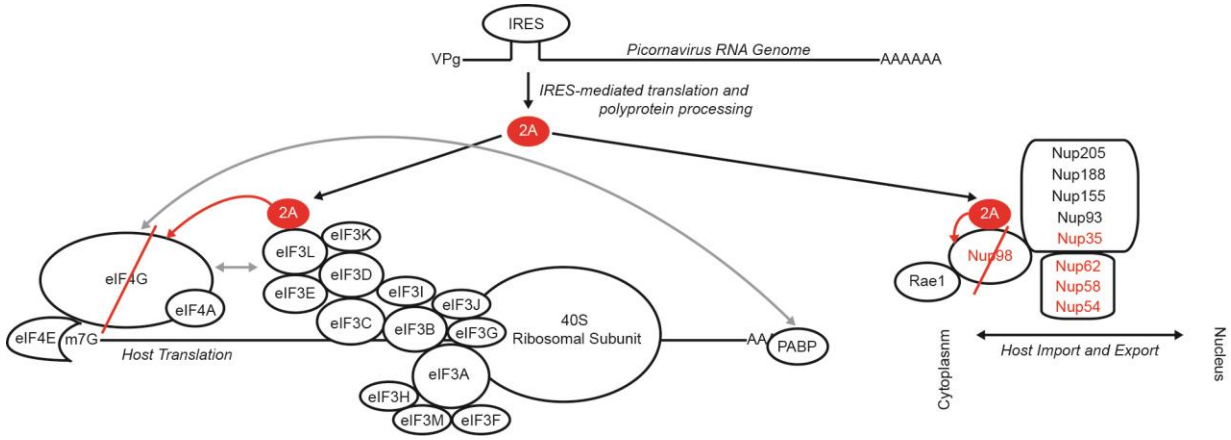

Figure 3.6. Unified model of initial stages of picornaviral protease expression and function. Upon virion intake and genome release, the picornaviral RNA genome is translated as a polyprotein that is proteolytically processed into individual protein subunits by proteases 2A and 3C. The 2A protease proceeds to cleave Nup98 and eIF4G, with the latter cleavage facilitated by $2A^{pro}$ association with the eIF3 complex. Cleavage of Nup98 dissociates Rae1 from the NPC, and the loss of both proteins impacts transport of proteins and mRNA across the NPC and relocalizes nuclear factors that promote IRES-mediated translation. In parallel, eIF4G cleavage results in a shutdown of the host cell's translation capability, preventing infected cells from reacting to the picornaviral infection. As the infection continues and additional viral proteins are translated, $2A^{pro}$ activity results in dozens of secondary and tertiary cleavage targets, such as MAVS and TRIF, among many others.

We conclude that prior to exponential viral protein production, $2A^{pro}$ makes surgical strikes against eIF4G (likely by binding to the adjacent eIF3L) and Nup98, key players in regulating critical functions of host cells. eIF4G cleavage results in an arrest of host translation, preventing accumulation of new proteins, and creating $eIF4G^{cp}$, which partakes in formation of picornaviral IRESes and promotion of viral translation. Nup98 degradation abrogates a number of protein import and export pathways, which results in accumulation of nuclear-localized proteins to the cytosol, including some proteins that facilitate the formation of the viral IRES. eIF4G cleavage and mRNA localization changes attenuates the ability of infected cells to mount an innate immune response. Once the picornaviral infection runs for 4-6 hours, viral protein production increases exponentially to produce orders of magnitude more $2A^{pro}$ compared to the earliest time points. This higher concentration of $2A^{pro}$ favorably drives the cleavage of secondary and tertiary protein targets, such as MAVS and TRIF, among many others.

Our proteomic analyses indicated that $2A^{pro}$ has preferential affinity for binding predominantly two proteins, Nup98 and eIF3L. Nup98 is one of two primary cleavage targets for picornavirus $2A^{pro}$, and our immunofluorescence microscopy experiments highlight how significant Nup98 degradation is to protein export from the nucleus. eIF4G, the other primary cleavage target of $2A^{pro}$, plays a critical role in eukaryotic translation, a key host function targeted during picornaviral infections. Based on our proteomic analyses, we can propose a novel function for $2A^{pro}$. We believe the $2A^{pro}$ binds directly to eIF3L, which then serves as a platform for $2A^{pro}$-mediated degradation of eIF4G. Altogether, our studies propel our understanding of $2A^{pro}$ specificity during picornaviral infections and the impact two surgical strikes by this protease has on infected cells.

CHAPTER 4. Materials and Methods

4.1 Molecular Cloning

4.1.1 Reagents and equipment

- pcDNA3.1NT-GFP-TOPO CVB3 2A and 3C and vectors with a catalytically inactive mutant were graciously provided by the Rice laboratory (The Rockefeller University).
- epB-Puro-TT-CVB3 2A plasmids for PiggyBac transfection were also generously provided by the Rice laboratory (The Rockefeller University).
- pHR39-CMV-GFP-LacZ with NLS sequences were generously provided by Melissa Kane (University of Pittsburgh).
- pRS426-GPD-mCherry-4xMS2 vector was kindly provided by Peter Fridy from the Rout laboratory (The Rockefeller University).
- PTC-200 DNA engine with 2x 48 well blocks for microcentrifuge tubes from BIO-RAD.
- NanoDrop™ 2000 Spectrophotometer (ND-2000) from ThermoFisher Scientific.
- UltraPure Agarose (REF 16500-100) from Invitrogen.
- *Dpn*I (R0176S) from New England BioLabs.
- *Not*I (R0189S) from New England BioLabs.
- Gibson Assembly® Master Mix (E2611S) from New England BioLabs.
- AccuTaq™ LA DNA Polymerase (D8045-125UN) from Millipore Sigma.
- QIAquick Gel Extraction Kit (28704) from Qiagen.
- QIAprep Spin Miniprep Kit (27106) from Qiagen.
- Plasmid Maxi Kit (12163) from Qiagen.
- QuikChange II XL Site-Directed Mutagenesis Kit (#200521) from Agilent.
- XL10-Gold Ultracompetent Cells (200315) from Agilent.
- SURE 2 SUPERCOMP CELLS (200152) from Agilent.
- Super PiggyBac Transposase Expression Vector (PB210PA-1) from System Biosciences.

Sequencing primers were designed in-house, some based on commercially available primers, others based on plasmid sequence. Primers were ordered from Integrated DNA Technologies (IDT).

Primer Name	**DNA Sequence**
M13Fwd	GTTTTCCCAGTCACGAC
M13Rev	CACACAGGAAACAGCTATGACCAT
GFP_5_Fwd	ATGGCCAGCAAAGGAGA
GFP_5_Rev	CATCACCATCTAATTCAACAAGAA
GFP_3_Fwd	AGTTTGTAACTGCTGCTGG
GFP_3_Rev	TTTGTAGAGCTCATCCATGC
2A_5_Fwd	GGACAACAATCAGGGGCAG
2A_5_Rev	GCACTGGTAGCTAGATGTCT
2A_3_Fwd	GGTCGGCTTTGCAGACATCC
2A_3_Rev	CTGTTCCATTGCATCATCTTC
EGFP_5_Fwd	GTGAGCAAGGGCGAGGAGCT
EGFP_5_Rev	CATCGCCCTCGCCCTCGC
EGFP_3_Fwd	CCCCAACGAGAAGCGCGATCAC
EGFP_3_Rev	TTGTACAGCTCGTCCATGCCG

mCherry_5_Fwd	ATGGTGAGCAAGGGCGAGGAG
mCherry_5_Rev	CTCGATCTCGAACTCGTGGCCG
mCherry_3_Fwd	CAACGTCAACATCAAGTTGGAC
mCherry_3_Rev	CTTGTACAGCTCGTCCATGCCG

4.1.2 Large scale preparation of plasmids for transient transfection

Prior to initiating transient transfection experiments, we needed to evaluate the quantity of plasmid DNA available for experiments. We prepared large amounts of plasmid DNA using Maxiprep kits from Qiagen.

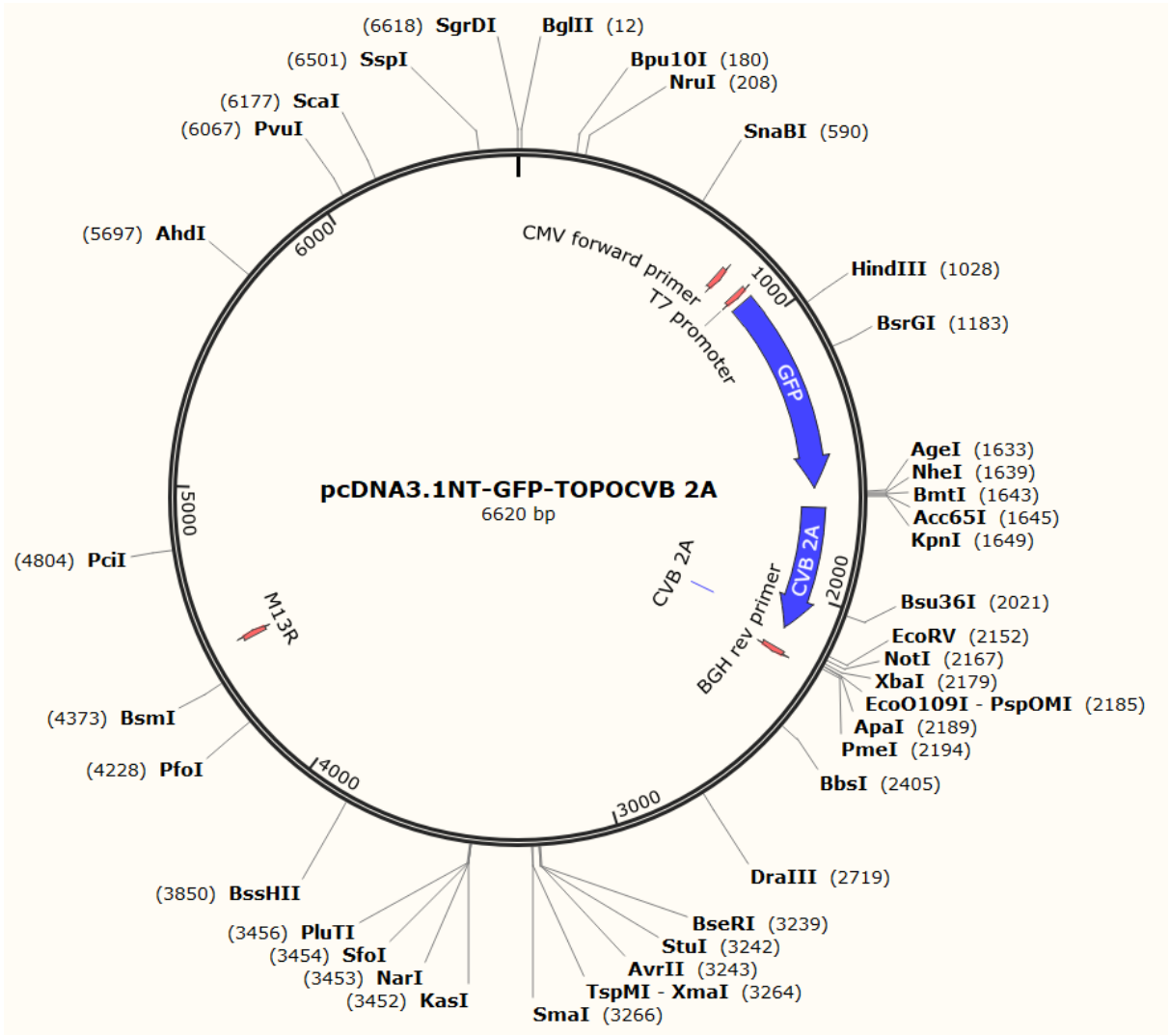

Figure 4.1. pcDNA3.1NT-GFP-TOPO CVB3 2A plasmid map.
The pcDNA3.1 vector includes an Ampicillin resistance gene for bacterial selection. The gene of interest ($2A^{pro}$) is tagged with an N-terminal GFP, with the fusion protein downstream of the CMV transcription promoter.

1) pcDNA3.1NT-GFP-TOPO CVB3 2A and 3C plasmids were transformed into XL10 Gold Ultracompetent cells (Agilent) and plated on LB-Agar plates with 100 µg/ml ampicillin for selection of plasmid-bearing clones (Fig. 4.1).
2) A clone was picked for overnight (~16 hr) growth in 100 ml LB broth with 100 µg/ml ampicillin for selection.
3) Plasmid DNA was extracted per QIAGEN Maxi kit instructions.
4) Purified DNA concentration was measured by Nanodrop prior to sequence verification using Genewiz Sanger sequencing services. Gene sequences were validated iusing commercially available sequencing primers (CMV Forward and BGHR), as well as in-house primers (GFP_5_Fwd and 2A_3_Rev), which hybridize to portions of the fusion protein to ensure complete sequence coverage.

4.1.3 Molecular cloning of plasmids for stable cell line transfection

epB-Puro-TT-CVB3 2A (wildtype) and 2A^{C110A} (catalytically inactive mutant) plasmids for PiggyBac stable cell transfection were utilized as a backbone for the development of the GFP control plasmid, as well as 3C and 3C^{C147A} plasmids.

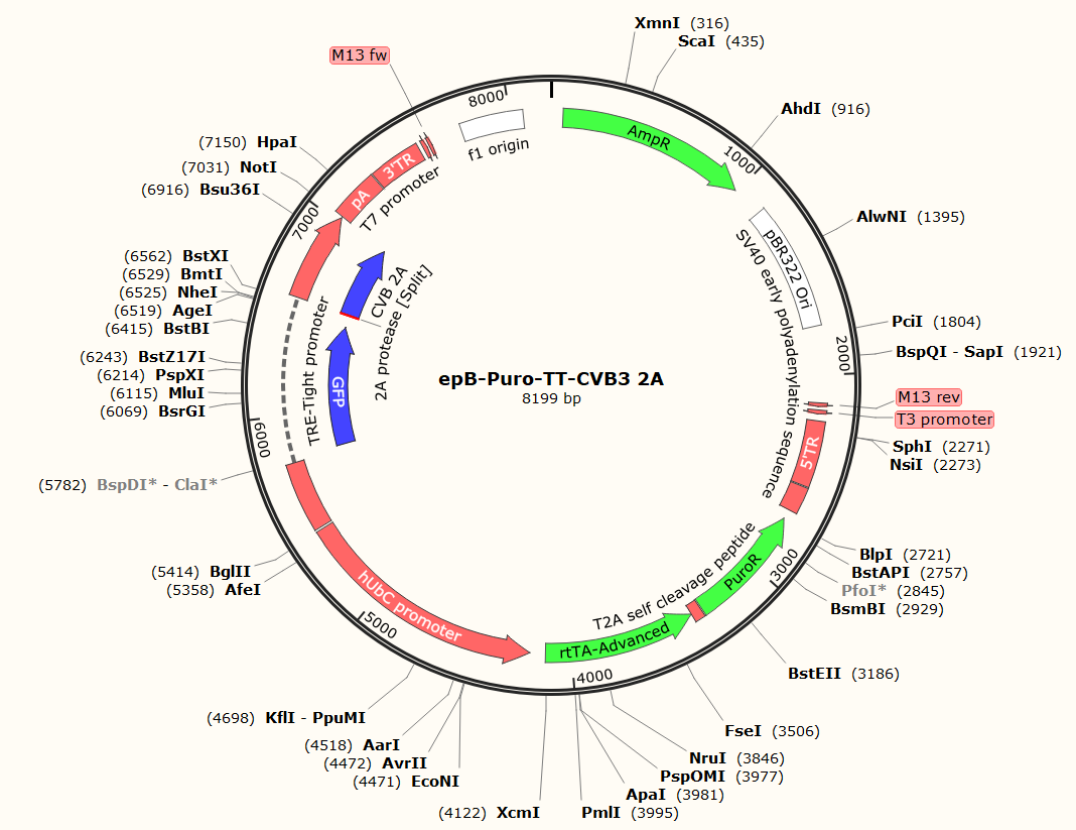

Figure 4.2. epB-Puro-TT-CVB3 2A plasmid map.
The PiggyBac vector includes an ampicillin resistance gene for bacterial selection, a puromycin resistance gene for selection in cell culture, and two translocation sites for genetic recombination into chromosomal DNA in cell culture cells. The gene of interest (2A^{pro}) is tagged with an N-terminal GFP, with the fusion protein placed downstream of the CMV transcription promoter.

Gibson Assembly Kit (New England Biolabs) was utilized to prepare the final plasmids, with primers designed in-house and ordered from IDT. Gibson Assembly is a method of molecular cloning that does not require any specific restriction sites, and instead depends on amplicons with overlapping DNA regions. The isothermal cloning reaction is catalyzed by three different enzymes, the T5 exonuclease, Phusion polymerase, and Taq ligase (Fig. 4.2). The standard Gibson workflow includes preparing at least one PCR-amplified DNA fragment with regions of overlapping DNA sequence. The ends of the amplicon(s) are recessed by T5 exonuclease activity, preparing complimentary DNA regions for hybridization. The Phusion DNA polymerase and Taq ligase re-extend and seal the sequence, yielding a plasmid with an insert for transformation.

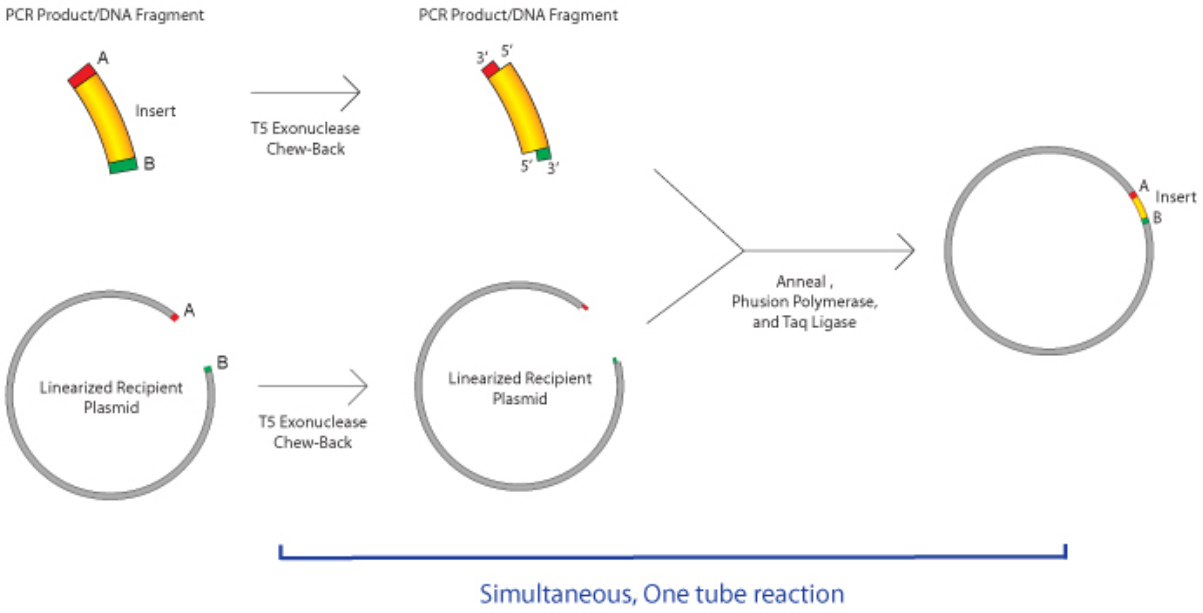

Figure 4.3. Schematic of Gibson Cloning.
PCR products are formed for an 'Insert' and 'Recipient' by PCR. Both PCR amplified fragments contain complimentary flanking sequences. Combination of fragments with Gibson Assembly Kit will fuse and seal the fragments together at sites of complimentarity. Source: *AddGene protocols*.

To convert the epB-Puro-TT-CVB3 2A plasmid into an epB-Puro-TT-GFP vector, we decided to amplify the entire plasmid without the coding region for $2A^{pro}$. The standard protocol for primer design in Gibson Cloning involves the preparation of at least two primers per amplicon (Fig. 4.4).

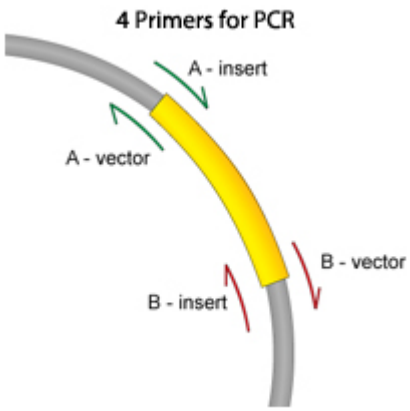

Figure 4.4. Gibson Cloning primer design. Primer design for Insert and Recipient/Vector fragments. Each fragment consists of two primers, the form a complete double stranded DNA fragment after PCR amplification. Source: *AddGene protocols*.

We prepared two sets of primers for PCR amplification, one located at the 3′ end of the GFP sequence, aiming 'reverse' (A-Vector), with the second primer complimentary to the stop codon after the $2A^{pro}$ sequence, aiming 'forward' (B-vector) (Fig. 4.3). These primers have an overlapping region corresponding to an *Eco*RV restriction site for future cloning endeavors.

Primer Name	**DNA Sequence**
3_EV_EcorV_PiggyBac_GFP	AGTCTGATATCTTATTTGTAGAGCTCATCC
5_EV_EcorV_PiggyBac_GFP	ATTATGATATCGCGGCCGCGACTCTAG

The PCR protocol was based on the recommended conditions in the Accutaq LA DNA polymerase manual. The various reagents, stock and final concentrations, and volumes used are listed below (Table 4.1).

Table 4.1. List of reagents and their respective volumes for a PCR reaction to amplify DNA.

Reagent	**Stock Concentration**	**Final Concentration**	**Volume (µL)**
Accutaq LA buffer (X)	10	1	5.000
dNTP mix (mM)	10	0.5	2.500
DMSO (%)	100	2	1.000
Fwd Primer (uM)	10	0.5	2.500
Rev Primer (uM)	10	0.5	2.500
Template DNA (ng/uL)	194	4	1.031
Accutaq LA DNA polymerase			0.500
Water			35.000
Final Volume:			50

After assaying a number of recommended PCR conditions (including the recommended cycles), we found that amplifying DNA was most efficient and reproducible using Touchdown PCR, where the initial cycles have a decreasing annealing temperature, eventually settling on a lower final annealing temperature for the remaining cycles. The PCR cycles used for large backbone amplification are listed below (Table 4.2).

Table 4.2. Cycles used for Touchdown PCR to amplify the large backbone DNA.

	Cycles:	Temp (C)	Time (sec)
	Initial Denaturation:	98	30
6 Cycles	Denaturation	94	15
	Annealing	68-0.5/cyc	20
	Extension	68	840
24 Cycles	Denaturation	94	15
	Annealing	65	20
	Extension	68	840
	Final Extension	68	600

After PCR amplification, we removed the original template DNA through *Dpn*I restriction digestion (per NEB protocol). *Dpn*I is a restriction endonuclease that only cleaves methylated DNA, which is a modification found on bacterial DNA. PCR-amplified DNA does not have the methyl modifications and is resistant to cleavage. After *Dpn*I digestion of our PCR samples, we purified our DNA of interest (Fig. 4.5) with gel electrophoresis (1% agarose gel), and excised the DNA for gel extraction and PCR purification (per Qiagen kit manuals).

Figure 4.5. Agarose gel purification of amplified DNA.
Agarose gel electrophoresis of PCR amplified DNA. 1 kb DNA ladder is in the left lane. The observed band corresponds to a ~6.5 kb long DNA fragment.

After PCR purification, we used Gibson Assembly to fuse the ends of the amplicon, per NEB guidelines. We subsequently transformed the plasmid into SURE2 Ultracompetent cells. These competent cells are specifically designed for cloning of genes involved in rearrangement and deletion of DNA and, therefore, are capable of improving cloning efficiency for PiggyBac vectors that contain sites for DNA recombination. After isolating and identifying successfully transformed clones, we prepared large quantities of DNA for eventual transfection, as per Chapter 4.1.3.

4.1.4 Molecular cloning of pHR39-NLS-CMV-mCherry-LacZ vectors

We utilized vectors expressing EGFP with various N-terminal NLS sequences as fluorescent reporters for studying localization and transport effects of viral proteases. The pHR39-CMV-GFP-LacZ plasmid backbone with each NLS sequence (Table 4.3) was used to prepare new vectors

with the EGFP sequence replaced by an mCherry sequence (from the pRS426-GPD-mCherry-4xMS2 plasmid) for downstream fluorescent imaging during GFP-2A^{pro} gene expression. These mCherry-NLS reporters were also prepared through Gibson Cloning procedure.

Table 4.3. Table of NLS names, corresponding amino acid sequence, and their NLS types.

NLS	Sequence (Amino Acid)	NLS Type
C-Myc	PAAKRVKLD	Monopartite class 2
Nucleopasmin	KRPAATKKAGQAKKKK	Bipartite
HTLV-1 Rex	PKTRRRPRRSQRKRPPT	N/A
MX2	GLMSKAHKPWPYRRRSQFSSRKYLKKEGA	N/A

Source: https://www.jbc.org/content/284/1/478.full. Kosugi et al, 2008[205]

Similarly to the process described in Chapter 4.1.3, we designed primers to PCR amplify two DNA fragments, one for the vector backbone of each NLS reporter, and one fragment with an mCherry tag (to replace the EGFP) and complimentary flanking regions for Gibson Assembly. The backbone consisted of an Ampicillin resistance gene, each unique NLS sequence (or none for the control), and a LacZ gene downstream of the fluorescent tag (Fig. 4.6). The LacZ gene adds significant size (over 115 kDa) to the fluorescent fusion protein, preventing any passive diffusion, so that re-localization would depend entirely on active transport pathways[181].

Figure 4.6. Schematic of an NLS-mCherry-LacZ reporter, and a corresponding reporter control without an NLS sequence.
Fluorescent reporter consisted of an NLS sequence bound to an mCherry fluorescent tag, which was bound to LacZ. NLS sequences were variable. LacZ was designed solely to add a large molecular weight to the final fusion protein.

We designed primers (Table 4.4) to have a melting temperature (Tm) within 2-6 ºC of each other to facilitate PCR amplification of them as a group. After PCR amplification of both fragments per construct, we followed the previously described steps for DNA purification, and eventually for Gibson Cloning itself. Sequences were verified with CMV_Forward primers (universal) and an mCherry specific primer.

Table 4.4. List of primers for molecular cloning of NLS-mCherry-LacZ constructs.

Primer Name	Primer Sequence
mCherry_Vector_Fwd	CGGCGGCATGGACGAGCTGTACAAGGCGGCCGCCGTCGTTTTACAA
mCherry_Vector_Rev	TCCTCGCCCTTGCTCACCATGGCCCTCTCGGCCCTCGAGGAAT
mCherry_Insert_Fwd	ATTCCTCGAGGGCCGAGAGGGCCATGGTGAGCAAGGGCGAGGA
mCherry_Insert_Rev	TTGTAAAACGACGGCGGCCGCCTTGTACAGCTCGTCCATGCCGCCG
CMyc_mCherry_Vector_Fwd	GGCATGGACGAGCTGTACAAGGCGGCCGCCGTCGTTTTACAACGT
CMyc_mCherry_Vector_Rev	CATGTTATCCTCCTCGCCCTTGCTCACCATGGCCCTCTTGTCCAACTTGACCCT
CMyc_mCherry_Insert_Fwd	AGGGTCAAGTTGGACAAGAGGGCCATGGTGAGCAAGGGCGAGGAGGATAACATG
CMyc_mCherry_Insert_Rev	ACGTTGTAAAACGACGGCGGCCGCCTTGTACAGCTCGTCCATGCC
Nucleo_mCherry_Vector_Fwd	GCGGCATGGACGAGCTGTACAAGGCGGCCGCCGTCGTTTTACAA

Nucleo_mCherry_Vector_Rev	ATCCTCCTCGCCCTTGCTCACCATGGCCCTCTTGTCAAGTTTCTTC
Nucleo_mCherry_Insert_Fwd	GAAGAAACTTGACAAGAGGGCCATGGTGAGCAAGGGCGAGGAGGAT
Nucleo_mCherry_Insert_Rev	TTGTAAAACGACGGCGGCCGCCTTGTACAGCTCGTCCATGCCGC
HTLV1_mCherry_Vector_Fwd	GGCGGCATGGACGAGCTGTACAAGGCGGCCGCCGTCGTTTTACAACGT
HTLV1_mCherry_Vector_Rev	ATGTTATCCTCCTCGCCCTTGCTCACCATGGCCCTCTTGGTCGGCGGGCGTTT
HTLV1_mCherry_Insert_Fwd	AAACGCCCGCCGACCAAGAGGGCCATGGTGAGCAAGGGCGAGGAGGATAACAT
HTLV1_mCherry_Insert_Rev	ACGTTGTAAAACGACGGCGGCCGCCTTGTACAGCTCGTCCATGCCGCC
MX2_mCherry_Vector_Fwd	GGCGGCATGGACGAGCTGTACAAGGCGGCCGCCGTCGTTTTACAACGT
MX2_mCherry_Vector_Rev	ATCCTCCTCGCCCTTGCTCACCATGGCCCTCTCGGCCCCTTCTTTTTTCAG
MX2_mCherry_Insert_Fwd	CTGAAAAAAGAAGGGGCCGAGAGGGCCATGGTGAGCAAGGGCGAGGAGGAT
MX2_mCherry_Insert_Rev	ACGTTGTAAAACGACGGCGGCCGCCTTGTACAGCTCGTCCATGCCGCC

Primer sequence is color coded, with red nucleotides matching the DNA sequence of the mCherry fragment, and the black sequence matching the backbone fragment.

4.2 Tissue culture

4.2.1 Reagents

- DMEM with high glucose and pyruvate, Invitrogen cat. # 11995-065
- 200 mM L-Glutamine (100x), Life Technologies Cat. # 25030-081
- Penicillin-Streptomycin (10,000 U/mL), Life Technologies Cat. # 15140-122
- Fetal Bovine Serum, Sigma-Aldrich Cat. # F2442-500ml
- Bright-Line™ Hemacytometer, Sigma-Aldrich Cat. # Z359629-1EA
- 6-well tissue culture plate 353046, Fisher Scientific Cat. # 087721B
- Tissue Culture Dish 353003 100X20MM CS/200, Fisher Scientific Cat. # 08772E
- DPBS 1X Liquid 500 ml (No calcium, no magnesium), Invitrogen Cat. # 14190-250
- PageRuler™ Plus Prestained Protein Ladder, 10-250 kDa, Life Technologies Cat. # 26619
- Nitrocellulose Membrane, 1 roll, 0.45 µm, 30 cm x 3 m, Bio-Rad Cat. # 1620094
- Lumi-Light Western Blotting Substrate, Sigma-Aldrich Cat. # 12015200001, Roche

Growth media (550 ml)

Reagent or solution	Final concentration	Volume (ml)
DMEM 11995	-	500
FBS (100%)	10%	50
Glutamine (200 mM)	2 mM	5.5
Penicillin/Streptomycin (10,000 U/ml)	100 U/ml	5.5

Buffer A (50 ml)

Reagent or solution	Final conc.	Mass (g)	Volume (ml)
Tris Base	0.5 M	3.03 g	-
SDS	5%	2.5 g	-
MilliQ H_2O	-	-	50

Buffer B (50 ml)

Reagent	Final conc.	Mass (g)	Volume (ml)

DTT	0.125 M	0.96 g	-
Bromophenol Blue	0.05 %	2.5 mg	-
Glycerol	75%	-	37.5
Water	N/A	-	12.5

Store A and B at -20ºC or room temp.

1x Tris-Glycine Running Buffer

Reagent	Volume (ml)
10x Tris-Glycine buffer	100
Water	900

Western Transfer Buffer

Reagent	Volume (ml)
10x Transfer buffer	100
Methanol	200
Water	700

5% BSA (100 ml)

Reagent	Final conc.	Mass (g)	Volume (ml)
BSA	5%	5 g	-
Sodium azide	0.02 %	2 mg	-
Water	N/A	-	100

Filter through 0.45 µm filters and store at +4ºC

4.2.2 Thawing mammalian cells

Mammalian cell lines are stored in cryovials inside liquid nitrogen containers for long term. Cryo-freezing storage medium for cell lines is 90% FBS and 10% DMSO. This medium does not support growth and does not ensure efficient survival after thawing. As such, cells need to be rapidly thawed and moved into normal growth media.

1) Obtain a vial of cells stored in liquid nitrogen dewars.
2) Quickly thaw frozen cells in +37 ºC water bath for ~1-2 min.
3) Move 1 ml of thawed cells to 15 ml Falcon tube.
4) Add 9 ml of growth media, mix, and centrifuge at 1,000 g for 3-5 min.
5) Check for cell pellet and proceed with aspiration of media.
6) Add 10 ml of fresh cell media, mix cells, and move to 100 x 20 mm plate.
7) Refresh media after 1 day(s) or passage the cells if they are too confluent.

4.2.3 Maintaining cell line growth

Mammalian cells grow relatively quickly and need to be passaged 1:10 or 1:20 in 100 x 20 mm plates every 2-3 days. Passaging cells ensures optimal cell growth and health, and minimizes accumulation of any potentially negative or undesirable epigenetic effects.

1) Aspirate media and wash cells with 5-10 ml of DPBS.
2) Aspirate DPBS and re-suspend cells with 1-2 ml trypsin (in tissue culture incubator for 3-5 min).
3) Deactivate trypsin with 8-9 ml growth media and lift cells with pipette. Triturate cells and move 0.5-1 ml to new dish.

4.2.4 Transient transfection protocol

Figure 4.7. Timeline of cell transfection.
During a typical cell transfection, one has to seed cells 1-2 days prior to the experiment. Time points are flexible and cells can also be harvested after 24 hrs.

1) Harvest cells as previously described.
2) Count cells with Hemacytometer based on provided protocol.
3) Seed 100,000 cells per well into 6 well plates. It is typically easier to dilute cells to a concentration of 100,000 per ml (Fig. 4.7).
4) Make up volume to 2 ml final per well.
5) Once cells reach 40-60% confluence, transfect cells with JetPrime reagent.
6) Prepare scaled up mastermixes of JetPrime buffer, DNA, and JetPrime reagents for transfection. JetPrime buffer and reagent should be held on ice.
7) Aliquot JetPrime buffer, add DNA, vortex for 10 seconds, and briefly spin down tubes.
8) Add JetPrime reagent, vortex for 10 seconds, and briefly spin down tubes.
9) Incubate at room temperature for 10 minutes before transfection.
10) Carefully pipette the mixture onto cells (200 µl) drop by drop (use P200 and filter tips) and mix the media.

4.2.5 Harvesting transfected cells

1) At the designated timepoint, aspirate media and wash transfected cells with DPBS.
2) Aspirate DPBS and add 0.5 ml trypsin. Move the plate to incubator for 3-5 min.
3) Add 0.5 ml growth media to deactivate trypsin. Harvest cells with P1000 pipette (using filter tips) and transfer them into 1.5 ml Eppendorf tubes.
4) For cell count normalization, use 10 µl of re-suspended cells for cell counting with Hemacytometer.
5) Spin down cells at 1,000 RCF and +4 ºC for 5 min.
6) Aspirate media (use gel loading tip), briefly spin down at 1,000 RCF, and aspirate leftovers media.
7) Store cell pellet at -20 ºC until sample processing.

4.2.6 Lysis of harvested cells

1) Briefly warm cell pellets (from step 7 of 4.2.5) in hands or on ice and re-suspend cells in 75 µl of Buffer A.

2) Sonicate samples with a probe at 1.5 power for 3 cycles of 3 seconds each.
3) Add 75 µl buffer B, briefly vortex, and incubate lysates at +95 ºC for 5 min.
4) Briefly spin down at max RPM (~15,000) to bring down water vapor.
5) Normalize cell counts in samples (with 1:1 solution of Buffers A + B) based on previously obtained cell counts.

4.2.7 SDS-PAGE and Western Blot analysis of lysates

1) Load 5-15 µl of sample (5 µl of Ladder) on 4-12% Bis-Tris gel.
2) Initially run samples at 50-70 V (~10-15 min). Once samples enter the gel, run at 120-150 V (~60-120 min). Samples can be run slower for better resolution, but for a longer duration.
3) Shortly before the gel run ends, prepare tray for blotting paper, sponges, and nitrocellulose membrane and incubate them in the Western transfer buffer. Put 4 pieces of pre-cut blotting paper into the transfer buffer (two per side – or use thicker blotting paper).
4) Remove the gel from the cast, cut off bottom part (that protrudes into cast) and top part of the gel (~1 cm below lane lines). Incubate the gel in the transfer buffer.
6) Prepare transfer gel sandwich (white side, sponge, blotting paper (2 thin or 1 thick piece), nitrocellulose paper, gel, blotting paper, sponge, black side – Fig. 4.8). Roll air bubbles out of the sandwich before transfer.
7) Transfer at 35-45 V overnight in cold room.

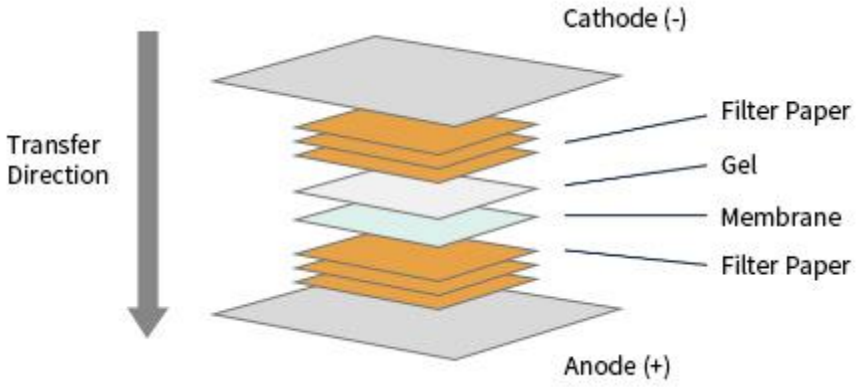

Figure 4.8. Schematic of Western Blot sandwich set-up.
Typical set-up for a Western Blot transfer. The SDS-PAGE gel is placed on top of a nitrocellulose membrane, which is oriented over the anode. The gel/membrane are subsequently sandwiched between filter papers and sponges, before being secured. Source: Sino Biological.

4.2.8 Blocking, antibody incubations, and imaging

1) Take apart gel sandwich, wash membrane in water, dry it between paper towels, and stain the blot with Ponceau dye. Ponceau stain illuminates protein bands as they were transferred onto the nitrocellulose blot. This is useful to assess any transfer issues, such as uneven transfer across the blot or presence of air bubbles that could interfere with immunodetection of key proteins.
2) Wash the stain off with water and TBS-T, and block the membrane in 5% non-fat dry milk (NFDM) in TBS-T for 30-120 min.
3) Wash the membrane in water and cut it with scalpel or scissors according to which antibodies are being used (can assay up to four different antibodies if they evenly span the molecular weight range of the gel).

4) Incubate primary antibodies in 2.5% NFDM (5% BSA or 5% NFDM can also work, depending on antibody) at room temperature for 2 hours. I utilize a thermal sealer and pouch method (uses only 0.5-1 ml for primary antibody incubation): the tube rack is placed on top of the pouch to distribute pressure on the solution equally.
5) Wash membranes 3 times in 5-10 ml 1xTBST at room temperature for 10 min each time.
6) Incubate membranes in secondary antibody at room temperature (1:5,000 in 2.5% Milk / 1x TBST) for 1.5 hours.
7) Wash membranes 4-6 times in 1x TBST at room temperature for 10 min.
8) Combine equal volumes of Reagents A and B from Lumi Light Western Blotting kit, incubate ECL reagent in a tube for 1 min, pipette it onto the membrane and incubate for another 1-3 minutes. Dry off ECL reagents with paper towel.
9) Image immunoblots with Chemiluminescence setting on ImageQuant LAS 4000 instrument. Exposure times vary among various antibodies.

4.3 Stable cell line generation

Stable cell lines with inducible protein expression were prepared following the PiggyBac Transposon System protocol (System Biosciences). PiggyBac plasmids flank the gene of interest with transposition sites, which can be activated during parallel production of Transposase. The result is integration of the gene of interest into chromosomal DNA of the transfected cells (Fig. 4.9).

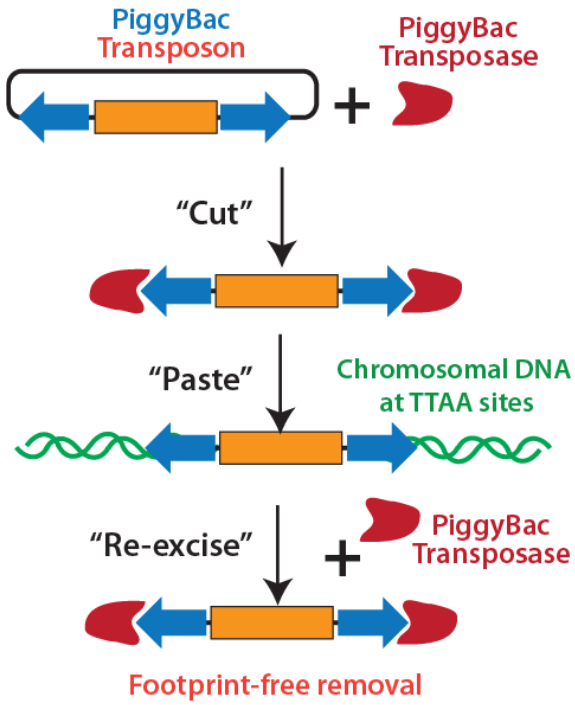

Figure 4.9 Schematic of PiggyBac integration into chromosomal DNA. PiggyBac Transposon is flanked by ITRs. Addition of the transposon to a cell, along with a vector expressing the PiggyBac Transposase, initiates integration events. The Transposase cuts the transposon at the ITR sites and pastes the gene into chromosomal DNA, with a preference to TTAA DNA sites. PiggyBac Transposase can also be utilized to reverse this integration event and excise added DNA.

We followed the provided protocol for stable cell line preparation from PiggyBac plasmids with our genes of interest.
1) Grow target cells to 60-80% confluency.

2) For one well of a 6-well dish (~1 x 10^6 cells), combine 0.5 µg PiggyBac Transposon vector clone (our plasmids) and 0.2 µg PiggyBac Transposase vector (PB210PA-1, System Biosciences).
3) Combine plasmid DNA with transfection reagents of choice and incubate the mixture according to protocols.
4) Gently add the DNA-transfection mixture drop-wise to cell culture and swirl to disperse the mixture.
5) The PiggyBac transposase activity will terminate after 72 hours resulting in integration of the transposon vector into the genome.
6) After 72 hours, switch growth media to include 1 µg/mL puromycin, and replace media daily. Continue antibiotic selection for 10 days before passaging cells.
7) Cells with integrated genes of interest will also retain a puromycin resistance gene and will survive the selective pressure.

4.4 Cleavage assay to detect $2A^{pro}$ expression

Given that $2A^{pro}$ shuts down host translation, preventing and limiting its own detectable accumulation by immunoassays, development of an alternative detection method for the protease has become imperative. We have developed a cleavage assay, whereby we measured the cleavage of known proteolytic targets as a proxy for $2A^{pro}$ expression. With either transient transfection or inducible protein expression, we can detect cleavage of Nup98 and eIF4G as early as 6 hours post-transfection/induction. Nup98 is usually undetectable when immunoassayed side-by-side with control samples. Likewise, eIF4G levels decrease significantly during $2A^{pro}$ expression, and a cleavage product of ~130 kDa can also be visualized by immunoblotting.

4.5 Cryogenic lysis

Cryogenic lysis is an effective approach pioneered by the Rout laboratory for large-scale preparation of eukaryotic cells prior to immunoprecipitation or other biochemical assays. Cells are grown in large quantities, collected, and ground to fine powder under -140 ºC conditions with a mill and steel balls. This lysis process creates homogeneous cell powder and provides an opportunity to assay a variety of immunoprecipitation conditions.

4.5.1 Large scale expansion of mammalian cell lines

1) Transfer stable cell lines into 8-16x 245 mm x 245 mm square treated tissue culture dishes (Fisher Scientific 431110).
2) Induce protein production with Doxycycline (100 ng/mL)
3) After 12-24 hours of protein production, prepare to harvest cells.
4) Gently wash cells with ice cold DPBS, decant, and collect cells with cell lifters (Corning 3008) while on ice.
5) Pool cells in 50 ml falcon tubes, wash cells in DPBS (2 rounds of washes) by spinning down cells at 500 g for 10-20 minutes. With each wash, concentrate cells into a Falcon tube.
6) Collect cells in a 10 mL syringe (with end capped) after last wash, spin cells down at 500 g for 10 minutes.
7) “Noodle” cells into 50 mL Falcon tube with liquid nitrogen by pushing pelleted cell material out of syringe.
8) Store Falcon tube(s) at -80 ºC. Initially, place tubes vertically to let remnants of liquid nitrogen evaporate.

4.5.2 Wet grind using liquid nitrogen

1) For samples up to 3g, use a 50 ml jar with 3x 20mm steel balls, large insulated Teflon jar, and Teflon hat (total weight about 3.5 Kg).
2) Pre-chill everything in liquid nitrogen.
3) Add liquid nitrogen to the jar to about 1cm from the top.
4) Add sample and balls to the jar. Alternatively, sample and steel balls can be added first and liquid nitrogen second, but there is a risk of dispersing sample if done incorrectly.
5) Put the lid on and then the Teflon hat.
6) Clamp it down and pour liquid nitrogen into the large Teflon jar until it is full around the inner jar. Liquid nitrogen will pour out of the jar when it is full.
7) Do 3 x 3 min grinding (400rpm) with 1 min intervals in the manual mode.
8) Pour liquid nitrogen into the large Teflon jar after each 3 min cycle.
9) After 3 cycles, add liquid nitrogen to cool the 50 ml jar before opening the lid.
10) Slowly untighten the clamp and let the pressure release gradually before opening the lid.
11) If there is still liquid nitrogen in the jar, let it slowly evaporate.
12) Scoop up the powder into a pre-cooled 50 ml Falcon tube and store it at -80 freezer (leave the lid loose if the powder is still wet to let nitrogen evaporate).

4.6 Nanobody dynabead conjugation

Magnetic Dynabeads conjugated to nanobodies is a key tool in our arsenal for immunoprecipitation experiments. Nanobodies are small and usually have high binding affinity to their substrates. In our experiments, we utilized Dynabeads conjugated to anti-GFP and anti-Nup214 nanobodies.

1) Weigh out 50 mg Dynabeads (ThermoFisher 14302D). Scale as needed – adjust nanobody amount and buffer volumes proportionately.
2) Wash with 5 ml 0.1M Na-phosphate, pH 7.4. Incubate 10 min on nutator or rotator.
3) Wash again with 5 ml 0.1M Na-phosphate, pH 7.4. No incubation needed.
4) Prepare nanobody mix during Dynabead washes. Mix Na-phosphate, ammonium sulfate, and water first and then add nanobody and quickly mix.

1 ml of nanobody mixture:
333 µl of 3M ammonium sulfate
200 µl 0.5M Na-phosphate, pH 8.0
0.5 mg nanobody (10µg nanobody per mg Dynabeads)
Water to 1ml final volume

5) Add the nanobody mixture to washed beads and transfer everything to 14 ml round bottom culture tube.
6) Incubate 20-24 hrs at 30 °C on rotating wheel.
7) Wash 4 times with 1 ml PBS: incubate 5 minutes per wash, nutating or rotating.
8) Wash with 1 ml PBS with 0.5% Triton X-100. Incubate 5 minutes nutating or rotating.
9) Wash again with 1 ml PBS with 0.5% Triton X-100. Incubate 15 minutes nutating or rotating.
10) Resuspend beads in 333 ul PBS supplemented with 50% glycerol and 0.02% NaN_3.
11) Store at -20 °C.

4.7 Immunoprecipitation of picornaviral proteases

Affinity capture protocols were established based on existing in-house Rout laboratory protocols. Several different types of buffer conditions were assayed before we decided to stick to specific buffers for quantitative MS analyses downstream of pulldowns.

4.7.1 Standard immunoprecipitation

Buffers:
1 - 20mM HEPES, pH 7.4, 150 mM NaCl, 0.5% Triton X-100
2 - 20mM HEPES, pH 7.4, 300 mM NaCl, 0.5% Triton X-100
3 - 20mM HEPES, pH 7.4, 500 mM NaCl, 0.5% Triton X-100

Keep buffers on ice, except for an aliquot for cell lysis/resuspension. Keep the lysis aliquot at room temperature. Take out beads and warm them at room temperature in the meantime to simplify bead mixing and aliquoting.

1) Weigh out 50/100 mg of powder and prepare 500/1000 µl buffer with Protease Inhibitor cocktail (Complete-EDTA free at 100x and 100x Solution P). Keep powder in liquid nitrogen until ready to re-suspend with lysis powder. Use regular 1.5 ml tubes for powder.
2) Remove the powder from liquid nitrogen, one tube at a time. Briefly warm a tube enough to open the lid and resuspend the powder with the lysis buffer by pipetting up and down multiple times. Vortex for 1 sec.
3) Sonicate the resuspended powder twice for 2 sec at power setting 2.5.
4) Clarify the lysate at the maximum speed (14,000 RPM/21,000 g) for 15 min.
5) Mix bead stock with pipette and aliquot 5/10 µl per tube. Use 2 ml Eppendorf tubes with wide bottom to mix the beads properly during incubations.
6) Wash beads 3 times with the lysis buffer (no protein inhibitor cocktail), gently mix them with pipette or flip the tube.
7) Add the clarified supernatant to the beads and rotate the tubes at +4 ºC for 30-45 min.
8) Aspirate supernatant and wash 3 times with 1 ml buffer. At the 2nd or 3rd wash, transfer the sample to a new 1.5 ml tube.
9) Spin down the tube after the 3rd aspiration and aspirate again with a P2 tip to ensure that no residual buffer is left in the tube.

Elution (two options):

1x LDS Elution:
10) Add 18 µl LDS (no DTT) and incubate at 72 ºC while shaking for 10 min.
11) Spin down briefly, transfer the eluate to a fresh tube, and add 2µl DTT from 1 M stock up to 100 mM final concentration to each sample.
12) Boil the eluate at +95 ºC for 3-5 min.

NH_4OH Elution:
10) Do an extra wash with 100 µl ammonium acetate (100 mM) and 0.1 mM $MgCl_2$. Mix beads by flicking tube and letting sit for 1-2 min.
11) Spin down the beads and aspirate twice to fully remove all buffer. Turn on SpeedVac to warm it up.
12) Add 400 µl of NH_4OH (1N) and 0.01 mM EDTA.

13) Rotate at +4 ºC for 3 hrs.
14) Transfer the eluate to fresh 1.5 mL Eppendorf tubes. Clarify the eluate at the maximum speed (14,000 RPM/21,000 g) for 15 min. This procedure occasionally removes some beads.
15) Transfer the clarified eluate to fresh tube. Take a 10% aliquot for gel electrophoresis and silver staining.
16) Speedvac for over 3 hrs, checking for buffer evaporation. Sometimes buffer takes overnight to evaporate.

4.7.2 Immunoprecipitation after chemical crosslinking of interacting partners

Buffers:
2 – 20 mM HEPES, pH 7.4, 300 mM NaCl, 0.5% Triton X-100
2 - 2x – 40 mM HEPES, pH 7.4, 1,000 mM NaCl, 1% Triton X-100
100 mM Ammonium Bicarbonate (make fresh), ~791 mg per 100 mL
10 mM Sulfo-NHS Acetate (make fresh), ~6.2 mg per 2.4 mL water - may need to adjust volume according to number of samples. 2.4 mL is typically sufficient for 4 reactions (0.5 mL per reaction with Buffer 2-2X; 1 mL buffer for 100 mg powder).
DSS-H12 – 50 mM - 1 mg (small aliquots) in PCR tubes (add 53 µl DMSO). Vortex to dissolve.

1) Prepare Sulfo-NHS Acetate for final concentration of 10 mM.
2) Aliquot beads for pulldown.
3) Wash beads twice with IP buffer.
4) Dilute Sulfo-NHS Acetate and 2x-2 immunoprecipitation (IP) buffer (1-to-1). Pre-treat beads with Sulfo-NHS Acetate for 1 hr rotating at room temp.
5) Measure out cell powder for experiment at the ~40 min after the start of the incubation (100 mg). Prepare all tubes for IP.
6) Wash beads with IP buffer.
7) Quench pretreatment with Ammonium Bicarbonate: dilute 100 mM 1-to-1 with 2x-2 IP buffer and incubate at room tempretaure on a rotator for 20 min.
8) Resuspend 100 mg cell powder in1 ml of buffer 2 (all protease inhibitor cocktails) by pipetting and sonicate twice for 2 seconds at power 2.5. Clarify lysates at the maximum speed (14,000 RPM) for 10-15min.
9) Wash beads twice with IP buffer.
10) Add lysates to beads and incubate rotating at +4 ºC for 30-45 min.
11) Prepare aliquots of DSS in IP buffer. Leave at room temperature (DMSO freezes on ice). I prepared DSS aliquots with 0, 0.05, 0.2, and 1 mM DSS.
12) Wash the beads trice with IP buffer. On the 2nd and 3rd wash, transfer the beads to fresh tube.
13) Add DSS in IP buffer to the beads and crosslink at room temperature on a rotator for 30 min.
14) Quench with 50 mM Ammonium Bicarbonate (in 1x IP buffer) at room temperature on a rotator for 20 min.
15) Wash beads with IP buffer.
16) Add 18 µl LDS (no DTT) to the beads and incubate at 72 ºC with shaking for 10 min.
17) Spin down briefly, transfer eluate to a fresh tube, and add 2µl DTT from1M stock up to 100 mM final concentration to each sample.
18) Boil the eluate at +95 ºC for 3-5 min.

4.8 Mass spectrometry sample preparation by centrifugation using OMIX C18 tips

MS processing of proteins is initiated by analyzing samples by SDS-PAGE. Immunoprecipitation samples can be run through a gel, with specific protein bands excised for analysis. Alternatively, a 5 min PAGE run ("gel plug") allows us to analyze the entirety of a sample without numerous and laborious excisions, and downstream gel piece processing. Immunoprecipitation samples were analyzed by gel plugs and MS by Erica Jacobs, our collaborator from the Chait laboratory.

Day 1

1) Cut bands and chop each one into $1mm^3$ cubes.
2) Add 200 µl 50mM Ammonium Bicarbonate /50% Acetonitrile.
3) Mix the solution with the gel pieces by vortexing.
4) Incubate at 37 °C for 30 min; discard the supernatant.
5) Add another 200 µl 50mM Ammonium Bicarbonate /50% Acetonitrile if the gel pieces are still blue. Destain more as needed; usually 2 incubations for 30 min are enough for a single band.
6) Remove 50 mM Ammonium Bicarbonate / 50% Acetonitrile when the gel pieces are completely destained.
7) Add 100 µl Acetonitrile, vortex, let the tubes set at room temperature for 2 min or more.
8) Remove Acetonitrile from all samples.
9) Dehydrate in speedvac for 10 min. Samples can be stored at -20 °C or used for to trypsin digestion.

Day 2

10) Prepare trypsin working solution: 12.5 ng/µl in 50 mM Ammonium Bicarbonate (trypsin stock 100 ng/µl in 1 mM HCl). Prepare tubes on ice.
11) Add 12.5ng/µl trypsin to cover gel pieces. It is typically 15 µl per tube for a single band cut from the 15-well gel; may need to add more for 10-well gel band.
12) Let samples swell on ice for 45 min.
16) After swelling, add 50 mM ammonium bicarbonate to cover gel pieces if necessary (~5 µl for 15-well gel or 10 µl for 10-well gel).
17) Move the tubes to 37 °C incubator to digest overnight (6 hrs at least).

Day 3

18) Add 0.5% TFA (w/v, final concentration) to stop digestion:

- Dilute 20% TFA stock to 2% first.
- Add 1/3 of digestion vol. of 2% TFA to digestion mix.
- Mix TFA with gel pieces and incubate @ room temp for 5 min

19) Transfer the digestion solution to 0.65ml low-binding tubes; hold at room temperature or +4 °C.
20) Extract with 30 ul of 0.1% TFA at room temperature for 45 sec.
21) Remove extractant and combine with the digestion solution. Total volume is ~50 µl for each 15-well gel band.

Desalt sample using OMIX tips (C18, 10 ul for gel band) by centrifugation

22) Tip wet: 2x 10 µl of 50% ACN (v/v), 0.1% TFA (w/v).
23) Spin at 1,000 rpm for 1 min (same speed and time for later spinning steps).

24) Wash the tips twice with 10 µl of 0.1% TFA (w/v).
25) Sample binding: let the sample pass through the filter once. Load 20 µl at a time; may have to load multiple times for each sample.
26) Save the flow-through at -20°C in case the binding is not complete.
27) Wash the sample 5 times with 10 µl of 0.1% TFA (w/v).

Elute sample by centrifugation
28) Pre-wash one set of low-binding tubes with 100% can to hold elution (for both elutions 1 and 2)
29) Elution 1: 20 µl 40% Acetonitrile / 0.5% Acetic acid. Use clean collecting tube pre-washed with 100% ACN. Let everything pass through.
30) Elution 2: 20 µl 80% Acetonitrile / 0.5% Acetic acid. Let everything pass through. Collect both eluates in the same tube.
31) Put the tube containing combined eluates in the SpeedVac and dry completely.

4.9 Proteomic data analysis

Raw MS data was analyzed with Proteome Discoverer software (Thermo Fisher Scientific) with an in-house generated list of protein database to compare peptides (Erica Jacobs, Chait Laboratory, St. John's University). Key data metrics generated during output included protein identity (gene name), number of PSMs, unique peptides identified in MS/MS, coverage of protein, and raw peptide quantity. Data output was generated in CSV format and converted to an Excel sheet for curation and analysis. Data was averaged by pulldown type (n=3), and sorted by the number of unique peptides. Identified proteins with fewer than 3 unique peptides were removed from the list (Fig. 4.10). The new datasets were normalized by the GFP protein levels ($2A^{pro}$ or 2AC110A subtracted by GFP), and finally curated by a list of non-specific GFP interactors identified in the CRAPome database (Table 4.2). The remaining proteins are enriched during affinity capture and represent interacting partners of the handle. Data analysis included plotting proteins ranked by peptide quantity and assessing fold enrichment between data sets.

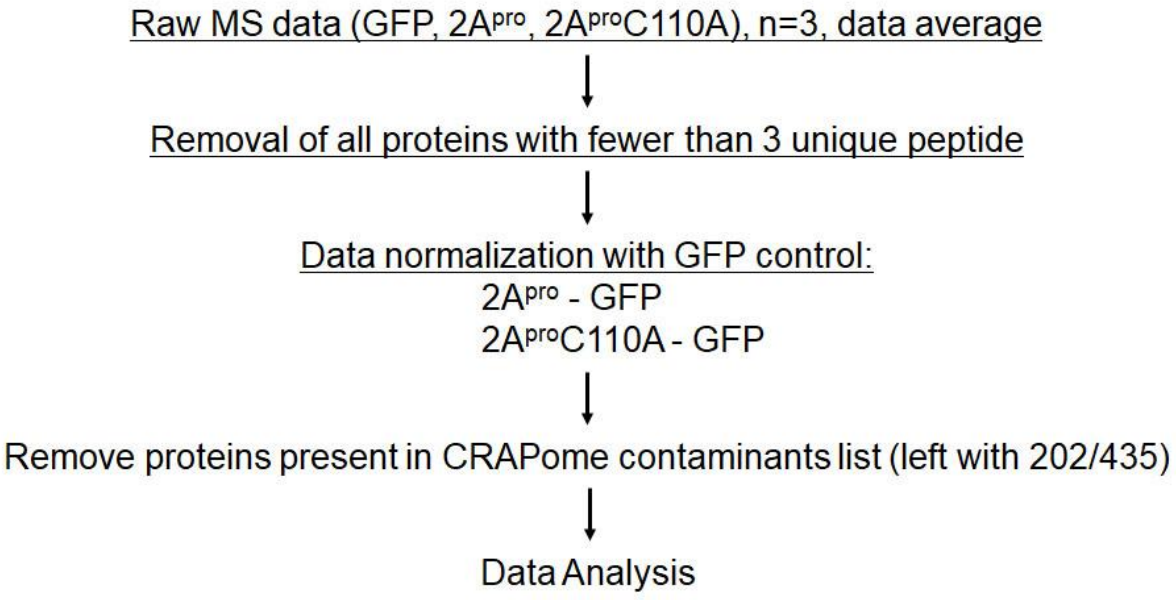

Figure 4.10. Schematic of interactome curation and analysis pipeline for $2A^{pro}$ pulldowns.

Raw MS data was analyzed with Proteome Discoverer software, which output a protein list of putative interacting partners. The data was averaged within data sets, ranked by unique peptides, and proteins with fewer than 3 unique peptides were removed. The remaining data was normalized by the GFP data set (raw peptide quantities were subtracted) and curated with the CRAPome contaminants list. The final data was ready for analysis such as rankings or fold-enrichments.

Nup214 MS analysis pipelines were modified based from the $2A^{pro}$ protocol (Fig. 4.11). Data sets were still averaged (n=3), curated for unique peptide counts, and interrogated against the CRAPome contaminants list resulting in 372 identified proteins from the initial list of 839 proteins. However, datasets were not normalized against the GFP "control" pulldown. Instead, during downstream analysis via fold enrichment, datasets were internally normalized to their own Nup214 levels.

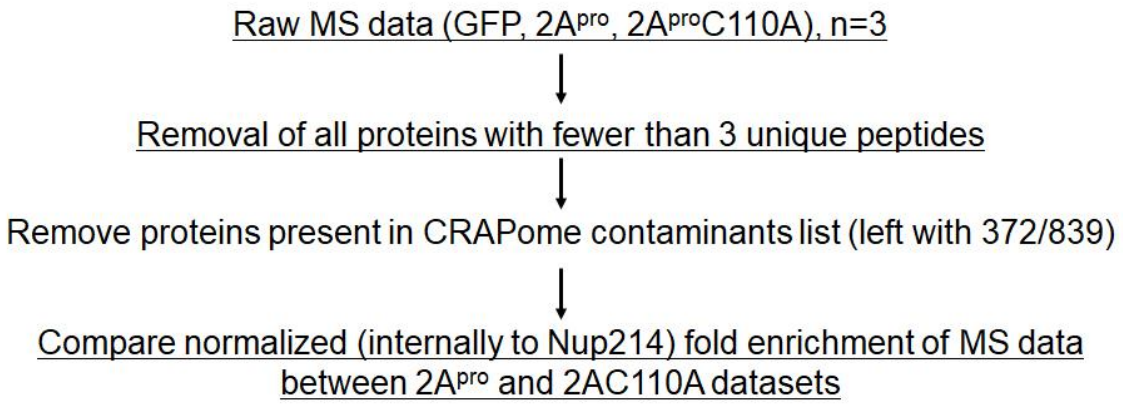

Figure 4.11. Schematic of interactome curation and analysis pipeline for Nup214 pulldowns.
MS data analysis pipeline was modified from $2A^{pro}$ protocol. The initial curation steps were the same, however, data sets were not normalized by the GFP data set. MS data was analyzed by fold enrichments and datasets were internally normalized to Nup214 enrichment.

4.10 Immunofluorescence and immunostaining of mammalian cell lines

1) Wash cells with PBS supplemented with 0.5 mM $MgCl_2$ and 0.9 mM $CaCl_2$ for 1-2 min.
2) Fix the cells in 4% PFA at room temp for 15 min.
3) Wash trice with PBS for 1-2 min.
4) Permeabilize the cells using 0.2% Triton-X 100 in PBS at room temperature for 10 min.
5) Block with 5% goat serum, 1% BSA, in PBS at room temperature for 1 hour.
6) Incubate the solution with primary antibody in blocking solution at +4 ºC overnight.
7) Wash with PBS 4 times at room temperature for 2 min.
8) Incubate with the 2^{nd} antibody in PBS at room temperature for 2 hours.
9) Wash trice with PBS at room temperature for 2 min.
10) Stain nuclei with DAPI (1:1000) in PBS at room temperature for 10 min.
11) Mount coverslips with ProLong Gold Antifade.

4.11 Fluorescent reporters to assay $2A^{pro}$ effects on nuclear transport

Fluorescently tagged (GFP or mCherry tags) fusion proteins with localization tags were developed by the Rout laboratory as reporters to study nuclear-cytoplasmic transport. These reporters are useful for a number of biological contexts: for instance, at over- or under-production of various Nups implicated in transport, during addition of chemical blockers of transport, or during expression of viral protein genes implicated in affecting transport. In our case, we were keen on exploring the effects of the $2A^{pro}$ on nuclear-cytoplasmic trafficking. We and other researchers established the $2A^{pro}$ mediated cleavage of Nup98 as a rapid and specific event. However, it is not fully explored how Nup98 cleavage affects cells on the protein or RNA level.

4.11.1 Poly-T FISH staining for assaying protease-mediated effects on mRNA localization

Buffers:

20x SSC: 3M NaCl, 400 mM Na-citrate.

Hybridization buffer: 1 mg/mL yeast tRNA, 0.005% Goat Serum, 10% dextran sulfate, 25% formamide, 2x SSC.

Oligo-dT(30) conjugated with Tye563 were ordered from IDT.

1) Stable cell lines were grown and induced for overnight expression of proteases.
2) Cells were washed, fixed with formaldehyde, permeabilized with 0.2% Triton X-100 in PBS, and washed again.
3) Cells were stained with 100 nM Oligo-dT in Hybrization buffer at +37 ºC in a humidity chamber overnight.
4) Wash cells with 4 times with SSC pre-warmed to +37 ºC.
5) Wash cells with 2x SSC pre-warmed to +37 ºC.
6) Wash cells twice with 2x SSC at room temperature.
7) Follow DAPI staining protocol before mounting coverslips for imaging.

4.11.2 Stable cell lines constitutively expressing NLS- or NES-tagged fluorescent reporters

The Rout laboratory developed stable cell lines constitutively expressing GFP-GFP-NLS/NES fusion proteins using lentiviral systems. Stable lines with HOS, HT1080, HeLa, and HEK293T cells were formed, expressing GFP_2-NLS/NES/NLS-NES protein fusions. The NLS sequence was cloned from SV40 Large T-antigen, the NES peptide sequence was from PKI, and the NLS-NES was the combination of both. Reporters would localize to their respective compartments, with the NLS-NES fusion mostly localizing to the nucleus. Any external stress, such as $2A^{pro}$ expression, would relocalize reporters to a new compartment accordingly. Stable cell lines constitutively expressing fluorescent reporters were transiently transfected with $2A^{pro}$ or 2AC110A, as per established protocol. Cells were subsequently fixed with formaldehyde and treated as per immunostaining protocol.

4.11.3 HeLa cells expressing NLS-tagged fluorescent-LacZ fusion reporters

NLS/NES-mCherry-LacZ fusion reporters were also developed to study nuclear-cytoplasmic trafficking. These fusion proteins are considerably larger than most assayed NLS/NES reporters, and as such, should not be affected by passive transport effects. We assayed these reporters by transiently transfecting them into HeLa stable cell lines with integrated GFP/GFP-$2A^{pro}$/GFP-2AC110A, 12-16 hours before induction of protease expression. Cells produced

protease for 12-16 hours before being fixed with formaldehyde and treated as per immunostaining protocol.

4.12 Biochemical fractionation of mammalian cell lines into nuclear and cytoplasmic fractions

1) Cells from 2 x 10 cm plates were harvested with 1-2 mL trypsin per plate, incubated at 37 ºC as necessary (Fig. 4.12). Some cell lines like HeLa will need additional incubation.
2) Add 10 mL DMEM to each plate (DMEM, P/S, 10% FBS) and transfer cells to 15 or 50 mL tubes and centrifuge at 50 g for 10 mins.
3) Aspirate media and resuspend gently with 1 mL cold PBS.
4) Transfer to 1.7 ml tubes and centrifuge at 50 g for 2 min.
5) Aspirate PBS and add fresh PBS. Let the cells sediment by gravity for ~5-10 min.
6) Add cell slurry (75 µL) to the lysis buffer (600-750 µL), vortex on medium speed for 5 sec, and let the cells swell on ice for 5 mins. Lysis buffer: 6% polyvinylpyrrolidone (PVP), 0.045% digitonin and Triton X-100, 1 mM DTT, 4 µM CytoB, 1:100 solution P (100 mg of PMSF, 2 mg of pepstatin A in 5 ml of ethanol).
7) Stroke cells with 1 ml insulin syringe (28 gauge). Cellular fractionation may occur anywhere from 30-50 strokes. Monitor by phase contrast microscopy for sufficient lysis and dispersal of cytoplasmic material away from nuclei.
8) Underlay lysed cells with 200 µL of 20% sucrose and centrifuge at 3,500 g at 4 ºC for 10 mins. The resulting supernatant, including the sucrose portion, is the Cytoplasmic fraction.
9) Gently resuspend the pellet with 1,000 µl of 6% PVP supplemented with 1 mM DTT and Solution P (1:100). Polytron twice on mid power for 10 sec.
10) Add 1 ml of 2.01 M sucrose in PVP to an SW55 tube. Overlay the resuspended cells with a layer of sucrose. Then overlay and fill the tube to the top with 6% PVP. Spin 20,000 RPM in ultracentrifuge for 40 mins.
11) Aspirate the buffer to the interface at ~1 cm from the bottom of the tube. Collect the interface and the sucrose underlay (~1 ml). This is the Membrane fraction.
Note: If there is no interface, the membrane fraction is integrated into the nuclear fraction.
12) Resuspend the remaining pellet in 200 µL 6% PVP. Confirm nuclei under phase contrast microscopy. This is the Nuclear fraction.
13) Precipitate the samples with methanol. Take 100 µl of each fraction (vortex the samples vigorously prior) and add 900 µl methanol. Vortex vigorously again and place the samples in -20 ºC freezer for overnight precipitation.
14) Pellet the samples by centrifugation at 14,000 RPM for 20 mins.
15) Aspirate supernatant and add 500 µL of 90% methanol. Sonicate at power 3 for 5 sec. Incubate samples at -20 ºC for 30 min.
16) Pellet samples again by centrifugation at 14,000 RPM for 20 mins.
17) Aspirate the supernatant and resuspend the pellet with 50 µL buffer A (0.5 M Tris-HCl, pH 10, 5% SDS). Sonicate to resuspend proteins at power 2.5 for 5 sec.
18) Add the equal volume (50 µL) of buffer B (75% glycerol, 0.125 M DTT, 0.05% Bromophenol Blue).

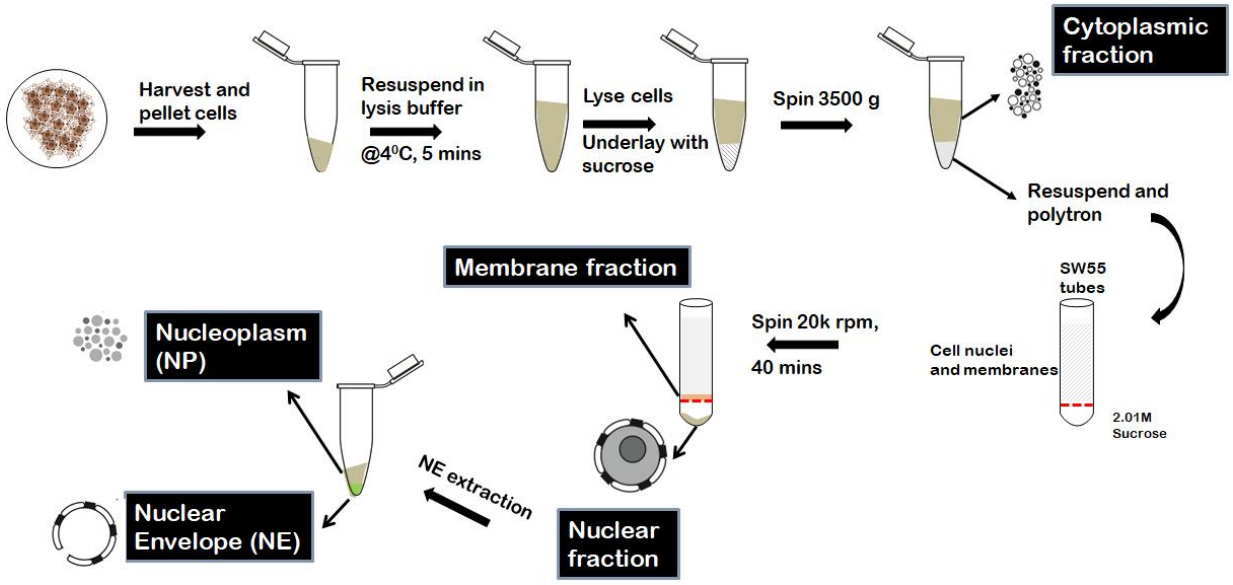

Figure 4.12. Schematic of biochemical fractionation.
Cellular fractionation is a flexible protocol, pliable to a number of cell lines and even tissue types (data not shown). The Rout laboratory has developed this protocol and assayed it for HeLa, HEK293T, HOS, and HT1080 cell lines. Cells are grown and collected for the protocol, gently spun down, washed, and eventually lysed in a 6% PVP buffer with a 28-gauge needle. Cells are monitored by phase contrast the separation of cytosol from nuclei. Cell material is spun down in a sucrose underlay to obtain a cytoplasmic fraction. The remaining fraction can be further separated into a membrane and nuclear fraction with another high-speed centrifugation and a sucrose underlay. All samples are eventually methanol precipitated for downstream processing.

4.13 Cellular viability assay

Picornaviral proteases, particularly $2A^{pro}$, are known to trigger apoptosis in mammalian cell lines, resulting in the eventual cell death. Utilizing our HeLa stable cell lines, we can assay and quantify cellular viability during expression of genes of interest, and especially $2A^{pro}$.
1) 50,000 HeLa cells were seeded in 6-well plates for the assay.
2) At time point 0, cells were collected and counted by Hemacytometer to establish baseline for growth. All remaining cells had their growth media replaced, either with standard media or media with Dox to induce protein expression.
3) Cells were collected at 12, 24, and 36 hours post-induction and counter by Hemacytometer.

4.14 List of CRAPome proteins identified as non-specific interactors in GFP-related affinity capture

Utilizing the publically available CRAPome database, we filtered all known contaminants of GFP immunoprecipitation experiments and generated a list containing ~1,300 proteins.

Table 4.5. List of CRAPome non-specific interactors we curated during proteomic analysis.

AAR2	CDK16	EHMT1	HIST1H3F	KRT76	ORC3	RBM39	SART1	TBPL2	ZC3H18
AATF	CDK17	EIF2AK2	HIST1H3G	KRT77	OS9	RBM42	SCAF1	TBX4	ZC3H4
ABCC2	CDK18	EIF2S1	HIST1H3H	KRT79	PABPC1	RBM5	SCAF11	TCEA1	ZC3HAV1
ABCD3	CDK2	EIF2S2	HIST1H3I	KRT8	PABPC3	RBM7	SCAF4	TCEA2	ZCCHC10
ABCF1	CDK3	EIF2S3	HIST1H3J	KRT80	PABPN1	RBM8A	SCAF8	TCEB3	ZCCHC17
ACIN1	CDK4	EIF4A1	HIST1H4A	KRT84	PAF1	RBMX	SCYL2	TCERG1	ZCCHC8
ACSS3	CDK5	EIF4A2	HIST1H4B	KRT9	PAK1IP1	RBMX2	SDAD1	TCF20	ZFC3H1
ACTA1	CDK6	EIF4A3	HIST1H4C	LACTB	PALB2	RBMXL1	SDCBP	TCOF1	ZFP1

ACTA2	CDK9	EIF5B	HIST1H4D	LARP1	PALM	RBMXL2	SEMA3B	TCTEX1D1	ZHX1-C8ORF76
ACTB	CDX1	EIF6	HIST1H4E	LARP1B	PAPD5	RBMXL3	SENP2	TDRD3	ZMYM1
ACTBL2	CDYL	ELAVL1	HIST1H4F	LARP4	PARP1	RCN2	SENP3	TECR	ZMYM4
ACTC1	CEBPZ	ELL2	HIST1H4H	LARS	PARP2	RECQL5	SERBP1	TEX10	ZMYND11
ACTG1	CENPB	ELOF1	HIST1H4I	LAS1L	PARP4	REXO4	SERPINH1	TFB1M	ZNF280B
ACTG2	CENPF	EMB	HIST1H4J	LEO1	PARVB	RFC1	SETD2	TFIP11	ZNF280C
ACTL6A	CENPV	EMD	HIST1H4K	LEPRE1	PAXBP1	RFC2	SF3A1	TGFBR3	ZNF280D
ACTL6B	CEP290	EMG1	HIST1H4L	LGALS7	PCBP1	RFC3	SF3A2	THAP11	ZNF281
ACTR1A	CETN2	ENY2	HIST2H2AA3	LGALS7B	PCBP2	RFC4	SF3A3	THEM6	ZNF326
ADAR	CHAMP1	EPB41L4B	HIST2H2AA4	LIG3	PCBP3	RFC5	SF3B1	THOC1	ZNF451
AFF4	CHD1	EPB41L5	HIST2H2AB	LIMK1	PCBP4	RICTOR	SF3B2	THOC2	ZNF512
AGBL1	CHD2	EPHB4	HIST2H2AC	LLPH	PCSK1	RING1	SF3B3	THOC3	ZNF593
AHCTF1	CHD4	EPPK1	HIST2H2BE	LMNA	PDCD11	RNF113A	SF3B4	THOC5	ZNF616
AHSA1	CHD6	EPRS	HIST2H2BF	LMNB1	PDCD6	RNF13	SF3B5	THOC6	ZNF638
AIFM1	CHD7	ERH	HIST2H3A	LMNB2	PDP2	RNF2	SFN	THOC7	ZNF655
AIMP1	CHD8	ERLIN1	HIST2H3C	LRRC59	PDRG1	RNMTL1	SFPQ	THRAP3	ZNF830
AIMP2	CHD9	ERLIN2	HIST2H3D	LRWD1	PELP1	RNPC3	SFSWAP	THSD7A	ZNF839
AK9	CHERP	ESCO2	HIST2H4A	LSM11	PES1	RNPS1	SGSM1	TIAM1	ZRANB2
AKAP17A	CHMP3	ESPL1	HIST3H2A	LSM2	PFKFB4	RP9	SKIV2L	TIMM13	
AKAP8L	CHMP4B	EXOSC1	HIST3H2BB	LSM3	PGAM5	RPAP1	SKIV2L2	TIMM50	
ALYREF	CHTOP	EXOSC10	HIST3H3	LSM4	PHC3	RPAP2	SLC1A2	TIMM8B	
AP2M1	CIR1	EXOSC2	HIST4H4	LSM5	PHF14	RPF1	SLC22A24	TJP2	
APOBEC3B	CIRBP	EXOSC3	HMG20A	LSM6	PHF15	RPF2	SLC25A1	TMA16	
APOBEC3C	CIRH1A	EXOSC4	HMGN1	LSM7	PHF16	RPL10	SLC25A10	TMCO1	
APOBEC3D	CKAP2	EXOSC5	HMGN2	LUC7L	PHF17	RPL10A	SLC25A11	TMEM26	
APOBEC3F	CKAP4	EXOSC6	HMGN4	LUC7L3	PHF3	RPL10L	SLC25A13	TMEM33	
AQR	CLASRP	EXOSC7	HMGXB4	LYAR	PHF5A	RPL11	SLC25A3	TMPO	
ARGLU1	CLK1	EXOSC8	HNRNPA0	MAGOH	PHF6	RPL12	SLC25A31	TNFAIP1	
ARHGAP35	CLK2	EXOSC9	HNRNPA1	MAGOHB	PHGDH	RPL13	SLC25A4	TNFRSF10B	
ARHGAP42	CLK3	F5	HNRNPA1L2	MAK16	PHIP	RPL13A	SLC25A5	TNRC18	
ARHGAP9	CLK4	FAM133A	HNRNPA2B1	MAP4	PHLDA2	RPL14	SLC25A6	TOE1	
ARHGEF2	CLTC	FAM133B	HNRNPAB	MAP7	PHRF1	RPL15	SLC3A2	TOP1	
ARHGEF28	CLTCL1	FAM207A	HNRNPC	MAPKAPK2	PIP4K2A	RPL17	SLC6A7	TOP1MT	
ARHGEF39	CMSS1	FAM208A	HNRNPCL1	MARS	PIWIL2	RPL17-C18orf32	SLTM	TOP2A	
ARID2	CNTNAP5	FAM32A	HNRNPD	MATR3	PKP2	RPL18	SLU7	TOP2B	
ARL6IP4	COG1	FAM98A	HNRNPDL	MB21D1	PKP3	RPL18A	SMARCA1	TOP3B	
ASCC1	COIL	FARSA	HNRNPF	MBD4	PLCG1	RPL19	SMARCA2	TOPORS	
ASCC3	COL15A1	FAU	HNRNPH1	MDC1	PLEC	RPL21	SMARCA4	TPX2	
ASH2L	COL4A1	FBL	HNRNPH2	MDM1	PLRG1	RPL22	SMARCA5	TRA2A	
ASPH	COPA	FER	HNRNPK	MEAF6	PNISR	RPL22L1	SMARCC1	TRA2B	
ASPHD1	CPS1	FGF2	HNRNPL	MED19	PNN	RPL23	SMC2	TRAP1	
ATAD3A	CPSF1	FIP1L1	HNRNPLL	MEPCE	PNPLA6	RPL23A	SMN1	TRIM21	
ATP11A	CPSF2	FLOT1	HNRNPM	MFAP1	POGZ	RPL24	SMN2	TRIM26	
ATP11B	CPSF3	FLYWCH1	HNRNPR	MIB1	POLDIP3	RPL26	SMNDC1	TRIM27	
ATP11C	CPSF4	FMN2	HNRNPU	MICAL3	POLR1A	RPL26L1	SMU1	TRIM28	
ATP2A2	CPSF6	FMR1	HNRNPUL2	MKI67	POLR1B	RPL27	SNIP1	TRIM56	
ATP2A3	CPSF7	FNBP4	HP1BP3	MKI67IP	POLR1C	RPL27A	SNRNP200	TRIM7	
ATP5A1	CRNKL1	FRG1	HPS6	MLH3	POLR1D	RPL28	SNRNP27	TRIP13	
ATP5B	CRTAP	FTSJ3	HS2ST1	MLLT4	POLR1E	RPL29	SNRNP40	TRMT10C	
ATP5C1	CSMD2	FUS	HSP90AB1	MLLT6	POLR2A	RPL3	SNRNP70	TRMT1L	
ATP5J2	CSNK1A1	FXR1	HSPA1A	MORF4L2	POLR2B	RPL30	SNRPA	TRPC1	
ATP5L	CSNK1A1L	FXR2	HSPA1B	MOS	POLR2C	RPL31	SNRPA1	TSGA10IP	
ATRX	CSNK1D	FYTTD1	HSPA1L	MOV10	POLR2D	RPL32	SNRPB	TSPYL1	
ATXN10	CSNK1E	G3BP1	HSPA2	MPG	POLR2E	RPL34	SNRPB2	TSR1	
AURKA	CSNK2A1	G3BP2	HSPA5	MPHOSPH10	POLR2F	RPL35	SNRPC	TSSK2	
AURKB	CSNK2B	GALNT15	HSPA6	MPHOSPH6	POLR2G	RPL35A	SNRPD1	TUBA1A	
BACH2	CTGF	GAPDH	HSPA8	MPHOSPH8	POLR2H	RPL36	SNRPD2	TUBA1B	
BAG2	CTNNBL1	GAR1	HSPA9	MPP7	POLR2I	RPL36A	SNRPD3	TUBA1C	
BANF1	CTR9	GCK	HSPB1	MPV17	POLR2J	RPL36AL	SNRPE	TUBA3C	
BAZ1B	CTSZ	GCN1L1	HSPD1	MRPL11	POLR2J3	RPL37	SNRPF	TUBA3D	
BAZ2A	CUL4A	GEMIN4	HSPG2	MRPL22	POLR2K	RPL37A	SNRPG	TUBA3E	
BCAS2	CUL4B	GEMIN8	IARS	MRPL46	POLR2L	RPL38	SNRPN	TUBA4A	
BCCIP	CWC15	GFAP	IFI16	MRPL47	POLR3A	RPL39	SNW1	TUBA8	
BCL2L2-PABPN1	CWC22	GLTSCR2	IGF2BP1	MRPS12	POLRMT	RPL3L	SOAT1	TUBAL3	
BCLAF1	CWC25	GLUD1	IGF2BP2	MRPS28	POP1	RPL4	SON	TUBB	
BLM	CWF19L2	GLUD2	IGF2BP3	MRPS34	POTEE	RPL5	SOWAHA	TUBB1	
BMS1	CYR61	GLYR1	IK	MRPS5	POTEF	RPL6	SPATS2	TUBB2A	
BOP1	DARS	GNL2	IKZF4	MRPS7	PPAN	RPL7	SPATS2L	TUBB2B	
BRD7	DDB1	GNL3	ILF2	MRPS9	PPAN-P2RY11	RPL7A	SPEN	TUBB4A	
BRD9	DDX1	GNL3L	ILF3	MRTO4	PPHLN1	RPL7L1	SPPL3	TUBB4B	
BRIX1	DDX17	GPALPP1	IMP3	MSH6	PPIA	RPL8	SPTAN1	TUBB6	
BRPF1	DDX18	GPATCH1	IMP4	MTDH	PPIB	RPL9	SPTY2D1	TUBB8	
BRPF3	DDX20	GPATCH11	INA	MTF2	PPIE	RPLP0	SQSTM1	TUFM	
BRWD1	DDX21	GPATCH4	INCENP	MTHFD1L	PPIG	RPLP1	SRBD1	TWISTNB	
BRWD3	DDX23	GPATCH8	ING4	MTM1	PPIH	RPLP2	SREK1	TXNDC11	

BUB3	DDX24	GPKOW	ING5	MTPAP	PPIL1	RPN1	SREK1IP1	TXNL4A	
BUD13	DDX27	GRWD1	IQGAP1	MXRA8	PPIL2	RPN2	SRGAP1	U2AF1	
BUD31	DDX28	GTF2H4	IQSEC2	MYBBP1A	PPIL3	RPP30	SRP14	U2AF1L4	
BYSL	DDX31	GTPBP4	ISG20L2	MYH11	PPP6R2	RPRD1A	SRP19	U2AF2	
C10orf2	DDX39A	GTSE1	ISY1	MYH14	PPWD1	RPRD1B	SRP68	U2SURP	
C11orf57	DDX39B	H1F0	ISY1-RAB43	MYH9	PQBP1	RPRD2	SRP72	UBA52	
C14orf166	DDX3X	H1FX	ITGA10	MYL6	PRC1	RPRML	SRP9	UBAP2L	
C15orf52	DDX3Y	H2AFJ	IWS1	MYL6B	PRDX1	RPS10	SRPK1	UBB	
C16orf80	DDX41	H2AFV	JPH1	MYO1C	PRDX2	RPS10-NUDT3	SRPK2	UBC	
C17orf85	DDX46	H2AFX	KARS	MYO1E	PRDX4	RPS11	SRPK3	UBL5	
C19orf53	DDX47	H2AFY	KAT7	MYO1F	PRKCDBP	RPS12	SRRM1	UBTF	
C1orf226	DDX5	H2AFY2	KCTD10	NAA38	PRKDC	RPS13	SRRM2	UFM1	
C1orf35	DDX50	H2AFZ	KCTD13	NAP1L1	PRKRA	RPS14	SRRT	UHMK1	
C7orf50	DDX51	H3F3A	KDM2A	NAT10	PRMT1	RPS15	SRSF1	UPF3B	
C7orf55-LUC7L2	DDX52	H3F3B	KDM3A	NCBP1	PRPF19	RPS15A	SRSF10	URB1	
C8orf34	DDX54	H3F3C	KEAP1	NCBP2	PRPF3	RPS16	SRSF11	URI1	
C8orf59	DDX55	HAS1	KIAA0020	NCL	PRPF31	RPS17	SRSF12	USP10	
C8orf76	DDX56	HBA1	KIAA1429	NCOA5	PRPF38A	RPS17L	SRSF2	USP24	
C9orf114	DECR1	HBA2	KIF18A	NDUFA9	PRPF38B	RPS18	SRSF3	USP36	
C9orf43	DEK	HBB	KIF22	NDUFB10	PRPF4	RPS19	SRSF4	USP39	
CAAP1	DES	HBD	KIF23	NEFH	PRPF40A	RPS2	SRSF5	USP42	
CACTIN	DFNB31	HBE1	KIF2A	NEFM	PRPF40B	RPS20	SRSF6	UTP14A	
CALM1	DGCR14	HBG1	KIF2B	NFKBIL1	PRPF4B	RPS23	SRSF7	UTP14C	
CALM2	DHX15	HBG2	KIF2C	NFX1	PRPF6	RPS24	SRSF9	UTP18	
CALM3	DHX16	HDAC1	KIFC1	NHP2	PRPF8	RPS25	SSR1	UTP23	
CALU	DHX29	HDAC2	KLB	NHP2L1	PRPH	RPS26	SSR3	UTP3	
CAPRIN1	DHX30	HDGF	KMT2A	NIP7	PRR3	RPS27	SSR4	VASH2	
CASP8	DHX33	HEATR1	KNOP1	NIPBL	PRRC2A	RPS27A	SSRP1	VIM	
CBFA2T3	DHX35	HERC5	KPNA1	NKAP	PRRC2B	RPS27L	STAMBPL1	VRK3	
CBLL1	DHX37	HIST1H1A	KPNA2	NKAPL	PRRC2C	RPS28	STAU2	WASF3	
CBX1	DHX57	HIST1H1B	KPNA5	NKRF	PRSS23	RPS29	STOML2	WBP11	
CBX3	DHX8	HIST1H1C	KPNA6	NKTR	PRSS56	RPS3	STT3A	WBP4	
CBX5	DHX9	HIST1H1D	KRI1	NLE1	PSEN2	RPS3A	STYK1	WBSCR16	
CBX8	DIDO1	HIST1H1E	KRR1	NLRC3	PSIP1	RPS4X	SUB1	WDR18	
CBY3	DIMT1	HIST1H1T	KRT1	NOC2L	PTCD1	RPS4Y1	SUGP1	WDR3	
CCDC112	DISP1	HIST1H2AA	KRT10	NOC3L	PTK6	RPS4Y2	SUGP2	WDR33	
CCDC12	DKC1	HIST1H2AB	KRT13	NOC4L	PTPMT1	RPS5	SUPT16H	WDR36	
CCDC124	DNAJA1	HIST1H2AC	KRT14	NOL10	PTRF	RPS6	SUPT4H1	WDR61	
CCDC137	DNAJA3	HIST1H2AD	KRT15	NOL11	PUF60	RPS7	SUPT5H	WDR74	
CCDC59	DNAJC17	HIST1H2AE	KRT16	NOL6	PVRL4	RPS8	SUPT6H	WDR75	
CCDC71	DNTTIP2	HIST1H2AG	KRT17	NOL7	PWP1	RPS9	SURF6	WDR76	
CCDC86	DOCK6	HIST1H2AH	KRT18	NOL8	PWP2	RRBP1	SUV39H1	WDR82	
CCDC9	DOT1L	HIST1H2AI	KRT19	NOL9	QARS	RRNAD1	SUV420H2	WHSC1	
CCNB1	DPEP1	HIST1H2AJ	KRT2	NOLC1	QSER1	RRP1	SUZ12	WIBG	
CCNB2	DPM1	HIST1H2AK	KRT24	NOM1	RACGAP1	RRP12	SYF2	WRAP53	
CCNK	DPY30	HIST1H2AL	KRT25	NONO	RAD23B	RRP15	SYMPK	WTAP	
CCNL1	DPYSL5	HIST1H2AM	KRT27	NOP10	RAI1	RRP1B	SYNCRIP	XAB2	
CCNT1	DROSHA	HIST1H2BA	KRT28	NOP16	RALY	RRP36	TAF1	XIRP2	
CCT3	DSC2	HIST1H2BB	KRT3	NOP2	RARS	RRP7A	TAF10	XPC	
CD2BP2	DSCAML1	HIST1H2BC	KRT31	NOP56	RBBP4	RRP8	TAF11	XPO1	
CD3EAP	DST	HIST1H2BD	KRT32	NOP58	RBBP6	RRS1	TAF12	XPO5	
CDC14A	DSTYK	HIST1H2BE	KRT33B	NOS1AP	RBBP7	RSBN1	TAF13	XRCC5	
CDC40	DUSP11	HIST1H2BF	KRT35	NOS3	RBM10	RSBN1L	TAF1D	XRN2	
CDC42BPA	DYNC1H1	HIST1H2BG	KRT36	NPM1	RBM14	RSF1	TAF1L	YBX1	
CDC42BPB	DYNC1LI1	HIST1H2BH	KRT37	NSA2	RBM14-RBM4	RSL1D1	TAF2	YBX2	
CDC5L	DYNLL1	HIST1H2BI	KRT38	NSUN2	RBM15	RSL24D1	TAF3	YBX3	
CDC73	EBF2	HIST1H2BJ	KRT4	NSUN5	RBM15B	RSRC1	TAF4	YTHDC1	
CDCA2	EBNA1BP2	HIST1H2BK	KRT5	NTHL1	RBM17	RSRC2	TAF4B	YTHDC2	
CDCA8	ECT2	HIST1H2BL	KRT6A	NUCKS1	RBM19	RTCB	TAF5	YWHAB	
CDHR1	EED	HIST1H2BM	KRT6B	TMOD3	RBM22	RTF1	TAF6	YWHAE	
CDK1	EEF1A1	HIST1H2BN	KRT6C	NUMA1	RBM23	RUVBL1	TAF7	YWHAG	
CDK11A	EEF1A2	HIST1H2BO	KRT7	NUPL2	RBM25	RUVBL2	TAF8	YWHAH	
CDK11B	EEF1E1	HIST1H3A	KRT71	NUSAP1	RBM26	S100A4	TAF9	YWHAQ	
CDK12	EEF1G	HIST1H3B	KRT72	NVL	RBM27	SAFB	TAF9B	YWHAZ	
CDK13	EEF2	HIST1H3C	KRT73	NXF1	RBM28	SAFB2	TBL2	ZC3H11A	
CDK14	EEFSEC	HIST1H3D	KRT74	OASL	RBM3	SAP18	TBL3	ZC3H13	
CDK15	EFTUD2	HIST1H3E	KRT75	ORC1	RBM34	SAP30BP	TBP	ZC3H14	

CHAPTER 5. References

[1] Fan, Y., Sanyal, S., and Bruzzone, R. (2018) Breaking Bad: How Viruses Subvert the Cell Cycle, *Front Cell Infect Microbiol 8*, 396.

[2] Thaker, S. K., Ch'ng, J., and Christofk, H. R. (2019) Viral hijacking of cellular metabolism, *BMC Biol 17*, 59.

[3] Walsh, D., and Mohr, I. (2011) Viral subversion of the host protein synthesis machinery, *Nat Rev Microbiol 9*, 860-875.

[4] Yarbrough, M. L., Mata, M. A., Sakthivel, R., and Fontoura, B. M. (2014) Viral subversion of nucleocytoplasmic trafficking, *Traffic 15*, 127-140.

[5] Best, S. M. (2008) Viral subversion of apoptotic enzymes: escape from death row, *Annu Rev Microbiol 62*, 171-192.

[6] Kirkegaard, K. (2009) Subversion of the Cellular Autophagy Pathway by Viruses, *Current Topics in Microbiology and Immunology 335*, 323-333.

[7] Epperson, M. L., Lee, C. A., and Fremont, D. H. (2012) Subversion of cytokine networks by virally encoded decoy receptors, *Immunol Rev 250*, 199-215.

[8] Murphy, P. M. (2001) Viral exploitation and subversion of the immune system through chemokine mimicry, *Nature Immunology 2*, 116-122.

[9] Davey, N. E., Trave, G., and Gibson, T. J. (2011) How viruses hijack cell regulation, *Trends Biochem Sci 36*, 159-169.

[10] Zell, R. (2018) Picornaviridae-the ever-growing virus family, *Arch Virol 163*, 299-317.

[11] Conzemius, R., Ganjian, H., Blaas, D., and Fuchs, R. (2016) ICAM-1 Binding Rhinoviruses A89 and B14 Uncoat in Different Endosomal Compartments, *J Virol 90*, 7934-7942.

[12] Bowers, J. R., Readler, J. M., Sharma, P., and Excoffon, K. (2017) Poliovirus Receptor: More than a simple viral receptor, *Virus Res 242*, 1-6.

[13] Patzke, C., Max, K. E., Behlke, J., Schreiber, J., Schmidt, H., Dorner, A. A., Kroger, S., Henning, M., Otto, A., Heinemann, U., and Rathjen, F. G. (2010) The coxsackievirus-adenovirus receptor reveals complex homophilic and heterophilic interactions on neural cells, *J Neurosci 30*, 2897-2910.

[14] van der Linden, L., Wolthers, K. C., and van Kuppeveld, F. J. (2015) Replication and Inhibitors of Enteroviruses and Parechoviruses, *Viruses 7*, 4529-4562.

[15] Kerkvliet, J., Edukulla, R., and Rodriguez, M. (2010) Novel roles of the picornaviral 3D polymerase in viral pathogenesis, *Adv Virol 2010*, 368068.

[16] Wessels, E., Duijsings, D., Lanke, K. H., van Dooren, S. H., Jackson, C. L., Melchers, W. J., and van Kuppeveld, F. J. (2006) Effects of picornavirus 3A Proteins on Protein Transport and GBF1-dependent COP-I recruitment, *J Virol 80*, 11852-11860.

[17] Jiang, P., Liu, Y., Ma, H. C., Paul, A. V., and Wimmer, E. (2014) Picornavirus morphogenesis, *Microbiol Mol Biol Rev 78*, 418-437.

[18] de Jong, A. S., de Mattia, F., Van Dommelen, M. M., Lanke, K., Melchers, W. J., Willems, P. H., and van Kuppeveld, F. J. (2008) Functional analysis of picornavirus 2B proteins: effects on calcium homeostasis and intracellular protein trafficking, *J Virol 82*, 3782-3790.

[19] Sonenberg, N., and Hinnebusch, A. G. (2009) Regulation of translation initiation in eukaryotes: mechanisms and biological targets, *Cell 136*, 731-745.

[20] Jackson, R. J., Hellen, C. U., and Pestova, T. V. (2010) The mechanism of eukaryotic translation initiation and principles of its regulation, *Nat Rev Mol Cell Biol 11*, 113-127.

[21] Petrenko, N., Jin, Y., Dong, L., Wong, K. H., and Struhl, K. (2019) Requirements for RNA polymerase II preinitiation complex formation in vivo, *Elife 8*.

[22] Martinez-Salas, E., Francisco-Velilla, R., Fernandez-Chamorro, J., and Embarek, A. M. (2017) Insights into Structural and Mechanistic Features of Viral IRES Elements, *Front Microbiol 8*, 2629.

[23] Khong, A., Bonderoff, J. M., Spriggs, R. V., Tammpere, E., Kerr, C. H., Jackson, T. J., Willis, A. E., and Jan, E. (2016) Temporal Regulation of Distinct Internal Ribosome Entry Sites of the Dicistroviridae Cricket Paralysis Virus, *Viruses 8*.

[24] Thompson, S. R., and Sarnow, P. (2003) Enterovirus 71 contains a type I IRES element that functions when eukaryotic initiation factor eIF4G is cleaved, *Virology 315*, 259-266.

[25] Dobrikova, E. Y., Grisham, R. N., Kaiser, C., Lin, J., and Gromeier, M. (2006) Competitive translation efficiency at the picornavirus type 1 internal ribosome entry site facilitated by viral cis and trans factors, *J Virol 80*, 3310-3321.

[26] Semler, B. L., and Waterman, M. L. (2008) IRES-mediated pathways to polysomes: nuclear versus cytoplasmic routes, *Trends Microbiol 16*, 1-5.

[27] Flather, D., and Semler, B. L. (2015) Picornaviruses and nuclear functions: targeting a cellular compartment distinct from the replication site of a positive-strand RNA virus, *Front Microbiol 6*, 594.

[28] Bedard, K. M., Daijogo, S., and Semler, B. L. (2007) A nucleo-cytoplasmic SR protein functions in viral IRES-mediated translation initiation, *EMBO J 26*, 459-467.

[29] Fitzgerald, K. D., Chase, A. J., Cathcart, A. L., Tran, G. P., and Semler, B. L. (2013) Viral proteinase requirements for the nucleocytoplasmic relocalization of cellular splicing factor SRp20 during picornavirus infections, *J Virol 87*, 2390-2400.

[30] Fitzgerald, K. D., and Semler, B. L. (2011) Re-localization of cellular protein SRp20 during poliovirus infection: bridging a viral IRES to the host cell translation apparatus, *PLoS Pathog 7*, e1002127.

[31] Alber, F., Dokudovskaya, S., Veenhoff, L. M., Zhang, W., Kipper, J., Devos, D., Suprapto, A., Karni-Schmidt, O., Williams, R., Chait, B. T., Sali, A., and Rout, M. P. (2007) The molecular architecture of the nuclear pore complex, *Nature 450*, 695-701.

[32] Wente, S. R., and Rout, M. P. (2010) The nuclear pore complex and nuclear transport, *Cold Spring Harb Perspect Biol 2*, a000562.

[33] Fernandez-Martinez, J., Kim, S. J., Shi, Y., Upla, P., Pellarin, R., Gagnon, M., Chemmama, I. E., Wang, J., Nudelman, I., Zhang, W., Williams, R., Rice, W. J., Stokes, D. L., Zenklusen, D., Chait, B. T., Sali, A., and Rout, M. P. (2016) Structure and Function of the Nuclear Pore Complex Cytoplasmic mRNA Export Platform, *Cell 167*, 1215-1228 e1225.

[34] Krull, S., Thyberg, J., Bjorkroth, B., Rackwitz, H. R., and Cordes, V. C. (2004) Nucleoporins as components of the nuclear pore complex core structure and Tpr as the architectural element of the nuclear basket, *Mol Biol Cell 15*, 4261-4277.

[35] Ghavami, A., van der Giessen, E., and Onck, P. R. (2016) Energetics of Transport through the Nuclear Pore Complex, *PLoS One 11*, e0148876.

[36] Zeitler, B., and Weis, K. (2004) The FG-repeat asymmetry of the nuclear pore complex is dispensable for bulk nucleocytoplasmic transport in vivo, *J Cell Biol 167*, 583-590.

[37] Hayama, R., Rout, M. P., and Fernandez-Martinez, J. (2017) The nuclear pore complex core scaffold and permeability barrier: variations of a common theme, *Curr Opin Cell Biol 46*, 110-118.

[38] Timney, B. L., Raveh, B., Mironska, R., Trivedi, J. M., Kim, S. J., Russel, D., Wente, S. R., Sali, A., and Rout, M. P. (2016) Simple rules for passive diffusion through the nuclear pore complex, *J Cell Biol 215*, 57-76.

[39] Aitchison, J. D., and Rout, M. P. (2012) The yeast nuclear pore complex and transport through it, *Genetics 190*, 855-883.

[40] Kabachinski, G., and Schwartz, T. U. (2015) The nuclear pore complex--structure and function at a glance, *J Cell Sci 128*, 423-429.

[41] Raices, M., and D'Angelo, M. A. (2012) Nuclear pore complex composition: a new regulator of tissue-specific and developmental functions, *Nat Rev Mol Cell Biol 13*, 687-699.

[42] Hayama, R., Sparks, S., Hecht, L. M., Dutta, K., Karp, J. M., Cabana, C. M., Rout, M. P., and Cowburn, D. (2018) Thermodynamic characterization of the multivalent interactions underlying rapid and selective translocation through the nuclear pore complex, *J Biol Chem 293*, 4555-4563.

[43] Raveh, B., Karp, J. M., Sparks, S., Dutta, K., Rout, M. P., Sali, A., and Cowburn, D. (2016) Slide-and-exchange mechanism for rapid and selective transport through the nuclear pore complex, *Proc Natl Acad Sci U S A 113*, E2489-2497.

[44] Ibarra, A., and Hetzer, M. W. (2015) Nuclear pore proteins and the control of genome functions, *Genes Dev 29*, 337-349.

[45] Salas-Pino, S., Gallardo, P., Barrales, R. R., Braun, S., and Daga, R. R. (2017) The fission yeast nucleoporin Alm1 is required for proteasomal degradation of kinetochore components, *J Cell Biol 216*, 3591-3608.

[46] Saroufim, M. A., Bensidoun, P., Raymond, P., Rahman, S., Krause, M. R., Oeffinger, M., and Zenklusen, D. (2015) The nuclear basket mediates perinuclear mRNA scanning in budding yeast, *J Cell Biol 211*, 1131-1140.

[47] Kim, S. J., Fernandez-Martinez, J., Nudelman, I., Shi, Y., Zhang, W., Raveh, B., Herricks, T., Slaughter, B. D., Hogan, J. A., Upla, P., Chemmama, I. E., Pellarin, R., Echeverria, I., Shivaraju, M., Chaudhury, A. S., Wang, J., Williams, R., Unruh, J. R., Greenberg, C. H., Jacobs, E. Y., Yu, Z., de la Cruz, M. J., Mironska, R., Stokes, D. L., Aitchison, J. D., Jarrold, M. F., Gerton, J. L., Ludtke, S. J., Akey, C. W., Chait, B. T., Sali, A., and Rout, M. P. (2018) Integrative structure and functional anatomy of a nuclear pore complex, *Nature 555*, 475-482.

[48] Simon, D. N., and Rout, M. P. (2014) Cancer and the nuclear pore complex, *Adv Exp Med Biol 773*, 285-307.

[49] Leslie, D. M., Timney, B., Rout, M. P., and Aitchison, J. D. (2006) Studying nuclear protein import in yeast, *Methods 39*, 291-308.

[50] Waldmann, I., Spillner, C., and Kehlenbach, R. H. (2012) The nucleoporin-like protein NLP1 (hCG1) promotes CRM1-dependent nuclear protein export, *J Cell Sci 125*, 144-154.

[51] Port, S. A., Monecke, T., Dickmanns, A., Spillner, C., Hofele, R., Urlaub, H., Ficner, R., and Kehlenbach, R. H. (2015) Structural and Functional Characterization of CRM1-Nup214 Interactions Reveals Multiple FG-Binding Sites Involved in Nuclear Export, *Cell Rep 13*, 690-702.

[52] Derrer, C. P., Mancini, R., Vallotton, P., Huet, S., Weis, K., and Dultz, E. (2019) The RNA export factor Mex67 functions as a mobile nucleoporin, *J Cell Biol 218*, 3967-3976.

[53] Chook, Y. M., and Suel, K. E. (2011) Nuclear import by karyopherin-betas: recognition and inhibition, *Biochim Biophys Acta 1813*, 1593-1606.

[54] Miyamoto, Y., Yamada, K., and Yoneda, Y. (2016) Importin alpha: a key molecule in nuclear transport and non-transport functions, *J Biochem 160*, 69-75.

[55] Richard Bayliss, T. L., and Murray Stewart. (2000) Structural Basis for the Interaction between FxFG Nucleoporin Repeats and Importin-β in Nuclear Trafficking, *Cell 102*, 99-108.

[56] Shah, S., Tugendreich, S., and Forbes, D. (1998) Major binding sites for the nuclear import receptor are the internal nucleoporin Nup153 and the adjacent nuclear filament protein Tpr, *The Journal of cell biology 141*, 31-49.

[57] Beck, M., Schirmacher, P., and Singer, S. (2017) Alterations of the nuclear transport system in hepatocellular carcinoma - New basis for therapeutic strategies, *J Hepatol 67*, 1051-1061.

[58] Xiaosheng Wu, L. H. K., Ralitsa T. Mantcheva, George T. Mantchev, Margaret J. Springett, and Jan M. A. van Deursen. (2001) Disruption of the FG nucleoporin NUP98 causes selective changes in nuclear pore complex stoichiometry and function, *PNAS 98*, 3191-3196.

[59] Eftekharzadeh, B., Daigle, J. G., Kapinos, L. E., Coyne, A., Schiantarelli, J., Carlomagno, Y., Cook, C., Miller, S. J., Dujardin, S., Amaral, A. S., Grima, J. C., Bennett, R. E., Tepper, K., DeTure, M., Vanderburg, C. R., Corjuc, B. T., DeVos, S. L., Gonzalez, J. A., Chew, J., Vidensky, S., Gage, F. H., Mertens, J., Troncoso, J., Mandelkow, E., Salvatella, X., Lim, R. Y. H., Petrucelli, L., Wegmann, S., Rothstein, J. D., and Hyman, B. T. (2018) Tau Protein Disrupts Nucleocytoplasmic Transport in Alzheimer's Disease, *Neuron 99*, 925-940 e927.

[60] Sakuma, S., and D'Angelo, M. A. (2017) The roles of the nuclear pore complex in cellular dysfunction, aging and disease, *Semin Cell Dev Biol 68*, 72-84.

[61] Puckelwartz, M. J. (2017) The Missing LINC for Genetic Cardiovascular Disease?, *Circ Cardiovasc Genet 10*.

[62] Pal, K., Bandyopadhyay, A., Zhou, X. E., Xu, Q., Marciano, D. P., Brunzelle, J. S., Yerrum, S., Griffin, P. R., Vande Woude, G., Melcher, K., and Xu, H. E. (2017) Structural Basis of TPR-Mediated Oligomerization and Activation of Oncogenic Fusion Kinases, *Structure 25*, 867-877 e863.

[63] Nerea Martínez, A. A., María Dolores Moragues, José Pontón and José Schneider. (1999) The Nuclear Pore Complex Protein Nup88 Is Overexpressed in Tumor Cells, *Cancer Research 59*, 5408-5411.

[64] Isnard, A., Christian, J. G., Kodiha, M., Stochaj, U., McMaster, W. R., and Olivier, M. (2015) Impact of Leishmania infection on host macrophage nuclear physiology and nucleopore complex integrity, *PLoS Pathog 11*, e1004776.

[65] Lussignol, M., Kopp, M., Molloy, K., Vizcay-Barrena, G., Fleck, R. A., Dorner, M., Bell, K. L., Chait, B. T., Rice, C. M., and Catanese, M. T. (2016) Proteomics of HCV virions reveals an essential role for the nucleoporin Nup98 in virus morphogenesis, *Proc Natl Acad Sci U S A 113*, 2484-2489.

[66] Quan, B., Seo, H. S., Blobel, G., and Ren, Y. (2014) Vesiculoviral matrix (M) protein occupies nucleic acid binding site at nucleoporin pair (Rae1 * Nup98), *Proc Natl Acad Sci U S A 111*, 9127-9132.

[67] W Glaser, T. S. (2000) Extremely efficient cleavage of eIF4G by picornaviral proteinases L and 2A in vitro, *FEBS J 480*, 151-155.

[68] Xiang, Z., Liu, L., Lei, X., Zhou, Z., He, B., and Wang, J. (2016) 3C Protease of Enterovirus D68 Inhibits Cellular Defense Mediated by Interferon Regulatory Factor 7, *J Virol 90*, 1613-1621.

[69] Watters, K., and Palmenberg, A. C. (2011) Differential processing of nuclear pore complex proteins by rhinovirus 2A proteases from different species and serotypes, *J Virol 85*, 10874-10883.

[70] Watters, K., Inankur, B., Gardiner, J. C., Warrick, J., Sherer, N. M., Yin, J., and Palmenberg, A. C. (2017) Differential Disruption of Nucleocytoplasmic Trafficking Pathways by Rhinovirus 2A Proteases, *J Virol 91*.

[71] Ling, H., Yang, P., Hou, H., and Sun, Y. (2018) Structural view of the 2A protease from human rhinovirus C15, *Acta Crystallogr F Struct Biol Commun 74*, 255-261.

[72] Tan, J., George, S., Kusov, Y., Perbandt, M., Anemuller, S., Mesters, J. R., Norder, H., Coutard, B., Lacroix, C., Leyssen, P., Neyts, J., and Hilgenfeld, R. (2013) 3C protease of enterovirus 68: structure-based design of Michael acceptor inhibitors and their broad-spectrum antiviral effects against picornaviruses, *J Virol 87*, 4339-4351.

[73] Lee, W., Watters, K. E., Troupis, A. T., Reinen, N. M., Suchy, F. P., Moyer, K. L., Frederick, R. O., Tonelli, M., Aceti, D. J., Palmenberg, A. C., and Markley, J. L. (2014) Solution structure of the 2A protease from a common cold agent, human rhinovirus C2, strain W12, *PLoS One 9*, e97198.

[74] Yang, J., Leen, E. N., Maree, F. F., and Curry, S. (2016) Crystal structure of the 3C protease from Southern African Territories type 2 foot-and-mouth disease virus, *PeerJ 4*, e1964.

[75] Sun, Y., Wang, X., Yuan, S., Dang, M., Li, X., Zhang, X. C., and Rao, Z. (2013) An open conformation determined by a structural switch for 2A protease from coxsackievirus A16, *Protein Cell 4*, 782-792.

[76] Farshid S Garmaroudi, D. M., Reid Hendry, Honglin Luo, Decheng Yang, Xin Ye, Junyan Shi, Bruce M McManus. (2015) Coxsackievirus B3 replication and pathogenesis, *Future Microbiology 10*, 629-653.

[77] Gao, F., Bian, L. L., Mao, Q. Y., Chen, P., Yao, X., Li, J. X., Zhu, F. C., and Liang, Z. L. (2016) An epidemic of coxsackievirus B3 infection in infants and children in Jiangsu Province, China: a prospective cohort study, *Arch Virol 161*, 1945-1947.

[78] Wang, Y., and Pfeiffer, J. K. (2016) Emergence of a Large-Plaque Variant in Mice Infected with Coxsackievirus B3, *mBio 7*, e00119.

[79] Glen R. Abedi, J. T. W., W. Allan Nix, M. Steven Oberste, Susan I. Gerber. (2018) Enterovirus and Parechovirus Surveillance — United States, 2014–2016, *MMWR Morb Mortal Wkly Rep 67*, 515-518.

[80] Lee, Y. G., Park, J. H., Jeon, E. S., Kim, J. H., and Lim, B. K. (2016) Fructus Amomi Cardamomi Extract Inhibit Coxsackievirus-B3 Induced Myocarditis in Murine Myocarditis Model, *J Microbiol Biotechnol 26*, 2012-2018.

[81] Lind, K., Svedin, E., Domsgen, E., Kapell, S., Laitinen, O. H., Moll, M., and Flodstrom-Tullberg, M. (2016) Coxsackievirus counters the host innate immune response by blocking type III interferon expression, *J Gen Virol 97*, 1368-1380.

[82] Rahnefeld, A., Klingel, K., Schuermann, A., Diny, N. L., Althof, N., Lindner, A., Bleienheuft, P., Savvatis, K., Respondek, D., Opitz, E., Ketscher, L., Sauter, M., Seifert, U., Tschope, C., Poller, W., Knobeloch, K. P., and Voigt, A. (2014) Ubiquitin-like protein ISG15 (interferon-stimulated gene of 15 kDa) in host defense against heart failure in a mouse model of virus-induced cardiomyopathy, *Circulation 130*, 1589-1600.

[83] Muto, S., Miyoshi, H., Nishikawa, H., and Nakashima, H. (2006) Novel recognition sequence of coxsackievirus 2A proteinase, *Biochem Biophys Res Commun 348*, 1436-1442.

[84] Zamora, M., Marissen, W. E., and Lloyd, R. E. (2002) Multiple eIF4GI-specific protease activities present in uninfected and poliovirus-infected cells, *J Virol 76*, 165-177.

[85] Fung, G., Ng, C. S., Zhang, J., Shi, J., Wong, J., Piesik, P., Han, L., Chu, F., Jagdeo, J., Jan, E., Fujita, T., and Luo, H. (2013) Production of a dominant-negative fragment due to G3BP1 cleavage contributes to the disruption of mitochondria-associated protective stress granules during CVB3 infection, *PLoS One 8*, e79546.

[86] Jagdeo, J. M., Dufour, A., Fung, G., Luo, H., Kleifeld, O., Overall, C. M., and Jan, E. (2015) Heterogeneous Nuclear Ribonucleoprotein M Facilitates Enterovirus Infection, *J Virol 89*, 7064-7078.

[87] Deng, H., Fung, G., Shi, J., Xu, S., Wang, C., Yin, M., Hou, J., Zhang, J., Jin, Z. G., and Luo, H. (2015) Enhanced enteroviral infectivity via viral protease-mediated cleavage of Grb2-associated binder 1, *FASEB J 29*, 4523-4531.

[88] Deng, H., Fung, G., Qiu, Y., Wang, C., Zhang, J., Jin, Z. G., and Luo, H. (2017) Cleavage of Grb2-Associated Binding Protein 2 by Viral Proteinase 2A during Coxsackievirus Infection, *Front Cell Infect Microbiol 7*, 85.

[89] Feng, Q., Langereis, M. A., Lork, M., Nguyen, M., Hato, S. V., Lanke, K., Emdad, L., Bhoopathi, P., Fisher, P. B., Lloyd, R. E., and van Kuppeveld, F. J. (2014) Enterovirus 2Apro targets MDA5 and MAVS in infected cells, *J Virol 88*, 3369-3378.

[90] Cathcart, A. L., Rozovics, J. M., and Semler, B. L. (2013) Cellular mRNA decay protein AUF1 negatively regulates enterovirus and human rhinovirus infections, *J Virol 87*, 10423-10434.

[91] Wong, J., Si, X., Angeles, A., Zhang, J., Shi, J., Fung, G., Jagdeo, J., Wang, T., Zhong, Z., Jan, E., and Luo, H. (2013) Cytoplasmic redistribution and cleavage of AUF1 during coxsackievirus infection enhance the stability of its viral genome, *FASEB J 27*, 2777-2787.

[92] Cathcart, A. L., and Semler, B. L. (2014) Differential restriction patterns of mRNA decay factor AUF1 during picornavirus infections, *J Gen Virol 95*, 1488-1492.

[93] Mukherjee, A., Morosky, S. A., Delorme-Axford, E., Dybdahl-Sissoko, N., Oberste, M. S., Wang, T., and Coyne, C. B. (2011) The coxsackievirus B 3C protease cleaves MAVS and TRIF to attenuate host type I interferon and apoptotic signaling, *PLoS Pathog 7*, e1001311.

[94] Kuyumcu-Martinez, N. M., Van Eden, M. E., Younan, P., and Lloyd, R. E. (2004) Cleavage of poly(A)-binding protein by poliovirus 3C protease inhibits host cell translation: a novel mechanism for host translation shutoff, *Mol Cell Biol 24*, 1779-1790.

[95] Kuyumcu-Martinez, N. M., Joachims, M., and Lloyd, R. E. (2002) Efficient cleavage of ribosome-associated poly(A)-binding protein by enterovirus 3C protease, *J Virol 76*, 2062-2074.

[96] Qiu, Y., Ye, X., Zhang, H. M., Hanson, P., Zhao, G., Tong, L., Xie, R., and Yang, D. (2017) Cleavage of osmosensitive transcriptional factor NFAT5 by Coxsackieviral protease 2A promotes viral replication, *PLoS Pathog 13*, e1006744.

[97] Hanson, P. J., Ye, X., Qiu, Y., Zhang, H. M., Hemida, M. G., Wang, F., Lim, T., Gu, A., Cho, B., Kim, H., Fung, G., Granville, D. J., and Yang, D. (2016) Cleavage of DAP5 by coxsackievirus B3 2A protease facilitates viral replication and enhances apoptosis by altering translation of IRES-containing genes, *Cell Death Differ 23*, 828-840.

[98] Harris, K. G., and Coyne, C. B. (2015) Unc93b Induces Apoptotic Cell Death and Is Cleaved by Host and Enteroviral Proteases, *PLoS One 10*, e0141383.

[99] Fung, G., Shi, J., Deng, H., Hou, J., Wang, C., Hong, A., Zhang, J., Jia, W., and Luo, H. (2015) Cytoplasmic translocation, aggregation, and cleavage of TDP-43 by enteroviral proteases modulate viral pathogenesis, *Cell Death Differ 22*, 2087-2097.

[100] Lim, B. K., Peter, A. K., Xiong, D., Narezkina, A., Yung, A., Dalton, N. D., Hwang, K. K., Yajima, T., Chen, J., and Knowlton, K. U. (2013) Inhibition of Coxsackievirus-associated dystrophin cleavage prevents cardiomyopathy, *J Clin Invest 123*, 5146-5151.

[101] Chase, A. J., and Semler, B. L. (2014) Differential cleavage of IRES trans-acting factors (ITAFs) in cells infected by human rhinovirus, *Virology 449*, 35-44.

[102] Shi, J., Wong, J., Piesik, P., Fung, G., Zhang, J., Jagdeo, J., Li, X., Jan, E., and Luo, H. (2013) Cleavage of sequestosome 1/p62 by an enteroviral protease results in disrupted selective autophagy and impaired NFKB signaling, *Autophagy 9*, 1591-1603.

[103] Wong, J., Zhang, J., Yanagawa, B., Luo, Z., Yang, X., Chang, J., McManus, B., and Luo, H. (2012) Cleavage of serum response factor mediated by enteroviral protease 2A contributes to impaired cardiac function, *Cell Res 22*, 360-371.

[104] de Breyne, S., Bonderoff, J. M., Chumakov, K. M., Lloyd, R. E., and Hellen, C. U. (2008) Cleavage of eukaryotic initiation factor eIF5B by enterovirus 3C proteases, *Virology 378*, 118-122.

[105] Saura, M., Lizarbe, T. R., Rama-Pacheco, C., Lowenstein, C. J., and Zaragoza, C. (2007) Inhibitor of NF kappa B alpha is a host sensor of coxsackievirus infection, *Cell Cycle 6*, 503-506.

[106] Hanson, P. J., Hossain, A. R., Qiu, Y., Zhang, H. M., Zhao, G., Li, C., Lin, V., Sulaimon, S., Vlok, M., Fung, G., Chen, V. H., Jan, E., McManus, B. M., Granville, D. J., and Yang, D. (2019) Cleavage and Sub-Cellular Redistribution of Nuclear Pore Protein 98 by Coxsackievirus B3 Protease 2A Impairs Cardioprotection, *Front Cell Infect Microbiol 9*, 265.

[107] Mohamud, Y., Shi, J., Qu, J., Poon, T., Xue, Y. C., Deng, H., Zhang, J., and Luo, H. (2018) Enteroviral Infection Inhibits Autophagic Flux via Disruption of the SNARE Complex to Enhance Viral Replication, *Cell Rep 22*, 3292-3303.

[108] Saeed, M., Kapell, S., Hertz, N. T., Wu, X., Bell, K., Ashbrook, A. W., Mark, M. T., Zebroski, H. A., Neal, M. L., Flodstrom-Tullberg, M., MacDonald, M. R., Aitchison, J. D., Molina, H., and Rice, C. M. (2020) Defining the proteolytic landscape during enterovirus infection, *PLoS Pathog 16*, e1008927.

[109] Park, N., Schweers, N. J., and Gustin, K. E. (2015) Selective Removal of FG Repeat Domains from the Nuclear Pore Complex by Enterovirus 2A(pro), *J Virol 89*, 11069-11079.

[110] Castello, A., Alvarez, E., and Carrasco, L. (2006) Differential cleavage of eIF4GI and eIF4GII in mammalian cells. Effects on translation, *J Biol Chem 281*, 33206-33216.

[111] Avanzino, B. C., Fuchs, G., and Fraser, C. S. (2017) Cellular cap-binding protein, eIF4E, promotes picornavirus genome restructuring and translation, *Proc Natl Acad Sci U S A 114*, 9611-9616.

[112] Barry J. Lamphear, R. K., Tim Skern, and Robert E. Rhoads. (1995) Mapping of Functional Domains in Eukaryotic Protein Synthesis Initiation Factor 4G (eIF4G) with Picornaviral Proteases, *Journal of Biological Chemistry 270*, 21975-21983.

[113] Carrasco, I. N. a. L. (1999) Cleavage of Eukaryotic Translation Initiation Factor 4G by Exogenously Added Hybrid Proteins Containing Poliovirus 2Apro in HeLa Cells: Effects on Gene Expression, *Molecular and Cellular Biology 19*, 2445-2454.

[114] Da Sacco, L., and Masotti, A. (2012) Recent insights and novel bioinformatics tools to understand the role of microRNAs binding to 5' untranslated region, *Int J Mol Sci 14*, 480-495.

[115] Michael L. Bovee, B. J. L., Robert E. Rhoads, and Richard E. Lloyd. (1998) Direct Cleavage of eIF4G by Poliovirus 2A Protease Is Inefficient in Vitro, *Virology 245*, 241-249.

[116] Carter, M., and Shieh, J. (2015) Gene Delivery Strategies, In *Guide to Research Techniques in Neuroscience*, pp 239-252.

[117] Atze T. Das, L. T., and Ben Berkhout. (2016) Tet-On Systems For Doxycycline-inducible Gene Expression, *Current Gene Therapy 16*, 156-167.

[118] Cadinanos, J., and Bradley, A. (2007) Generation of an inducible and optimized piggyBac transposon system, *Nucleic Acids Res 35*, e87.

[119] Yusa, K., Zhou, L., Li, M. A., Bradley, A., and Craig, N. L. (2011) A hyperactive piggyBac transposase for mammalian applications, *Proc Natl Acad Sci U S A 108*, 1531-1536.

[120] Chen, Q., Luo, W., Veach, R. A., Hickman, A. B., Wilson, M. H., and Dyda, F. (2020) Structural basis of seamless excision and specific targeting by piggyBac transposase, *Nat Commun 11*, 3446.

[121] Li, X., Burnight, E. R., Cooney, A. L., Malani, N., Brady, T., Sander, J. D., Staber, J., Wheelan, S. J., Joung, J. K., McCray, P. B., Jr., Bushman, F. D., Sinn, P. L., and Craig, N. L. (2013) piggyBac transposase tools for genome engineering, *Proc Natl Acad Sci U S A 110*, E2279-2287.

[122] Xiao Dong, S. Y., Gu Weiwang & Chen Xigu. (2007) Tetracycline-controlled transcriptional regulation systems: countermeasures to eliminate basal transgene leaks in Tet-based systems, *Progress in Natural Science 17*, 11-19.

[123] Goldstaub, D., Gradi, A., Bercovitch, Z., Grosmann, Z., Nophar, Y., Luria, S., Sonenberg, N., and Kahana, C. (2000) Poliovirus 2A protease induces apoptotic cell death, *Molecular and cellular biology 20*, 1271-1277.

[124] Visser, L. J., Langereis, M. A., Rabouw, H. H., Wahedi, M., Muntjewerff, E. M., de Groot, R. J., and van Kuppeveld, F. J. M. (2019) Essential Role of Enterovirus 2A Protease in Counteracting Stress Granule Formation and the Induction of Type I Interferon, *J Virol 93*.

[125] Walker, E., Jensen, L., Croft, S., Wei, K., Fulcher, A. J., Jans, D. A., and Ghildyal, R. (2016) Rhinovirus 16 2A Protease Affects Nuclear Localization of 3CD during Infection, *J Virol 90*, 11032-11042.

[126] Domanski, M., Molloy, K., Jiang, H., Chait, B. T., Rout, M. P., Jensen, T. H., and LaCava, J. (2012) Improved methodology for the affinity isolation of human protein complexes expressed at near endogenous levels, *Biotechniques 0*, 1-6.

[127] Hakhverdyan, Z., Domanski, M., Hough, L. E., Oroskar, A. A., Oroskar, A. R., Keegan, S., Dilworth, D. J., Molloy, K. R., Sherman, V., Aitchison, J. D., Fenyo, D., Chait, B. T., Jensen, T. H., Rout, M. P., and LaCava, J. (2015) Rapid, optimized interactomic screening, *Nat Methods 12*, 553-560.

[128] LaCava, J., Fernandez-Martinez, J., Hakhverdyan, Z., and Rout, M. P. (2016) Protein Complex Purification by Affinity Capture, *Cold Spring Harb Protoc 2016*.

[129] Faria, P. A., Chakraborty, P., Levay, A., Barber, G. N., Ezelle, H. J., Enninga, J., Arana, C., van Deursen, J., and Fontoura, B. M. (2005) VSV disrupts the Rae1/mrnp41 mRNA nuclear export pathway, *Mol Cell 17*, 93-102.

[130] Colin E.J. Pritchard, M. F., Lawryn H. Kasper, and Jan M.A. van Deursen. (1999) RAE1 Is a Shuttling mRNA Export Factor That Binds to a GLEBS-like NUP98 Motif at the Nuclear Pore Complex through Multiple Domains, *The Journal of Cell Biology 145*, 237-253.

[131] Ren, Y., Seo, H. S., Blobel, G., and Hoelz, A. (2010) Structural and functional analysis of the interaction between the nucleoporin Nup98 and the mRNA export factor Rae1, *Proc Natl Acad Sci U S A 107*, 10406-10411.

[132] Frank, A. M. (2009) A ranking-based scoring function for peptide-spectrum matches, *J Proteome Res 8*, 2241-2252.

[133] Masutani, M., Sonenberg, N., Yokoyama, S., and Imataka, H. (2007) Reconstitution reveals the functional core of mammalian eIF3, *EMBO J 26*, 3373-3383.

[134] LaCava, J., Jiang, H., and Rout, M. P. (2016) Protein Complex Affinity Capture from Cryomilled Mammalian Cells, *J Vis Exp*.

[135] Obado S.O., F. M. C., Chait B.T., Rout M.P (2016) *High-Efficiency Isolation of Nuclear Envelope Protein Complexes from Trypanosomes.*, Vol. 1411, Humana Press.

[136] Xiang Y., S. Z., Shi Y (2020) *Chemical Cross-Linking and Mass Spectrometric Analysis of the Endogenous Yeast Exosome Complexes.*, Humana.

[137] Zayas, J. F. (1997) Solubility of Proteins, In *Functionality of Proteins in Food* (Zayas, J. F., Ed.), pp 6-75, Springer Berlin Heidelberg, Berlin, Heidelberg.

[138] Liu, Y., Mi, Y., Mueller, T., Kreibich, S., Williams, E. G., Van Drogen, A., Borel, C., Germain, P.-L., Frank, M., Bludau, I., Mehnert, M., Seifert, M., Emmenlauer, M., Sorg, I., Bezrukov, F., Sloan Bena, F., Zhou, H., Dehio, C., Testa, G., Saez-Rodriguez, J., Antonarakis, S. E., Hardt, W.-D., and Aebersold, R. (2018) Genomic, Proteomic and Phenotypic Heterogeneity in HeLa Cells across

Laboratories: Implications for Reproducibility of Research Results, *bioRxiv*.

[139] Geiger, T., Wehner, A., Schaab, C., Cox, J., and Mann, M. (2012) Comparative proteomic analysis of eleven common cell lines reveals ubiquitous but varying expression of most proteins, *Mol Cell Proteomics 11*, M111 014050.

[140] Hodge, K., Have, S. T., Hutton, L., and Lamond, A. I. (2013) Cleaning up the masses: exclusion lists to reduce contamination with HPLC-MS/MS, *J Proteomics 88*, 92-103.

[141] Mellacheruvu, D., Wright, Z., Couzens, A. L., Lambert, J. P., St-Denis, N. A., Li, T., Miteva, Y. V., Hauri, S., Sardiu, M. E., Low, T. Y., Halim, V. A., Bagshaw, R. D., Hubner, N. C., Al-Hakim, A., Bouchard, A., Faubert, D., Fermin, D., Dunham, W. H., Goudreault, M., Lin, Z. Y., Badillo, B. G., Pawson, T., Durocher, D., Coulombe, B., Aebersold, R., Superti-Furga, G., Colinge, J., Heck, A. J., Choi, H., Gstaiger, M., Mohammed, S., Cristea, I. M., Bennett, K. L., Washburn, M. P., Raught, B., Ewing, R. M., Gingras, A. C., and Nesvizhskii, A. I. (2013) The CRAPome: a contaminant repository for affinity purification-mass spectrometry data, *Nat Methods 10*, 730-736.

[142] Beck, M., Schmidt, A., Malmstroem, J., Claassen, M., Ori, A., Szymborska, A., Herzog, F., Rinner, O., Ellenberg, J., and Aebersold, R. (2011) The quantitative proteome of a human cell line, *Mol Syst Biol 7*, 549.

[143] Kadrmas, J. L., and Beckerle, M. C. (2004) The LIM domain: from the cytoskeleton to the nucleus, *Nat Rev Mol Cell Biol 5*, 920-931.

[144] Nie, Z., Du, M. Q., McAllister-Lucas, L. M., Lucas, P. C., Bailey, N. G., Hogaboam, C. M., Lim, M. S., and Elenitoba-Johnson, K. S. (2015) Conversion of the LIMA1 tumour suppressor into an oncogenic LMO-like protein by API2-MALT1 in MALT lymphoma, *Nat Commun 6*, 5908.

[145] Maul, R. S., Song, Y., Amann, K. J., Gerbin, S. C., Pollard, T. D., and Chang, D. D. (2003) EPLIN regulates actin dynamics by cross-linking and stabilizing filaments, *J Cell Biol 160*, 399-407.

[146] Barrientos, T., Frank, D., Kuwahara, K., Bezprozvannaya, S., Pipes, G. C., Bassel-Duby, R., Richardson, J. A., Katus, H. A., Olson, E. N., and Frey, N. (2007) Two novel members of the ABLIM protein family, ABLIM-2 and -3, associate with STARS and directly bind F-actin, *J Biol Chem 282*, 8393-8403.

[147] Holaska, J. M., Rais-Bahrami, S., and Wilson, K. L. (2006) Lmo7 is an emerin-binding protein that regulates the transcription of emerin and many other muscle-relevant genes, *Hum Mol Genet 15*, 3459-3472.

[148] Vazquez-Calvo, A., Caridi, F., Gonzalez-Magaldi, M., Saiz, J. C., Sobrino, F., and Martin-Acebes, M. A. (2016) The Amino Acid Substitution Q65H in the 2C Protein of Swine Vesicular Disease Virus Confers Resistance to Golgi Disrupting Drugs, *Front Microbiol 7*, 612.

[149] Esfandi, F., Taheri, M., Namvar, A., Oskooei, V. K., and Ghafouri-Fard, S. (2019) AFAP1 and its naturally occurring antisense RNA are downregulated in gastric cancer samples, *Biomed Rep 10*, 296-302.

[150] Fridy, P. C., Li, Y., Keegan, S., Thompson, M. K., Nudelman, I., Scheid, J. F., Oeffinger, M., Nussenzweig, M. C., Fenyo, D., Chait, B. T., and Rout, M. P. (2014) A robust pipeline for rapid production of versatile nanobody repertoires, *Nat Methods 11*, 1253-1260.

[151] Franks, T. M., and Hetzer, M. W. (2013) The role of Nup98 in transcription regulation in healthy and diseased cells, *Trends Cell Biol 23*, 112-117.

[152] Bonnet, A., and Palancade, B. (2014) Regulation of mRNA trafficking by nuclear pore complexes, *Genes (Basel) 5*, 767-791.

[153] Yamada, J., Phillips, J. L., Patel, S., Goldfien, G., Calestagne-Morelli, A., Huang, H., Reza, R., Acheson, J., Krishnan, V. V., Newsam, S., Gopinathan, A., Lau, E. Y., Colvin, M. E., Uversky, V. N., and Rexach, M. F. (2010) A bimodal distribution of two distinct categories of intrinsically disordered structures with separate functions in FG nucleoporins, *Mol Cell Proteomics 9*, 2205-2224.

[154] Capelson, M., Liang, Y., Schulte, R., Mair, W., Wagner, U., and Hetzer, M. W. (2010) Chromatin-bound nuclear pore components regulate gene expression in higher eukaryotes, *Cell 140*, 372-383.

[155] van der Linden, L., Ulferts, R., Nabuurs, S. B., Kusov, Y., Liu, H., George, S., Lacroix, C., Goris, N., Lefebvre, D., Lanke, K. H., De Clercq, K., Hilgenfeld, R., Neyts, J., and van Kuppeveld, F. J. (2014) Application of a cell-based protease assay for testing inhibitors of picornavirus 3C proteases, *Antiviral Res 103*, 17-24.

[156] Deszcz, L., Cencic, R., Sousa, C., Kuechler, E., and Skern, T. (2006) An antiviral peptide inhibitor that is active against picornavirus 2A proteinases but not cellular caspases, *J Virol 80*, 9619-9627.

[157] Jagdeo, J. M., Dufour, A., Klein, T., Solis, N., Kleifeld, O., Kizhakkedathu, J., Luo, H., Overall, C. M., and Jan, E. (2018) N-Terminomics TAILS Identifies Host Cell Substrates of Poliovirus and Coxsackievirus B3 3C Proteinases That Modulate Virus Infection, *J Virol 92*.

[158] Citarella, A., and Micale, N. (2020) Peptidyl Fluoromethyl Ketones and Their Applications in Medicinal Chemistry, *Molecules 25*.

[159] Shi, Y., Fernandez-Martinez, J., Tjioe, E., Pellarin, R., Kim, S. J., Williams, R., Schneidman-Duhovny, D., Sali, A., Rout, M. P., and Chait, B. T. (2014) Structural characterization by cross-linking reveals the detailed architecture of a coatomer-related heptameric module from the nuclear pore complex, *Mol Cell Proteomics 13*, 2927-2943.

[160] Aumayr, M., Schrempf, A., Uzulmez, O., Olek, K. M., and Skern, T. (2017) Interaction of 2A proteinase of human rhinovirus genetic group A with eIF4E is required for eIF4G cleavage during infection, *Virology 511*, 123-134.

[161] Kumar, R., Khandelwal, N., Thachamvally, R., Tripathi, B. N., Barua, S., Kashyap, S. K., Maherchandani, S., and Kumar, N. (2018) Role of MAPK/MNK1 signaling in virus replication, *Virus Res 253*, 48-61.

[162] Le Sage, V., and Mouland, A. J. (2013) Viral subversion of the nuclear pore complex, *Viruses 5*, 2019-2042.

[163] Addetia, A., Lieberman, N. A. P., Phung, Q., Xie, H., Roychoudhury, P., Shrestha, L., Loprieno, M., Huang, M.-L., Jerome, K. R., and Greninger, A. L. (2020) SARS-CoV-2 ORF6 disrupts nucleocytoplasmic transport through interactions with Rae1 and Nup98.

[164] Alvarez, E., Castello, A., Carrasco, L., and Izquierdo, J. M. (2013) Poliovirus 2A protease triggers a selective nucleo-cytoplasmic redistribution of splicing factors to regulate alternative pre-mRNA splicing, *PLoS One 8*, e73723.

[165] Taha, M. S., Nouri, K., Milroy, L. G., Moll, J. M., Herrmann, C., Brunsveld, L., Piekorz, R. P., and Ahmadian, M. R. (2014) Subcellular fractionation and localization studies reveal a direct interaction of the fragile X mental retardation protein (FMRP) with nucleolin, *PLoS One 9*, e91465.

[166] Adam, S. A., Sengupta, K., and Goldman, R. D. (2008) Regulation of nuclear lamin polymerization by importin alpha, *J Biol Chem 283*, 8462-8468.

[167] Stefanie Hugel, R. D., Gunnar Dittmar, Franziska Rother, Ryan Cabot, Matthias D. Sury, Enno Hartmann, and Michael Bader. (2014) Identification of Importin α 7 Specific Transport Cargoes Using a Proteomic Screening Approach, *Molecular & Cellular Proteomics 13.5*, 1286-1298.

[168] He, B., Lu, N., and Zhou, Z. (2009) Cellular and nuclear degradation during apoptosis, *Curr Opin Cell Biol 21*, 900-912.

[169] An, S., Yoon, J., Kim, H., Song, J. J., and Cho, U. S. (2017) Structure-based nuclear import mechanism of histones H3 and H4 mediated by Kap123, *Elife 6*.

[170] Michael P. Rout, G. B., and John D. Aitchison. (1997) A Distinct Nuclear Import Pathway Used by Ribosomal Proteins, *Cell 89*, 715-725.

[171] Hung-Chuan Chiu, W.-R. H., Yu-Yang Wang, Jyun-Yi Li, Tsai-Ling Liao, Brent L. Nielsen, Hung-Jen Liua. (2019) Heterogeneous Nuclear Ribonucleoprotein A1 and Lamin A/C Modulate Nucleocytoplasmic Shuttling of Avian Reovirus p17, *Journal of Virology 93*, 00851-00819.

[172] Alberts B, J. A., Lewis J, et al. (2002) *Molecular Biology of the Cell. 4th edition. The Transport of Molecules between the Nucleus and the Cytosol.*, Garland Science, New York.

[173] Miorin, L., Kehrer, T., Sanchez-Aparicio, M. T., Zhang, K., Cohen, P., Patel, R. S., Cupic, A., Makio, T., Mei, M., Moreno, E., Danziger, O., White, K. M., Rathnasinghe, R., Uccellini, M., Gao, S., Aydillo, T., Mena, I., Yin, X., Martin-Sancho, L., Krogan, N. J., Chanda, S. K., Schotsaert, M., Wozniak, R. W., Ren, Y., Rosenberg, B. R., Fontoura, B. M. A., and Garcia-Sastre, A. (2020) SARS-CoV-2 Orf6 hijacks Nup98 to block STAT nuclear import and antagonize interferon signaling, *Proc Natl Acad Sci U S A 117*, 28344-28354.

[174] Abkallo, H. M., Kawano, H., Watanabe, K., and Kobayashi, N. (2011) A new cell-based reporter system for sensitive screening of nuclear export inhibitors, *Drug Discov Ther 5*, 286-292.

[175] Dougherty, J. D., Tsai, W. C., and Lloyd, R. E. (2015) Multiple Poliovirus Proteins Repress Cytoplasmic RNA Granules, *Viruses 7*, 6127-6140.

[176] Lloyd, R. E. (2016) Enterovirus Control of Translation and RNA Granule Stress Responses, *Viruses 8*, 93.

[177] Yang, X., Hu, Z., Fan, S., Zhang, Q., Zhong, Y., Guo, D., Qin, Y., and Chen, M. (2018) Picornavirus 2A protease regulates stress granule formation to facilitate viral translation, *PLoS Pathog 14*, e1006901.

[178] Guttler, T., Madl, T., Neumann, P., Deichsel, D., Corsini, L., Monecke, T., Ficner, R., Sattler, M., and Gorlich, D. (2010) NES consensus redefined by structures of PKI-type and Rev-type nuclear export signals bound to CRM1, *Nat Struct Mol Biol 17*, 1367-1376.

[179] Te-Tuan Yang, L. C., and Steven R. Kain. (1996) Optimized Codon Usage and Chromophore Mutations Provide Enhanced Sensitivity with the Green Fluorescent Protein, *Nucleic Acids Res 24*, 4592-4593.

[180] Oka, M., Asally, M., Yasuda, Y., Ogawa, Y., Tachibana, T., and Yoneda, Y. (2010) The mobile FG nucleoporin Nup98 is a cofactor for Crm1-dependent protein export, *Mol Biol Cell 21*, 1885-1896.

[181] Kane, M., Rebensburg, S. V., Takata, M. A., Zang, T. M., Yamashita, M., Kvaratskhelia, M., and Bieniasz, P. D. (2018) Nuclear pore heterogeneity influences HIV-1 infection and the antiviral activity of MX2, *Elife 7*.

[182] Engelke, H., Chou, C., Uprety, R., Jess, P., and Deiters, A. (2014) Control of protein function through optochemical translocation, *ACS Synth Biol 3*, 731-736.

[183] Thavarajah, R., Mudimbaimannar, V. K., Elizabeth, J., Rao, U. K., and Ranganathan, K. (2012) Chemical and physical basics of routine formaldehyde fixation, *J Oral Maxillofac Pathol 16*, 400-405.

[184] KATIE WELCH, J. F., MATTHIAS KOHLER, AND IAN G. MACARA. (1999) RanBP3 Contains an Unusual Nuclear Localization Signal That Is Imported Preferentially by Importin-α3, *Molecular and Cellular Biology 19*, 8400-8411.

[185] Dicks, M. D. J., Betancor, G., Jimenez-Guardeno, J. M., Pessel-Vivares, L., Apolonia, L., Goujon, C., and Malim, M. H. (2018) Multiple components of the nuclear pore complex interact with the amino-terminus of MX2 to facilitate HIV-1 restriction, *PLoS Pathog 14*, e1007408.

[186] Katherine E. Suel, H. G., Yuh Min Chook. (2008) Modular Organization and Combinatorial Energetics of Proline–Tyrosine Nuclear Localization Signals, *PLoS Biol 6*, 1253-1267.

[187] Nakano, K., and Watanabe, T. (2012) HTLV-1 Rex: the courier of viral messages making use of the host vehicle, *Front Microbiol 3*, 330.

[188] Bai, X. T., Sinha-Datta, U., Ko, N. L., Bellon, M., and Nicot, C. (2012) Nuclear export and expression of human T-cell leukemia virus type 1 tax/rex mRNA are RxRE/Rex dependent, *J Virol 86*, 4559-4565.

[189] Zhang, K., Xie, Y., Munoz-Moreno, R., Wang, J., Zhang, L., Esparza, M., Garcia-Sastre, A., Fontoura, B. M. A., and Ren, Y. (2019) Structural basis for influenza virus NS1 protein block of mRNA nuclear export, *Nat Microbiol 4*, 1671-1679.

[190] Morais, A. T. S., Terzian, A. C. B., Duarte, D. V. B., Bronzoni, R. V. M., Madrid, M. C. F. S., Gavioli, A. F., Gil, L. H. V. G., Oliveira, A. G., Zanelli, C. F., Valentini, S. R., Rahal, P., and Nogueira, M. L. (2013) The eukaryotic translation initiation factor 3 subunit L protein interacts with FlavivirusNS5 and may modulate yellow fever virus replication, *Virology Journal 10*, 205.

[191] Villa, N., Do, A., Hershey, J. W., and Fraser, C. S. (2013) Human eukaryotic initiation factor 4G (eIF4G) protein binds to eIF3c, -d, and -e to promote mRNA recruitment to the ribosome, *J Biol Chem 288*, 32932-32940.

[192] Querol-Audi, J., Sun, C., Vogan, J. M., Smith, M. D., Gu, Y., Cate, J. H., and Nogales, E. (2013) Architecture of human translation initiation factor 3, *Structure 21*, 920-928.

[193] Blanchard, S. C., Kim, H. D., Gonzalez, R. L., Puglisi, J. D., and Chu, S. (2004) tRNA dynamics on the ribosome during translation, *Proceedings of the National Academy of Sciences of the United States of America 101*, 12893.

[194] Fraser, C. S., Berry, K. E., Hershey, J. W., and Doudna, J. A. (2007) eIF3j is located in the decoding center of the human 40S ribosomal subunit, *Mol Cell 26*, 811-819.

[195] Jailson Brito Querido, M. S., Sebastian Kraatz, Yuliya Gordiyenko, J. Mark Skehel, Christopher S. Fraser, V. Ramakrishnan. (2020) Structure of a human 48S translational initiation complex, *Science 369*, 1220-1227.

[196] Feng, X., Li, J., and Liu, P. (2018) The Biological Roles of Translation Initiation Factor 3b, *Int J Biol Sci 14*, 1630-1635.

[197] Min Zhou, A. M. S., Christopher S. Fraser, Gabriela Ridlova, Elaine Stephens, Matthew R. Schenauer, Theresa Yokoi-Fong, Daniel Barsky, Julie A. Leary, John W. Hershey, Jennifer

A. Doudna, and Carol V. Robinson. (2008) Mass spectrometry reveals modularity and a complete subunit interaction map of the eukaryotic translation factor eIF3, *PNAS 105*, 18139-18144.

[198] Duvvuru Muni Rajasekhara Reddy, A. A., Bhushan Bhalchandra Dholakia, Vidya Shrikant Gupta. (2008) Evolutionary analysis of WD40 super family proteins involved in spindle checkpoint and RNA export: Molecular evolution of spindle checkpoint, *Bioinformation 2*, 461-468.

[199] Valasek, L. S., Zeman, J., Wagner, S., Beznoskova, P., Pavlikova, Z., Mohammad, M. P., Hronova, V., Herrmannova, A., Hashem, Y., and Gunisova, S. (2017) Embraced by eIF3: structural and functional insights into the roles of eIF3 across the translation cycle, *Nucleic Acids Res 45*, 10948-10968.

[200] Fung, H. Y., Fu, S. C., Brautigam, C. A., and Chook, Y. M. (2015) Structural determinants of nuclear export signal orientation in binding to exportin CRM1, *Elife 4*.

[201] Walker, E. J., Younessi, P., Fulcher, A. J., McCuaig, R., Thomas, B. J., Bardin, P. G., Jans, D. A., and Ghildyal, R. (2013) Rhinovirus 3C protease facilitates specific nucleoporin cleavage and mislocalisation of nuclear proteins in infected host cells, *PLoS One 8*, e71316.

[202] Redondo, N., Madan, V., Alvarez, E., and Carrasco, L. (2015) Impact of Vesicular Stomatitis Virus M Proteins on Different Cellular Functions, *PLoS One 10*, e0131137.

[203] Chemello, F., Bassel-Duby, R., and Olson, E. N. (2020) Correction of muscular dystrophies by CRISPR gene editing, *J Clin Invest 130*, 2766-2776.

[204] Hirakawa, M. P., Krishnakumar, R., Timlin, J. A., Carney, J. P., and Butler, K. S. (2020) Gene editing and CRISPR in the clinic: current and future perspectives, *Biosci Rep 40*.

[205] Kosugi, S., Hasebe, M., Matsumura, N., Takashima, H., Miyamoto-Sato, E., Tomita, M., and Yanagawa, H. (2009) Six classes of nuclear localization signals specific to different binding grooves of importin alpha, *J Biol Chem 284*, 478-485.